FATE AND TRANSPORT OF NUTRIENTS AND CONTAMINANTS UNDER THE IMPACT OF SURFACE WATER AND GROUNDWATER INTERACTIONS

A Dissertation

by

PIN SHUAI

Submitted to the Office of Graduate and Professional Studies of
Texas A&M University
in partial fulfillment of the requirements for the degree of

DOCTOR OF PHILOSOPHY

Chair of Committee,	Peter S. K. Knappett
Committee Members,	Hongbin Zhan
	Ethan L. Grossman
	Gretchen R. Miller
Head of Department,	Michael C. Pope

August 2017

Major Subject: Geology

ABSTRACT

Periodic river fluctuations are common in nature. River fluctuations propagate into the riparian aquifer meters to hundreds of meters inland. They greatly enhance the mixing of geochemically distinct river water with groundwater and lead to intensive biogeochemical transformation of solutes in the hyporheic zone (HZ). Here, we use a combination of field methods and numerical simulations to investigate the effects of BS induced by river fluctuations due to both natural (e.g. tides and floods) and anthropogenic (e.g. hydropeaking) events on nutrients, (i.e. nitrogen (N)) and contaminants, (i.e. arsenic (As)) fate and transport. We carried out our study in two study sites: a dam regulated river in Austin, Texas and a tidally fluctuating river in Bangladesh. In the first study site, we developed a two-dimensional (2-D) coupled flow, reactive transport model to study the influence of dam release induced river fluctuations on N cycling within the HZ. Sensitivity analyses were conducted to quantify the effects of river amplitude, sediment hydraulic conductivity (K) and dispersivity, and ambient groundwater flow on nitrate removal efficiency. Our results demonstrated that daily river fluctuations created denitrification hot spots within the HZ that would not otherwise exist under naturally neutral or gaining conditions. In the second study site, we investigated the effects of tidal fluctuations on the formation of a permeable natural reactive barrier (PNRB) consisting of iron oxide precipitates and the implications of this for As trapping and mobilization in an aquifer high in dissolved As concentrations adjacent to the Meghna River. We first characterized the hydraulic properties of

riverbank aquifer by using slug tests, pumping test and tidal methods. The characterized aquifer properties were used in a 2-D, flow and reactive transport model to simulate the spatial and temporal distributions of an PNRB in response to tidal and seasonal river stage fluctuations. Our study found that tidal and seasonal river stage fluctuations accelerate the formation of PNRB and broadened their spatial extent. This work, therefore, contributes to the understanding of the fate of several very important biogeochemical cycles (i.e. N, Fe and As) in a dynamically fluctuating river-aquifer system.

DEDICATION

This dissertation is dedicated to Fei and my parents.

ACKNOWLEDGEMENTS

I would first like to thank my major scientific advisor, Dr. Peter Knappett. Peter has always been very supportive both to my scientific advancement and personal growth in the past four years. He has always showed me that field work could have a tons of fun, encouraged me when things did not work out, and motivated me to push my limits to tackle the most challenging problems. Our first and only trip to Bangladesh was an unforgettable experience for me, although the rickshaw ride in Dhaka during the middle of the night was a little intimidating to me. I also want to thank my co-advisor Dr. Bayani Cardenas for his generous time and support. Bayani has introduced me to hyporheic zone and taught me step by step how to be a good groundwater modeler. I had great time debugging and playing with COMSOL. Many thanks also to my committee members, Dr. Hongbin Zhan, Dr. Ethan Grossman and Dr. Gretchen Miller, who have devoted their time to discuss my research findings and provided valuable feedback.

I would also like to thank people who have helped me walk through my PhD and made this dissertation become reality. I am thankful for the people in Bangladesh who have opened their homes and shared their experiences with me. I still remember the van driver who helped me get to the airport during the middle of the night, and Mukta's family who warmly welcomed me to their home in Char Para, Araihazar, Imtiaz Choudury with whom we had long conversations, and the many students from Dhaka University who have been both local guides and field helpers. In addition, I would like to thank Lizhi Zheng and Lichun Wang from University of Texas for their advice on

training reactive transport models and Jeff Watson for field help in collecting water samples. My graduate study became less stressful through conversations with my past and present officemates, Renjie Zhou, Matthew Wehner and Kyungho ‘Nehe’ Jeon. I also thank Kim Rhodes and Katrina Jewell in our research group for their help collecting some of the field data used to constrain the modeling and their companionship.

Last, but not least, I am grateful for the constant love and support from my family even when I am seven thousand miles away from home. My wife, Fei Gao Shuai, has always been there for me whenever I needed and has made my PhD life seem so much shorter yet enjoyable. Thanks to all the friends I met while in College Station, you have made my time at Texas A&M such a wonderful experience. I am proud to be an Aggie!

CONTRIBUTORS AND FUNDING SOURCES

Contributors

Part 1, faculty committee recognition

This work was supervised by a dissertation committee consisting of Dr. Peter Knappett, Dr. Hongbin Zhan and Dr. Ethan Grossman of the Department of Geology and Geophysics and Dr. Gretchen Miller of the Department of Civil Engineering.

Part 2, student/collaborator contributions

Chapter 2: Dr. Bayani Cardenas and Alyse Briody assisted with the collection of the data. Dr. Peter Knappett and Dr. Bayani Cardenas assisted with the interpretation of the model results.

Chapter 3: Dr. Peter Knappett assisted with the collection of the data. Ms. Kimberly Rhodes installed the monitoring wells. The resistivity survey was conducted and analyzed by Alamgir Hosain and Saddam Hossain from Dhaka University. Dr. Peter Knappett assisted with the interpretation of the field data and simulation results.

Chapter 4: Dr. Peter Knappett assisted with the interpretation of the field data and simulation results. Ms. Katrina Jewell and Dr. Kimberly Myers collected the aqueous chemistry field samples to constrain the modeling.

All other work conducted for the dissertation was completed by the student independently.

Funding Sources

This work was made possible in part by U.S. National Science Foundation under Grant no. EAR-1344547 and EAR-1343861, and by Geological Society of America under student research grant. Graduate study was also supported by Graduate Research/Teaching Assistantship from Department of Geology and Geophysics of Texas A&M University.

TABLE OF CONTENTS

Page

LIST OF FIGURES

Page

LIST OF TABLES

Page

CHAPTER I

INTRODUCTION AND LITERATURE REVIEW

1.1 Introduction

1.1.1 Periodic River Fluctuations and Bank Storage

Periodic river fluctuations are easily found in most coastal and regulated rivers. Levels of coastal rivers are often subjected to tidal influences and fluctuate semi-diurnally (12 h) or diurnally (24 h) with an amplitude ranging from a few centimeters to several meters [*Schultz and Ruppel,* 2002; *Trefry and Bekele,* 2004; *Musial et al.*, 2016]. Tidal pulses often travel upstream from the coast for tens or hundreds of kilometers in unregulated rivers [*Musial et al.,* 2016]. In areas with monsoonal climate, seasonal storm events cause river stage to fluctuate several meters annually. river stage

Similar to natural tidal fluctuations, river stages in regulated rivers fluctuate up to several meters over hours resulting from controlled dam release [*Friesz,* 1996; *Arntzen et al.*, 2006; *Sawyer et al.*, 2009; *Francis et al.*, 2010; *Gerecht et al.*, 2011; *Briody et al.*, 2016; *McCallum and Shanafield,* 2016]. Dammed rivers are the norm among large rivers. Over 50% of the world's major rivers are dammed for the purpose of flood control, hydropower production, reservoir storage and recreation [*Nilsson et al.,* 2005]. This body of related work broadly examines the significance of natural and regulated river fluctuations on biogeochemical processes impacting the chemical quality of ground and surface waters relied upon for human consumption and recreation, and for ecosystem sustainability.

Bank storage (BS) is driven by periodic river fluctuations (Figure 1). When rivers flow through porous aquifers which are well connected to the river [*Larkin and Sharp, Jr.*, 1992], rising river stage forces river water into the bank (bank inflow) and falling river stage draws water out of bank (bank outflow). The process of river water being stored and released is referred to as bank storage (BS) [*Squillace,* 1996]. Bank storage leads to dynamic pore-water flow and solute transport in the hyporheic zone (HZ), where surface and ground waters mix. As river water passes through the riverbank aquifer with accompanying reactions, bank storage may impact downstream transport of nutrients, heavy metals and toxic elements. This may occur by slowing the movement of nutrients down river or by removing them through biogeochemical reactions in the HZ. Nutrients and metals within groundwater discharging to rivers may be transformed or consumed prior to discharging into the river within the HZ. *Fritz and Arntzen* [2007] estimated water and uranium flux into and out of a riverbank in response to a regulated fluctuating river near Richland, Washington. They found that BS diluted the uranium flux discharging to the river from the aquifer, thereby fortunately minimizing the impact of this contamination source to the river. *Ensign et al.* [2008] quantified denitrification flux (the amount of nitrate being reduced to nitrogen gas) from the tidal freshwater riparian zone of a coastal river using an empirical model. The model predicted that BS reduced the daily riverine nitrate load through the riparian zone denitrification. This study will investigate the role of water exchanged between rivers and riverbank aquifers induced by periodic river fluctuation on removing unwanted nutrients from rivers, and heavy metals from groundwater.

1.1.2 Nitrogen cycling in the hyporheic zone

Surface waters are rich in dissolved oxygen (DO) and nutrients such as nitrate and phosphate, whereas groundwater is often depleted in these same essential components for biological activity. When these two differing bodies of water mix, it can lead to dynamic biogeochemical reactions in the hyporheic zone (HZ). The exchange of water and oxidizing and reducing agents across the HZ facilitates these biogeochemical reactions, thus regulating nutrient cycling. This exchange process is a critical factor in determining the fate of nitrogen within the river. For example, when DO from rivers enter the HZ, it reacts with the often co-advected dissolved organic carbon (DOC) during microbial heterotrophic respiration processes. Ammonia also reacts with DO during nitrification. As DO is progressively consumed, anaerobic conditions develop that promote denitrification using nitrate as the primary electron acceptor [*Gu et al.*, 2012]. Presumably, much less biogeochemical reactions would occur in the riverbanks without river stage fluctuations driving the mixing between oxidizing river water and relatively reducing ground waters.

Mixing of surface and ground waters, driven by river fluctuations, is not the only cause of denitrification in the HZ. However, many previous studies have focused on nitrogen cycling in the HZ driven by river bed forms, such as riffle-pool sequences [*Tonina and Buffington*, 2007; *Fox et al.*, 2014; *Hassan et al.*, 2015; *Naranjo*, 2015]. *Hassan et al.* [2015] investigated the effect of stream discharge, channel slope and sediment hydraulic properties on hyporheic exchange in step-pool morphologies through flume experiments and numerical modeling. They found that steeper riverbed gradients

in the direction of flow, combined with moderate discharges produced the deepest hyporheic flow. They also found that hydraulic conductivity (K) greatly impacted the extent of stream water intrusion into the streambed as others have found in [*Arntzen et al.,* 2006]. *Fox et al.* [2014] measured hyporheic exchange fluxes induced by dune-shaped bed forms in a laboratory flume system under gaining and losing streamflow conditions. They found that the hyporheic exchange fluxes under both conditions are similar. *Tonina and Buffington* [2007] examined the effect of discharge and bed form amplitude on hyporheic exchange using a set of flume experiments and 3-D modeling. They found that bedform-induced advection plays an important role in hyporheic exchange. Although field experiments and laboratory flumes are useful to explore the various important chemical and physical factors influencing nitrate reaction rates in pore-waters within the HZ, these experiments are often laborious and expensive. Numerical simulations, on the other hand, allow us to test the sensitivity of specific factors on hyporheic exchange and advance our quantitative understanding of the inter-relationships between simultaneously-occurring physical and chemical processes. These models can, in turn, be very useful for developing hypotheses that can be tested with specific field or laboratory experiments.

Coupled flow and reactive transport models may be used to evaluate the role of solute concentrations and reaction kinetics in determining whether the HZ acts as a net source or sink of nitrate [*Gu et al.,* 2007; *Boano et al.,* 2010; *Marzadri et al.,* 2011; *Bardini et al.,* 2012, 2013; *Zarnetske et al.,* 2012]. *Bardini et al.* [2012] simulated nutrient dynamics in the HZ induced by a duned streambed under steady flow. They

found that the availability of DOC determined whether the streambed functioned as a net sink or source of nitrate. *Bardini et al.* [2013] further showed that sediment heterogeneity at the bedform scale has minimal effect on streambed nutrient dynamics. *Zarnetske et al.* [2012] used a 1D coupled flow and reactive transport model to evaluate the factors controlling whether the HZ is a net source of sink of nitrate. They found that water residence time and the supply and demand rates of oxygen determined whether the HZ performed as a nitrate source or sink to the stream. *Gu et al.* [2007] investigated the impacts of flow and biogeochemical kinetics on nitrate reduction in streambed sediments using both laboratory column experiments and numerical simulations. They found that nitrate concentration discharging from groundwater increased with increasing flow rates.

Gu et al. [2012] was the first author to perform fully coupled flow and reactive transport modeling to identify the effect of BS on nutrient transport during river stage fluctuations. Their model showed that high biogeochemical reaction rates (i.e. aerobic respiration and denitrification) occurred in the near-stream HZ. Their model, however, did not account for total stress changes in response to river stage fluctuations. When sediment compressibility is considered, the governing equation should be modified to include total stress changes [*Reeves et al.*, 2000; *Wilson and Gardner*, 2006]. Also, for the sake of simplicity, their models only account for denitrification. One of our main objectives is to understand how changes in hydrological and biogeochemical processes under periodic river fluctuations impact nitrogen cycling within the HZ. This will be carried out though a more physically sound reactive transport model that accounts for both nitrification and denitrification.

1.1.3 Arsenic mobilization under tidal influence

The role of river stage fluctuations in releasing or trapping heavy metals and toxic elements discharged from aquifers within sediments, in the HZ, has not been widely explored. In deltas, transient water levels in rivers and aquifers cause pore-water flow directions to oscillate from towards to away from the river. This action causes changing redox conditions in HZ that may promote releasing and trapping of toxic elements such as As [*Datta et al.*, 2009; *Jung et al.*, 2015]. Coastal rivers fluctuate with semi-diurnal, diurnal and neap-spring tides (14 d) which drives surface water in and out of aquifers over a short term. Further, in regions with monsoonal climates and cold regions with spring snowmelts, seasonal changes in the river stage will drive surface water into and out of the aquifers over a long term.

In the area of the Ganges-Brahmaputra-Meghna Delta (GBMD), this fluctuating river stage will introduce oxygen- and nutrient- rich water into the reducing, ferrous iron (Fe(II))-rich aquifers, causing amorphous ferric (Fe(III)) oxide (FeOOH) minerals to precipitate. This process will tend to occur during the early monsoon when the river stage is rapidly rising and infiltrating into the aquifer. At falling stage, groundwater that is high in dissolved As in shallow aquifers in the GBMD, discharges into the river. These FeOOH minerals strongly sorb dissolved oxyanions such as As. Therefore, the oxidized Fe(III) may form a permeable natural reactive barrier (PNRB) along the riverbank [*Jung et al.*, 2009, 2012, 2015; *Lee et al.*, 2014; *MacKay et al.*, 2014; *Baken et al.*, 2015]. *Datta et al.* [2009] found extremely high As concentrations in the sediments lining the Meghna River, Bangladesh. Solid-phase concentrations of As of 23,000 mg/kg

where found, while most samples had levels greater than 400 mg/kg (or 0.04 percent by weight). They hypothesized that the elevated As concentration in the river sediments resulted from the discharge of Fe- and As-rich shallow groundwater. *Jung et al.* [2012] also found enrichment of solid-phase As exceeding 700 mg/kg along the redox transition zone within a riverbank aquifer along the Meghna River where reducing groundwater mixed with oxic river water. In a further study, *Jung et al.* [2015] concluded that the As content was so high (700 mg/kg) that it would take hundreds of years of steady groundwater discharge (~10 m/yr) to accumulate. These studies did not explicitly explore the role of transient river stage fluctuations on the formation of the Natural Reactive Barriers (PNRBs), neither do they examine the potential impact of human activities on remobilizing As from the riverbank sediment.

Human activities such as irrigation pumping are likely to perturb groundwater flow fields near rivers and re-mobilize As into shallow aquifers within the GBMD [*Stollenwerk et al.*, 2007; *Dhar et al.*, 2011; *Radloff et al.*, 2011; *van Geen et al.*, 2013; *Schaefer et al.*, 2016; *Stahl et al.*, 2016]. Irrigation pumping greatly alters flow patterns in groundwater systems in the vicinity of irrigation wells, switching flow direction from towards the river to away from the river. The reversal of flow might induce a much larger amount of surface water into shallow aquifers than caused by tidal or seasonal fluctuations, bringing in DOC. This is analogous to the previously suggested roles of ponds in introducing fresh, labile DOC to aquifers causing the mobilization of As through reductive dissolution broadly across the lower delta [*Neumann et al.*, 2010]. One important difference, however, is that the previously functioning PNRB may have built

up extremely high solid-phase concentrations of As along the river-aquiver interface. Thus, river water DOC may mobilize As into the dissolved phase, which may further contaminate groundwater [*Jung et al.*, 2015]. The net result of competing reducing and oxidizing reactions under the influence of persistent river water movement through an PNRB into an aquifer, however, is not obvious. Unlike pond water, which is typically very low in oxygen and high in DOC [*Knappett et al.*, 2012], river water commonly contains abundant oxygen and less DOC [*Berube et al.*, 2017]. This oxygen may cause the re-precipitation of any Fe that is mobilized by reductive dissolution from DOC derived from the river water or particulate organic matter (POC) within the aquifer sediments. Similarly, any newly released As from reductively dissolved FeOOH may then quickly re-attach to other FeOOH surfaces. A model is thus needed to study the impacts of these competing reactions on As mobilization, even under constant losing losing conditions.

None of the previously mentioned studies have examined how tidally- and seasonally- influenced river stage fluctuations determine the development of an PNRB or the impact of irrigation pumping located within several hundred meters of a river on the fate of As that had built up within that PNRB. To fill this gap, this study will investigate Fe and As cycling under the influence of natural tidal fluctuations and local irrigation pumping. The processes investigated in this study have implications for other hydrogeologically and chemically similar shallow aquifers lining rivers across South and Southeast Asia where dissolved concentrations of As and Fe are commonly high in shallow aquifers [*Fendorf et al.*, 2010]. These findings should also be applicable to other

coastal aquifers lining rivers in the U.S. which are contaminated with heavy metals and toxic elements like As from natural or industrial processes.

1.2 Objectives and Hypotheses

This research aims to study the effects of periodic river fluctuations on nitrogen cycling and arsenic trapping and mobilization in the HZ. This research also broadly analyzes how physical and biogeochemical processes interact to control the transport and transformation of reactive solutes (Figure 2). Previous studies have either focused on the biogeochemical aspects of the reactions or the physical aspects of the flow. That is, they either study the different reaction processes within the context of simple, 1-D, steady-state flow, or they focused on complex flow field but with few reactions. Very few investigations have coupled the transient flow with a set of the most important kinetically-controlled, biogeochemical reactions. Therefore, this dissertation fills this gap through field experiments and numerical modeling to fully couple dynamic physical transport with complex biogeochemical reactions. Our model could further be used elsewhere to study and predict the transport and transformation of other solutes under the influence of frequent mixing between surface and ground waters. The detailed objectives and hypotheses are listed below:

Objective 1 (O1): Understand the impacts of regular hydropeaking and physical aquifer properties on nitrate removal in the riparian zone

Hypothesis (H1): a) Biogeochemical reaction (respiration, nitrification, and denitrification) rates in the HZ increase with dynamic fluctuations induced by river fluctuations; b) respiration and nitrification in the HZ are dominant along flowpaths with

short residence times, while denitrification dominates along flowpaths with longer residence times; and c) hydraulic conductivity (K), aquifer dispersivity, river fluctuation amplitude and ambient groundwater flow direction impact nitrate removal efficiency.

Objective 2 (O2): Constrain aquifer properties of a tidally-influenced riverbank aquifer using a combination of slug tests, pumping test and tidal methods, and test the validity of Jacob-Ferris model in different aquifer settings. Many studies have used tidal methods (e.g. time lag and amplitude attenuation) to estimate aquifer diffusivity (D), the ratio between aquifer transmissivity (T) and storativity (S)) with the assumption of vertical bank, homogeneous and confined aquifer without regional groundwater flow [*Jacob*, 1950; *Ferris*, 1951]. How would a diffusive wave propagate in a more realistic hydrogeologic setting?

Hypothesis 2 (H2): Time lag and amplitude attenuation of a diffusive wave within an aquifer will be greater with sloped bank compared with a vertical bank, an unconfined aquifer compared with a confined aquifer, and in a homogeneous aquifer compared with a heterogeneous aquifer. These biases will result in aquifer diffusivity being overestimated when using the Jacob-Ferris 1-D analytical model. The hypothesis is tested with a combination of field measurements and numerical simulations.

Objective 3 (O3): Understand the hydro-geochemical processes that control the formation of a natural reactive barrier and subsequent arsenic mobilization under the influence of intensive irrigation pumping within a shallow riverbank aquifer.

Hypothesis 3 (H3): a) The enrichment of arsenic (As) in the sediments lining the Meghna River is the result of seasonally gaining river conditions; b) a highly reactive Fe-oxide barrier coats the sediments of the HZ along the Meghna River; c) the high dissolved concentrations of As discharging to the river through the HZ sorbs to the Fe-oxides; d) the temporal and spatial distribution of PNRBs is influenced by different tidal frequency and amplitude; and e) intensive groundwater pumping nearby, reverses the gaining river condition to a losing one, promoting the mobilization of As into the shallow aquifer.

1.3 Chapter Summaries

This dissertation is divided into three major chapters to address the above objectives and hypothesis in sequence. Chapter 2 focuses on the N cycling in riverbanks adjacent to Lower Colorado River (LCR) in Austin, Texas. Chapter 3 focuses on the application of various field methods to constrain aquifer properties and to validate assumptions of the 1-D Jacob-Ferris tidal pulse propagation model, whereas Chapter 4 uses a numerical model to simulate the PNRB formation and As mobilization processes. Both Chapter 3 and 4 are conducted in a shallow, deltaic aquifer adjacent to the Meghna River in Bangladesh.

Chapter 2: *Denitrification in the banks of fluctuating rivers: the effects of river stage amplitude, sediment hydraulic conductivity and dispersivity, and ambient groundwater flow.* A two-dimensional flow and reactive transport model was developed and used to simulate DO, nitrate, DOC and ammonia transport and reactions within the HZ driven by river stage fluctuations. Furthermore, the effects of river stage fluctuation

amplitude, sediment hydraulic conductivity and dispersivity, and ambient groundwater flow were tested separately through sensitivity analysis (Objective 1).

Chapter 3: *The impact of the degree of aquifer confinement and anisotropy on tidal pulse propagation*. 1-D tidal methods are widely used in coastal aquifers to estimate the diffusivity of an aquifer. The errors associated with these methods, caused by the limited dimensionality, however, have not been extensively investigated. Therefore, we developed a 2-D numerical model to test the sensitivity of tidal pulse propagation into a shallow aquifer to higher dimension riverbank aquifer properties (than 1-D), including riverbank slope, heterogeneity, and aquifer anisotropy. The errors introduced by calculating aquifer diffusivity using the 1-D model based on amplitude attenuation ratio and delayed time arrival were evaluated by comparing known aquifer diffusivity input into a 2-D numerical riverbank model to that calculated by applying the 1-D analytical model to the simulated signals. We then analyzed the suitability of 1-D analytical model specifically for our study site and discuss reasons why they yielded aquifer diffusivity, inconsistent with that obtained with pumping and slug tests (Objective 2).

Chapter 4: Modeling the formation of permeable natural reactive barriers in a riverbank aquifer under the influence of tidal and seasonal fluctuations, and subsequent mobilization of As under the influence of irrigation pumping. Solid-phase arsenic concentrations are strongly correlated to Fe-oxide content in aquifer sediments in shallow aquifers in Bangladesh. However, the distribution of Fe-oxide is vulnerable to the redox condition in the aquifer. River stage fluctuations alter the redox condition in

the HZ, resulting in complex temporal and spatial patterns of Fe-oxide. We developed a 2-D multi-species, reactive transport model to explain the dynamic formation of an PNRB. We also evaluated these PNRB as sources of dissolved As mobilized into shallow aquifers under the influence of irrigation pumping (Objective 3). A sensitivity analysis was conducted to identify impact of river stage fluctuations and groundwater table level on the rate of PNRB, its ultimate density of Fe deposited throughout, and its spatial extent.

Chapter 5*: Conclusions*. This chapter summarizes all the key findings and highlights the novelty of this body of work. The significance of this dissertation and broader impacts were also discussed to inform researchers, stake holders and practitioners of the role that dynamically fluctuating rivers may have on limiting nutrients and concentrating natural or industrial heavy metals and toxic elements within the HZ.

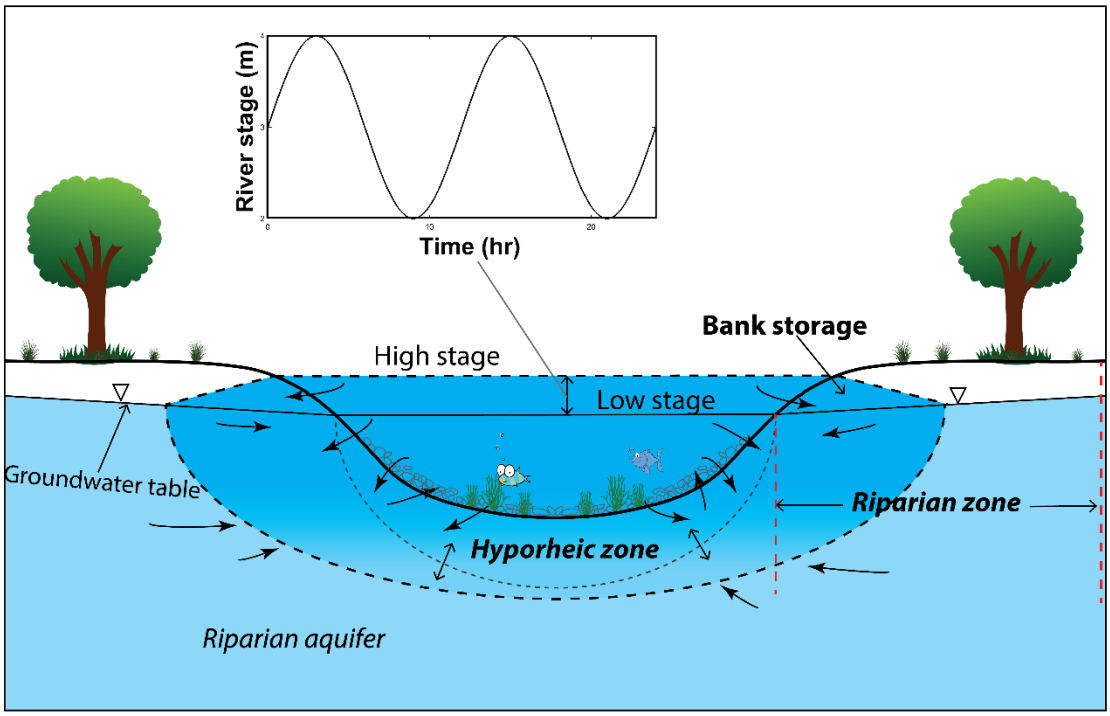

Figure 1. Cartoon showing how river fluctuations induce bank storage and the relative locations of hyporheic zone and riparian zone.

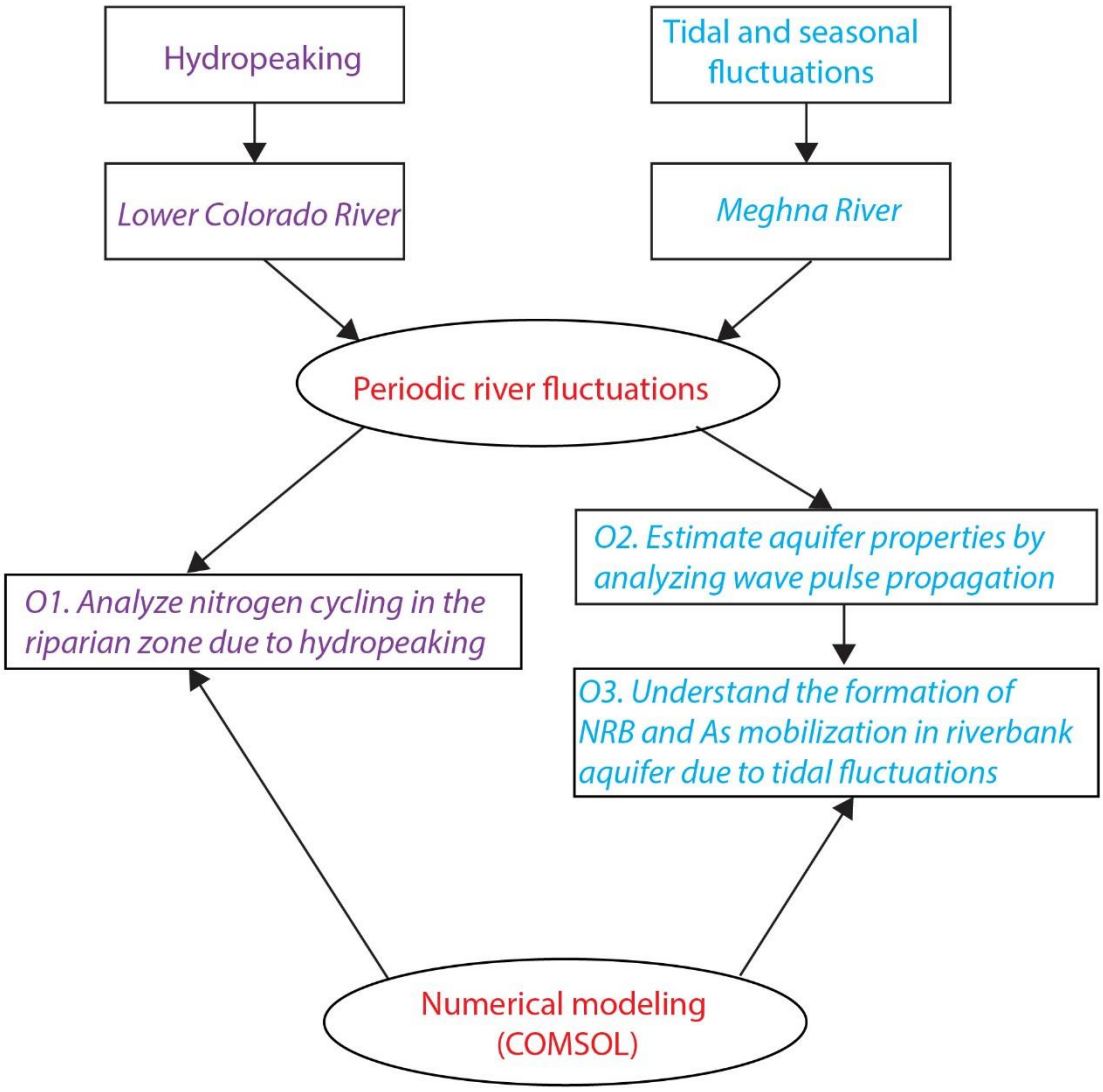

Figure 2. Flow chart of the study

CHAPTER II

DENITRIFICATION IN THE BANKS OF FLUCTUATING RIVERS: THE EFFECTS OF RIVER STAGE AMPLITUDE, SEDIMENT HYDRAULIC CONDUCTIVITY AND DISPERSIVITY, AND AMBIENT GROUNDWATER FLOW

2.1 Summary

Hyporheic exchange induced by periodic river fluctuations leads to important biogeochemical processes, particularly nitrogen cycling, in riparian zones (RZs) where chemically distinct surface water and groundwater mix. We developed a two-dimensional coupled flow, reactive transport model to study the influence of river fluctuations on nitrogen cycling within the RZ during a single 24 h pulse. Sensitivity analyses were conducted to quantify the effects of river amplitude, sediment hydraulic conductivity and dispersivity, and ambient groundwater flow on nitrate removal efficiency. The simulations showed that nitrification occurred in the shallower zone adjacent to the bank where oxic river water and groundwater interacted while denitrification occurred deeper into the aquifer and in the riverbed sediments where oxygen was depleted. River fluctuations greatly increased the amount of nitrate being removed; however, the removal efficiency decreased as river amplitude increased. Similarly, increasing hydraulic conductivity increased overall nitrate removal since it expanded the denitrifying zone but decreased efficiency. In contrast, increasing sediment dispersivity increased the removal efficiency of nitrate because it promoted mixing between electron acceptors and donors. The presence and direction of ambient

groundwater flow had a significant impact on nitrate removal efficiency when compared to neutral conditions. A losing river showed smaller removal efficiency (3.5%) while a gaining river showed larger removal efficiency (17.1%) compared to neutral conditions (5.4%). Our results demonstrated that daily river fluctuations created denitrification hot spots within the RZ that would not otherwise exist under naturally neutral or gaining conditions.

2.2 Introduction

Periodic river stage fluctuations are common in nature. River fluctuations propagate into the riparian aquifer meters to dozens of meters inland [*Sawyer et al.*, 2009] and may greatly enhance the mixing of geochemically distinct river water with groundwater and lead to intensive biogeochemical transformation of solutes in the riparian zone (RZ), or hyporheic zone [*Valett et al.*, 1993]. The hyporheic zone is defined as the area below and adjacent to river sediments where surface water and groundwater mix, however, it may also overlap with the RZ, which is defined as the region between uplands and the stream [*Merill and Tonjes*, 2014]. Here, the exchange occurring across a riverbank is also referred to as bank storage (BS), which is to be differentiated from in-stream hyporheic exchange that primarily occurs across the river bed [*Cooper and Rorabaugh*, 1963]. Bank storage plays an important role in removing nutrients or contaminants from rivers and reducing the nutrients transport downstream [*Musial et al.*, 2016]. River stage fluctuations are attributed to both natural hydrological events, such as tides [*Wilson and Gardner*, 2006; *Xin et al.*, 2011; *Musial et al.*, 2016], floods [*Pinder and Sauer*, 1971; *Squillace*, 1996; *Bates et al.*, 2000; *Gu et al.*, 2012],

snowmelt [*Loheide and Lundquist*, 2009] and anthropogenic influences such as dam releases [*Sawyer et al.*, 2009]. In regulated rivers, river stage fluctuates up to several meters over time periods measured in hours as a result of dam operations [*Friesz*, 1996; *Arntzen et al.*, 2006; *Sawyer et al.*, 2009; *Francis et al.*, 2010; *Gerecht et al.*, 2011; *Briody et al.*, 2016; *McCallum and Shanafield*, 2016]. Dammed rivers are the norm among large rivers with over 50% of the world's major rivers being dammed for the purpose of flood control, hydropower production, reservoir storage and recreation [*Nilsson et al.*, 2005]. Few studies, however, have analyzed nutrient and contaminant transport and transformation within the BS due to regular, periodic fluctuations such as daily dam releases.

Changes in BS is driven by river fluctuations. Under transient river fluctuations, rising river stage forces water into the bank (bank inflow) and falling river stage draws water out of bank (bank outflow). The exchange between rivers and riparian aquifers therefore leads to dynamic pore water flow and solute transport in the RZ, which increases the volume of water exchanged between aquifers and rivers, enhances the mobilization and transformation of solutes, and alters the microbial community [*Curry et al.*, 1994; *Arntzen et al.*, 2006; *Ensign et al.*, 2008; *Hanrahan*, 2008; *Stegen et al.*, 2016]. *Sawyer et al.* [2009] conducted field studies in a regulated river that fluctuated almost a meter daily due to dam operations. They found that river water penetrated several meters into the riparian aquifer and were able to estimate the daily hyporheic exchange volume to be 1 m^3 of water per meter of bank. *Musial et al.* [2016] conducted a field study in an incised tidal river that fluctuates 0.75 m semi-diurnally. They estimated that at least 11%

of the river's discharge was exchanged through tidal BS over a 17-km reach, corresponding to an average of 1.22 m^3 per meter of river per tidal cycle. Tidal rivers further increased aquifer dissolved oxygen (DO) concentration further away from the river compared to non-tidal rivers. A recent study by *Stegen et al.* [2016] suggested that BS induced by river fluctuations also promoted the accumulation of labile organic carbon within microsites during the falling stage and stimulated microbial respiration in the RZ during the rising stage. Together these studies indicate that periodic river fluctuations increase physical connectivity and biogeochemical transformation between rivers and riparian aquifers. With continued construction of dams around the world, we would expect to see more rivers with frequent periodic fluctuations. Yet little is known about the impact of dynamically fluctuating rivers on the migration and transformation of nutrients such as nitrate due to BS. This study investigates the role of BS induced by periodic river fluctuation on removing riverine nutrients.

Surface waters are typically saturated in DO and rich in nutrients such as nitrate and phosphate, whereas groundwater is often depleted in these same essential components for biological activity. When these two differing bodies of water mix, it can lead to dynamic biogeochemical exchange in the RZ. The exchange of water and chemicals in the RZ facilitates biogeochemical reactions and regulates nutrient cycling. This process of exchange is a critical factor in determining the fate of nitrogen. For example, when DO from rivers penetrates into the RZ, it reacts with the often co-advected dissolved organic carbon (DOC) via microbial heterotrophic respiration. Ammonia within the aquifer also reacts with DO via nitrification. As DO is consumed,

however, anaerobic conditions promote denitrification as nitrate becomes primary electron acceptor (Figure 3) [*Gu et al.*, 2012].

The role of solute concentration and reaction kinetics on determining whether the RZ is a source or sink of nitrate can be discerned using coupled flow and reactive transport models, [*Gu et al.*, 2007; *Boano et al.*, 2010; *Marzadri et al.*, 2011; *Bardini et al.*, 2012, 2013; *Zarnetske et al.*, 2012]. *Zarnetske et al.* [2012] used a 1D numerical model describing coupled physical transport and biogeochemical redox reactions to evaluate the factors controlling whether the hyporheic zone is a net source or sink of nitrate. Through Monte Carlo sensitivity analysis, they found that water residence time and the supply and demand rates of oxygen determined whether the hyporheic zone performed as a nitrate source or sink to the stream. *Bardini et al.* [2012] simulated nutrient dynamics in the hyporheic zone when exchange was induced by a duned streambed under steady flow. They found that the availability of DOC determined whether the streambed functioned as a net sink or source of nitrate. *Bardini et al.* [2013] further showed that sediment heterogeneity at the bedform scale has minimal effect on streambed nutrient dynamics. *Gu et al.* [2007] investigated the effect of flow and biogeochemical kinetics on nitrate reduction in streambed sediments using both laboratory column experiments and numerical simulations. They found that effluent nitrate concentrations increase with increasing groundwater discharge rates and aerobic respiration and denitrification rates both affect the fate of nitrate. However, none of these studies have looked at the effect of BS induced by river fluctuations on nitrogen cycling in the RZ.

Gu et al. [2012] was the first to use numerical models to identify the effect of BS induced by stage fluctuations on nutrient transport during storm events. Their results showed that intensive biogeochemical activity occurred in the near-stream RZ forming localized hot spots. However, this model contained two simplifications. First, it did not account for total stress changes in response to river stage fluctuations. When sediment poromechanics is considered, the governing equation should be modified to include total stress changes [*Reeves et al.*, 2000; *Wilson and Gardner*, 2006]. Second, it did not account for nitrification. When short residence times occur, nitrification might be dominant in the RZ [*Zarnetske et al.*, 2011a]. Our main objective is to understand more precisely how changes in hydrological and biogeochemical processes under periodic river fluctuations impact nitrogen cycling within the RZ. This will be carried out through a more comprehensive flow and reactive transport model that accounts for total stress changes and nitrification and denitrification.

Here we coupled a 2D flow and biogeochemical reaction model to study the influence of river fluctuation-induced hyporheic exchange on nitrogen cycling within the RZ during dam release and storage. Further, we used a suite of models to quantify the effect of river fluctuation amplitude, sediment hydraulic conductivity and dispersivity, and ambient groundwater flow on nitrate removal efficiency. For the sake of simplicity, our simulations were conducted over one 24 h cycle.

2.3 Materials and Methods

2.3.1 Study site which guided the models

This study is exclusively based on simulations, however the computational experiments are guided by field observations from a site along the Lower Colorado River (LCR). The study site is located at Hornsby Bend, 15 km downstream from Longhorn Dam in Austin, Texas, USA. Upstream from Longhorn Dam, the Tom Miller Dam is constantly releasing water to generate the hydroelectric power for Austin. The Longhorn Dam forms a cooling reservoir for an adjacent power plant and opens its gate automatically once the water level reaches a certain height. This gate opening produces pulses in river stage and discharge. At Hornsby Bend, the LCR is a regulated 4th-order river with a daily average discharge of ~70 m^3/s and a daily fluctuation upwards of 85 cm during dam operations, or so-called "hydropeaking" [*Sawyer et al.*, 2009]. However, the stage fluctuation varies and the amplitude may reach as high as 2 m, depending on lake level, rainfall, and water and energy demands. The releases at Longhorn Dam typically follow a square wave with a temporal width of a few hours, with most lasting about 12 hours (see for example https://waterdata.usgs.gov/nwis/uv?site_no=08158000). The river is about 60 m wide, with depth varying due to river fluctuations on the order of 1-2 m. The regional groundwater flow is towards the river [*Larkin and Sharp*, 1992]. But, during dam operation or flood events, the river changes from a gaining stream to a losing one due to the reversal of hydraulic head gradients.

Five kilometers north of Hornsby Bend, the Walnut Creek Wastewater Treatment plant discharges approximately 0.43 million m^3 treated wastewater into the LCR daily

(or 4.98 m^3/s) [*LCRA*, 2014]. With nitrate concentration in the effluent ranging between 88 and 111 mg/L, this causes an excess of nutrients in the river contributing to the observed overgrowth of algae and aquatic plants, especially under low-flow conditions [*Dawson et al.*, 2015; *Briody et al.*, 2016].

2.3.2 Model development

2.3.2.1 Governing equations

A 2D flow and reactive transport model was developed to simulate water exchange across a riverbank induced by hydropeaking using COMSOL Multiphysics, a generic finite-element program. The model couples unsaturated porous media flow based on Richard's equation and solute transport based on the advection-dispersion-reaction equation.

$$\rho\left(\frac{C_m}{\rho g}+S_e S\right)\frac{\partial p}{\partial t}+\nabla\cdot\rho\left(-\frac{k_s}{\mu}k_r(\nabla p+\rho g\nabla z)\right)=Q_m \tag{2.1}$$

$$\frac{\partial}{\partial t}(\theta C_i)=-\nabla\cdot\rho(uC_i)+\nabla\cdot(D\nabla C_i)+R_i \tag{2.2}$$

where p is pressure, ρ is the fluid density, C_m is specific moisture capacity, g is the acceleration of gravity, S_e is effective saturation, S is the storage coefficient, k_s is the saturated hydraulic permeability, k_r is the relative permeability, μ is the fluid dynamic viscosity and z is elevation head. Q_m in this equation represents a stress source term (see below). C_i is the concentration for species i, θ is water content, u is Darcy velocity, D is the hydrodynamic dispersion coefficient and R_i is the reaction rate for species i.

The coupled equations were solved with a segregated solver which solved flow and solute transport and reactions sequentially. Unlike similar steady-state flow models developed to study denitrification along riverbank aquifers, our model accounted for a transient flow field induced by river fluctuations, which was important to understand the dynamic, kinetically limited biogeochemical reactions in the RZ.

2.3.2.2 Flow model

The model geometry is taken from bank elevation profile surveyed with a Total Station (GTX-226, TopCon Positioning Systems, Inc., Tokyo, Japan) at the Hornsby Bend site, starting from the floodplain to the middle of the river channel (**Figure 4**). The model domain is 38 m wide with a maximum depth of 6 m and is homogeneous and isotropic. The bottom of the aquifer and center of the river channel are treated as a no flow boundary. A constant head boundary that is equal to the mean river stage is assigned to the landward vertical boundary. The upper boundary is a semi-pervious layer or seepage face without considering rainfall or evaporation. The seepage face boundary condition is implemented along the upper boundary using a mixed-boundary condition, which splits the boundary into zero-pressure for the nodes along the seepage face and zero-flux for the nodes above the seepage face using a conditional statement (see details in *Cardenas et al.*, [2015] and *Chui and Freyberg* [2009]). The nodes below the seepage face are set to a specific head equal to the river stage. To facilitate convergence, a smoothing function is used to switch between the Dirichlet condition (i.e. zero-pressure) and Neumann condition (i.e. zero-flux) [*Chui and Freyberg*, 2009]. The river stage is described as a sine function with a period of 24 hours for simplicity.

The addition or removal of water from the aquifer associated with total stress changes from loading of the aquifer with increased or decreased river stage is included in the model for the portion of the aquifer directly underneath the river [*Reeves et al.*, 2000]. The change in total stress is denoted as the time derivative of river stage and implemented in the source term Q_m (**Equation (2.1)**) [*Cardenas et al.*, 2015]. This modeling approach has been found to be useful in describing river water movement and residence times within the RZ bordering dynamic rivers [*Wilson and Gardner*, 2006; *Maji and Smith*, 2009; *Cardenas et al.*, 2015].

The triangular mesh is discretized uniformly throughout most of the domain but with a finer grid toward the upper boundary where dynamic fluctuations in the river cause imbibition and drainage of water into and out of the sediment. The mesh size is 0.01 m at the top layer and 0.3 m elsewhere consisting of over 80,000 domain elements. In addition, a boundary layer mesh is added to the upper layer to smooth the gradient towards the aquifer. A maximum time step of 500 seconds is enforced to ensure numerical stability and minimize numerical dispersion. The total simulation period is 24 hours. Typical van Genuchten parameters were assumed based on clean fine sand (Table 1). The initial hydraulic head field was obtained by running a steady-state model with a constant river stage and groundwater table.

2.3.2.3 Solute transport and biogeochemical reaction model

Solute transport is based on the velocity field from the flow model. A no flux boundary condition is applied to the bottom and center of the river channel (**Figure 4**). An outflow boundary condition is assigned to the landward side of the domain. An open

boundary condition with external concentration equal to solute concentrations in the river is assigned to the upper layer. This allows the solute to move in (advection and dispersion) and out (advection only) of the aquifer freely across the river-aquifer interface with dynamic flow and transport conditions [*Cardenas et al.*, 2015].

Four species (DOC, DO, nitrate and ammonium) were introduced into the aquifer from the river and these solutes were then produced and consumed via aerobic respiration, nitrification and denitrification (Figure 3). Surface water intrusion brings in DO, DOC, ammonium and nitrate to the RZ. The concentrations of the above species were initially assumed to be zero in the aquifer for simplicity and to isolate the effects of the factors that this study focuses on. In the aerobic region where aerobic respiration and nitrification happen simultaneously, a partition coefficient for DO demand is calculated based on bioenergetics [see more details in *Zarnetske et al.*, 2012]. When nitrate and the remaining DOC enters the deeper anaerobic region of RZ, nitrate becomes the thermodynamically favored electron acceptor and is therefore removed through denitrification. Other nitrogen cycling processes like dissimilatory nitrate reduction to ammonium (DNRA) and anaerobic ammonium oxidation (ANAMMOX) were not considered here due to their negligible effect on nitrogen dynamic in the RZ [*Zarnetske et al.*, 2012]. Besides being transported through advection from surface water, a considerable amount of DOC may originate from in situ POC dissolution or desorption; this process was simulated by a first-order mass transfer process [*Jardine et al.*, 1992; *Gu et al.*, 2007; *Zarnetske et al.*, 2012; *Sawyer*, 2015]:

$$\frac{dC_{POC}}{dt} = \alpha(k_d C_{DOC} - C_{POC}) \quad (2.3)$$

where C_{POC} is particulate organic carbon content in the sediment, C_{DOC} is the concentration of DOC, α is a first-order mass transfer coefficient, and k_d is a linear distribution coefficient for the hyporheic sediment.

Multiple Monod kinetics was used to represent aerobic respiration, denitrification and nitrification [*Molz et al.*, 1986]. Noncompetitive inhibition was used to suppress denitrification in the presence of DO [*Widdowson et al.*, 1988]. The reaction terms in **Equation (2.2)** are described as follows:

$$R_{O_2} = -\theta V_{AR} X_{AR} y_{O_2} \left(\frac{C_{DOC}}{K_{DOC}+C_{DOC}}\right)\left(\frac{C_{O_2}}{K_{O_2}+C_{O_2}}\right) - \theta V_{NT} X_{NT}(1 - y_{O_2})\left(\frac{C_{NH_4}}{K_{NH_4}+C_{NH_4}}\right)\left(\frac{C_{O_2}}{K_{O_2}+C_{O_2}}\right) \quad (2.4)$$

$$R_{NH_4} = -\theta V_{NT} X_{NT} \left(\frac{C_{NH_4}}{K_{NH_4}+C_{NH_4}}\right)\left(\frac{C_{O_2}}{K_{O_2}+C_{O_2}}\right) \quad (2.5)$$

$$R_{NO_3} = \theta V_{NT} X_{NT} \left(\frac{C_{NH_4}}{K_{NH_4}+C_{NH_4}}\right)\left(\frac{C_{O_2}}{K_{O_2}+C_{O_2}}\right) - \theta V_{DN} X_{DN} \left(\frac{K_I}{K_I+C_{O_2}}\right)\left(\frac{C_{DOC}}{K_{DOC}+C_{DOC}}\right)\left(\frac{C_{NO_3}}{K_{NO_3}+C_{NO_3}}\right) \quad (2.6)$$

$$R_{DOC} = -\theta V_{AR} X_{AR} y_{O_2} \left(\frac{C_{DOC}}{K_{DOC}+C_{DOC}}\right)\left(\frac{C_{O_2}}{K_{O_2}+C_{O_2}}\right) - \theta V_{DN} X_{DN} \left(\frac{K_I}{K_I+C_{O_2}}\right)\left(\frac{C_{DOC}}{K_{DOC}+C_{DOC}}\right)\left(\frac{C_{NO_3}}{K_{NO_3}+C_{NO_3}}\right) + \rho_b \alpha(C_{POC} - k_d C_{DOC}) \quad (2.7)$$

where C_{O_2} , C_{NH_4} , C_{NO_3} , and C_{DOC} are the concentrations for oxygen (O_2), ammonium (NH_4), nitrate (NO_3) and dissolved organic carbon (DOC) respectively. R_{O_2}, R_{NH_4} , R_{NO_3} and R_{DOC} are the reaction rates for O_2, NH_4, NO_3 and DOC, respectively. V_{AR}, V_{NT}, and V_{DN} are the maximum specific uptake rates of the substrate for aerobic respiration (AR),

nitrification (NT) and denitrification (DN), respectively. X_{AR}, X_{NT}, and X_{DN} are the biomass of the functional microbial group facilitating the different reaction components of AR, NT and DN, respectively. y_{O_2} is the O_2 partition coefficient, K_{O_2} , K_{NH_4} , K_{NO_3} , and K_{DOC} are the half-saturation constants for O_2, NH_4, NO_3 and DOC, respectively. K_I is an inhibition constant, and ρ_b is bulk density.

Parameters used in the flow and reactive transport model are either observations from field or from data found in the literature (**Table 1**) [*Gu et al.*, 2007, 2012; *Zarnetske et al.*, 2012; *Sawyer*, 2015]. To test the sensitivity of river stage amplitude (A), hydraulic conductivity (K) and longitudinal dispersivity (D_L) on denitrification in the RZ, a range of values with A (0.1~0.5 m), K (10~100 m/d) and D_L (0.5~2 m) were used. These ranges were established from previous studies at nearby locations [*Sawyer et al.*, 2009; *Francis et al.*, 2010; *Gerecht et al.*, 2011; *Briody et al.*, 2016]. Transversal dispersivity was assumed as one tenth of D_L which is typical for most aquifers [*De Marsily*, 1986].

The concentrations of the four aqueous species (i.e. O_2, DOC, NO_3 and NH_4) in the river were considered constant and were taken as the mean value of previous measurements of water samples [*LCRA*, 2014; *Briody et al.*, 2016]. One solid species (POC) was set to be 2% by mass for the whole aquifer to ensure excess DOC supply [*Gu et al.*, 2007]. It should be noted that POC content is richer at the river-aquifer interface and declines with depth. Our model, however, simplified the spatial distribution of POC by assuming uniform distribution throughout aquifer. The biomass of the functional microbial groups (X_{AR}, X_{NT}, and X_{DN}) were also set as constants and were implicitly

included as lumped parameters in the model because they are products of their respective uptake rates (V_{AR}, V_{NT}, and V_{DN}) [*Gu et al.*, 2007]. The partition coefficient for O_2 demand process (y_{O_2}) is calculated based on the known free energy yield between aerobic respiration and nitrification. In this case, y_{O_2} of O_2 in the system is used for the more energetic uptake reaction, i.e., aerobic respiration, such that the remaining O_2 ($1 - y_{O_2}$) is consumed by the less energetic uptake reaction, i.e., nitrification [*Zarnetske et al.*, 2012].

2.3.3 Quantifying nitrate removal efficiency

To quantify the amount of nitrate removal in the aquifer per unit river length, net denitrification rate is integrated over the 24 hour cycle and across the whole domain.

$$M_{DN} = \int_0^T \int_\Omega \theta R_{NO_3} d\Omega \, dT \tag{2.8}$$

where M_{DN} is the total mass of nitrate being removed from denitrification, Ω is the domain area, and T is the total simulation time (24 h).

The amount of nitrate being transported into the aquifer with flux per unit river length is calculated based on the inward boundary flux across the top boundary layer integrated across the river-aquifer interface over the whole cycle (24 h):

$$M_{in} = \int_0^T \int_l C_{0NO_3} F_{bnd} dl \tag{2.9}$$

where M_{in} is the total mass of nitrate that being transported into the aquifer, C_{0NO_3} is the initial concentration of nitrate in the river, F_{bnd} is the top boundary flux, and l is the total length of the top boundary layer.

Nitrate removal efficiency (N_{RE}) is quantified by the amount of nitrate being removed from the aquifer divided by the total nitrate that goes into the aquifer across the river-aquifer interface.

$$N_{RE} = \frac{M_{DN}}{M_{in}} \tag{2.10}$$

Nitrate removal efficiency ranges between 0 and 1 with a larger value indicating higher removal efficiency. The total nitrate that enters the aquifer is completely consumed in the RZ when N_{RE} equals one.

2.4 Results

2.4.1 Water flux across the seepage face: base case

To exemplify our simulation results, a baseline simulation (A=0.5 m, D_L=1 m and K=10 m/d) with imposed river stage and boundary flux was run (**Figure 5**). During the 24 h simulation, the boundary flux reflected the sinusoidal signal of the river stage. As river stage rose, water started infiltrating across the bank (negative value). As river stage dropped, water started flowing out of the aquifer (positive value). The infiltration flux reached its peak several hours before the river stage maximum, while the exfiltration flux reached its peak before river stage reached its minimum. This trend agrees with what *Musial et al.* [2016] found in a tidal freshwater zone adjacent to a creek. A maximum infiltration rate of 2.68×10^{-5} m^2/s and a maximum exfiltration rate of 1.97×10^{-5} m^2/s occurred during one cycle. This larger infiltration rate is caused by the filling of the upper unsaturated zone above the water table as river stage rises [*McCallum and Shanafield*, 2016] as the hydraulic gradient reaches its maximum.

2.4.2 Spatial and temporal distribution of flow, solutes and reaction rates: base case

The hydraulic gradient changed with river stage since the far-field groundwater table was kept constant. At river stage maximum (time at 6 h), flow was towards the aquifer with the largest Darcy velocity occurring at the river-aquifer interface (**Figure 6**). Then as river stage dropped below the mean groundwater table (time at 12 h), the hydraulic gradient direction reversed and water flowed towards the river. As river stage continued to drop, a seepage face developed along the bank reaching its maximum length at 18 h. As river stage recovered, the hydraulic gradient returned to its initial state.

All four species showed similar patterns of expansion and contraction in the RZ as river stage rose and fell (**Figure 6**(c)). Solute concentration hot spots occurred at the river-aquifer interface immediately below the water table and diminished with depth. There was, however, a considerable amount of solute left behind in the variably saturated zone above the water table as river's edge receded. At the minimum river stage (time at 18 h), the influx of solutes slowed while the majority of the solutes remained above the water table. Dissolved organic carbon penetrated the deepest into the aquifer because of its additional supply from the *in situ* dissolution of co-advected POC. The maximum DOC concentration in the aquifer reached 3.8 mg/L after the 24 h simulation. This fell within the range of 3.4-10.8 mg/L for the groundwater end members collected at our site [*Briody et al.*, 2016]. Nitrate penetrated slightly deeper than ammonium and DO since denitrification was suppressed when DO was present.

Nitrification occurred in the shallower zone where the river and aquifer interacted the most. The largest nitrification rate was found along the water-sediment interface across the river stage fluctuation range where oxygen and ammonium concentration were the highest. These nitrification hot spots were also dominated by short residence time. Moreover, the nitrification rate was limited by the relatively small concentration of ammonium (5×10^{-2} mg/L) entering the aquifer from the river compared to oxygen concentration (9 mg/L).

Denitrification occurred deeper within the aquifer and in the river bed where oxygen was depleted and residence time was generally long. The denitrification hot spots formed as a band surrounding the nitrification hot spots and thinned towards the middle of the river. The largest denitrification rate was found in the middle of the band and in general, denitrification rates were likely limited by short simulation times. As time increased from 0 to 24 h, the extent of the denitrification zone continued to grow along with its maximum reaction rate.

2.4.3 Effect of river fluctuation amplitude

Larger river amplitude greatly increased the amount of nitrate being removed; however, the N_{RE} decreased (**Table 2**). Amplitudes of 0.1 m, 0.3 m and 0.5 m were chosen to represent small, medium, and large fluctuations in the river that are similar to those observed at the study site. As amplitude increased from 0.1 to 0.5 m, the total nitrate being transported into the aquifer increased more than 5 times; however, the amount of nitrate being removed only increased about 2.5 times, causing N_{RE} to decrease from 12% to 5%. Larger river fluctuations deepened the penetration depth of

solutes and expanded the nitrification and denitrification zone both horizontally and vertically (**Figure 6**). The nitrification hot spots always occurred in the RZ adjacent to the bank between river stage maximum and minimum. The denitrification rate reached its peak at 24 h when oxygen was depleted but DOC concentrations remained high in the aquifer.

2.4.4 Effects of sediment hydraulic conductivity and dispersivity

Larger K significantly increased the total influx of nitrate and the amount of nitrate being reduced; however, N_{RE} decreased with K. By changing K from 10 m/d (fine sand) to 100 m/d (coarse sand) which are typical values for our site [*Sawyer et al.*, 2009], the total nitrate flux into the aquifer increased about six times while the amount of nitrate being reduced increased about three times (**Table 2**). As a result, N_{RE} decreased from 5% to 2.5% for K=10 m/d and K=100 m/d, respectively. Larger K also greatly increased the penetration depth of all solutes and the nitrification and denitrification rates (**Figure 7**). For K=10 m/d after 24 h, the hot spots of denitrification reached a maximum depth of 1.5 m to the middle of the aquifer, while for K=100 m/d after 24 h, they reached to a maximum depth of 3 m to the bottom of the aquifer. With DO being transported farther inland as K increased, denitrification occurred much farther into the banks and the hot spot band grew wider.

Large D_L had a minor influence on the amount of solutes transported into the aquifer, though the amount of nitrate being reduced slightly increased (**Table 2**). Longitudinal dispersivity was increased by a factor of two for each case from 0.5 m to 1 m and then to 2 m. Since river amplitude and K remained unchanged, D_L only changed

nitrate concentrations due to dispersive influences while the amount of nitrate being transported into the aquifer through the upper interface due to advection was approximately the same. Therefore, the N_{RE} increased from 4.0% to 7.5 % with increasing D_L. The denitrification hot spots moved deeper into the aquifer with larger dispersivity due to nitrate reaching deeper into the anoxic zone (**Figure 8**).

2.4.5 Effects of ambient river-groundwater interaction: losing vs. gaining condition

A losing river showed the smallest N_{RE} (3.5%) even though the influx of nitrate into the aquifer was the largest. In contrast, a gaining river showed the largest N_{RE} (17.1%) with only a small fraction of solutes able to penetrate into the aquifer (**Figure 9**). This was because the amount of nitrate being transported into the aquifer under losing conditions was eight times higher while the amount of nitrate being reduced was only about two times higher than that under gaining condition. Similarly, gaining conditions were three times more efficient in removing nitrate through BS compared to neutral river conditions. All solutes penetrated much deeper into the aquifer with denitrification hot spots located farther and deeper and were wider under losing conditions. Though the groundwater flow direction was mostly towards the river under gaining conditions, a narrow denitrification hot spot band was formed at 1 m depth adjacent to the water-sediment interface due to solute dispersion.

2.5 Discussion

2.5.1 Other factors that influence nitrate removal efficiency (N_{RE})

Admittedly, our sensitivity analysis was not exhaustive. Other hydrological and biogeochemical factors such as stream temperature, availability and ratio of nutrients,

sediment heterogeneity and residence times were not considered here but could potentially impact nitrogen cycling and thus N_{RE}.

Microbially-mediated biogeochemical reactions are sensitive to ambient temperature. *Zheng et al*. [2016] suggested that nitrate removal (or production) efficiency might be higher during warmer daytime temperatures when compared to colder nighttime temperatures. In the same study, the authors also found that whether the RZ functioned as nitrate source or sink was highly dependent on the ratio of $[NO_3]/[NH_4]$ in stream water. The RZ functioned as a nitrate sink at higher ratios and as a nitrate source at lower ratios. In our simulations, the $[NO_3]/[NH_4]$ ratio was high, resulting in negligible nitrification in the RZ. Therefore, the RZ functioned as nitrate sink in all our simulations.

The availability of nutrients such as labile DOC limits denitrification along hyporheic pathways [*Zarnetske et al.*, 2011b]. The addition of labile DOC strongly increased the amount of nitrate being removed because it stimulates aerobic respiration that consumes DO, creating anaerobic conditions for denitrification. In addition, the elevated DOC provides a carbon substrate supply that increases the denitrification rate. In our simulations, additional DOC came from *in situ* POC dissolution which led to increased DOC concentration in the aquifer over time and ensured denitrification was not DOC-limited. However, a maximum DOC concentration was set to 10.8 mg/L according to our field data [*Briody et al.*, 2016]. The content of POC also controls nitrate removal rate. *Knights et al.* [2017] showed that denitrification rate was greater with higher POC content in the sediments.

Heterogeneous sediment permeability has also been shown to influence hyporheic exchange [*Sawyer and Cardenas*, 2009] and results in more efficient in nitrate removal in upwelling groundwater [*Sawyer*, 2015]. However, a recent study by *Bardini et al.* [2013] showed that sediment heterogeneity at the bed form scale did not affect river bed nitrate source/sink function. This is because the reactions are controlled by the residence time which can be similar for both heterogeneous and homogeneous cases under steady flow.

For a transient flow situation, both residence and reaction time scales of water and solute are important. *Zarnetske et al.* [2012] demonstrated that the residence time of water and solutes in the RZ and the uptake rate of O_2 determines whether the RZ is nitrate source or sink. In general, nitrification rate is the greatest during short residence time, while denitrification rate is the greatest at long residence time [*Zarnetske et al.*, 2011a]. Our study shows that net nitrate production is dominant in shallower zones adjacent to the bank with shorter residence time, while net nitrate consumption occurs deeper in the aquifer or below the riverbed due to longer residence times. Across the whole domain, however, the RZ is a net nitrate consumption zone or nitrate sink for the river. A dimensionless Damkohler number (*Da*) for O_2, the ratio of residence time scales to O_2 reaction time scales or the ratio of O_2 uptake rates to transport rates, is used to indicate whether the RZ is a nitrate source (Da«1) or nitrate sink (Da»1) [*Zarnetske et al.*, 2012]. In general, our model produces *Da* much greater than 1, which indicates a nitrate sink for RZ. By assuming a constant oxygen uptake rate, increasing transport rates (for example, groundwater velocity increases with higher river amplitude and/or

larger sediment hydraulic conductivity) that contribute higher nitrate load to the RZ would decrease Da, and thus result in lower N_{RE}. Similarly, in a losing river condition where river discharge rates and nitrate fluxes are greater, N_{RE} is lower than in a gaining river condition. This is consistent with *Sawyer* [2015] that higher nitrate load often results in lower N_{RE}.

2.5.2 Limitations and future work of our study

Our model revealed the effect of river fluctuation induced exchange with the RZ and the controlling factors on N_{RE}. However, our model has the following key limitations. (1) Our model was two-dimensional, thus it ignored the third dimension such as bedforms [*Cardenas and Wilson*, 2007; *Bardini et al.*, 2012] and point bars [*Cardenas*, 2009] which could induce significant solute exchange and thus denitrification. *Zheng et al.* [2016] calculated N_{RE} in bed form-induced hyporheic exchange ranging from 42.4% to 49.9% for a polluted stream under varying aquifer temperature. (2) Only one single pulse cycle was simulated, although multiple river fluctuation cycles would be more realistic. Under the conditions described in our modeling, longer simulation period would greatly increase solute residence times and thus the removal of nitrate from the river, however nitrate removal would also vary as a function of the reoccurrence of the storage and release cycle. (3) A homogeneous aquifer permeability field was assumed. Sediment heterogeneity may have the effect of creating spatially differing localized biogeochemical reaction hot spots. *Briggs et al.* [2015] demonstrated how anoxic microzones could develop in less mobile pores of bulk-oxic hyporheic zones as a result of pore-scale heterogeneity. (4) Constant solute

concentration was assumed for the river. Rivers usually exhibit changing chemical and nutrient concentrations during high flows and low flows [*Sawyer et al.*, 2009; *Briody et al.*, 2016]. (5) Groundwater-borne nutrients were not considered. *Knights et al.* [2017] showed that riverbed sediments had the potential to remove more than 80% of the groundwater-borne nitrate load to the tidal freshwater zone of the White Clay Creek. In our study site, however, groundwater-borne nitrate is relatively low (3 mg/L) compared to river (20 mg/L) [*Briody et al.*, 2016]. Thus it is reasonable to assign zero nitrate concentration for the aquifer. In addition, to address the impact of ambient aquifer DOC concentrations, the model was run without POC dissolution. This resulted in a 3.2 % reduction in N_{RE}. Clearly the results presented in this paper are sensitive to reactive solute concentrations within the river and the aquifer, however a full sensitivity analysis covering the natural range of solute concentrations was beyond the scope of this study. Varying concentration of different species in the river over time as well as the lag time between peak river stage and concentration peaks should be investigated in the future. All of the above factors are worth investigating; however, they would further complicate our interpretation of the role of BS on nitrate cycling in the RZ. The numerical experiments in this study were designed to focus on the parameters we systematically varied.

2.5.3 Implication of fluctuating rivers in removing nitrate

Our results show that river fluctuations induced by dam operations have the potential to remove significant nitrate from the riverine system, which might alleviate the nitrate load downstream. This agrees with the "lung" model proposed by *Sawyer et*

al. [2009], which postulates that the mixing of river water and groundwater as a result of frequent river fluctuations greatly enhance the biogeochemical activity in the subsurface compared to a baseflow dominated river. For example, a neutral river with 0.5 m amplitude can remove nitrate up to 4.2 g/d per meter of river length, which translates to 378 kg/d for a 90 km river reach including the opposing bank. More importantly, N_{RE} would increase as water residence times in the subsurface increases. With a 7-day total timespan of daily fluctuation cycles for the same model, the N_{RE} increased from 5.4% to 22% in the RZ (results not shown). This suggests that regular dam releases and the associated increases in residence times in the RZ can be beneficial to the ecology of river in terms of buffering nitrogen loads.

Similar to dam regulations, tidal pumping induced frequent river fluctuations could mitigate nitrate loads to the coast. For example, *Knights et al.* [2017] used a modeling approach to investigate the effect of tidal pumping on riverbed denitrification along a tidal freshwater zone in White Clay Creek (Delaware). They found that riverbed sediments were only able to remove 4% of the riverine nitrate within the tidal freshwater zone that discharged to the coast over a day. However, these findings are limited because they used a simple 1-D model which ignores the bank storage effect on removing nitrate. By comparison, our 2-D simulations showed localized denitrification hot spots within the RZ deep into the bank as well as below the river sediments. Therefore, our model could be applied to any riverine systems with a dynamic flow.

2.6 Conclusions

We developed a 2D coupled unsaturated transient flow and biogeochemical model to investigate the fate of nitrogen through bank storage induced by regular and relatively short-lived river stage fluctuations, such as by dam release-and-storage cycles, within a riparian zone. Using a suite of models, we analyzed the effects of river fluctuation amplitude, sediment hydraulic conductivity and dispersivity, and the ambient groundwater flow on the spatial and temporal distribution of solutes, reaction rates, and on integrated nitrate removal efficiency. To our knowledge, this is the first study to illustrate the role of bank storage induced by periodic river fluctuations on nitrification and denitrification within a riparian zone. Our results showed that nitrification occurred in the shallower zone adjacent to the bank where oxic river water and groundwater interacted, while denitrification occurred deeper into the aquifer and below the riverbed where oxygen was depleted. River fluctuations greatly increased the amount of nitrate being removed; however, the removal efficiency decreased as river amplitude increased. Similarly, larger hydraulic conductivity induced larger influx of nitrate and the amount of nitrate being reduced; however, nitrate removal efficiency decreased with hydraulic conductivity. In contrast, increasing sediment dispersivity had a minor influence on the amount of solutes transported into the aquifer, though the amount of nitrate being reduced slightly increased. Additionally, the presence and direction of ambient groundwater flow had a significant impact on nitrate removal efficiency. A losing river showed the smallest nitrate removal efficiency (3.5%) even though the influx of nitrate into the aquifer was the largest. In contrast, a gaining river showed the largest nitrate

removal efficiency (17.1%) with only a small fraction of solutes able to penetrate into the aquifer. These results demonstrate that dam-induced river fluctuations increased the cycling of nitrate through exchange between the river and riparian aquifer. However, nitrate removal efficiency is sensitive to river fluctuation amplitude and sediment hydraulic conductivity, and ambient groundwater flow, and to a lesser extent sediment dispersivity. Among those factors, nitrate removal efficiency was more sensitive to river amplitude and ambient groundwater flow. Management of regulated rivers can thus benefit from consideration of the factors analyzed here if part of the management goals includes nutrient fate and loading.

Acknowledgments

This research was funded by the National Science Foundation (EAR-1344547 and EAR-1343861). Thanks to Kevin Anderson at Austin Water- Center for Environmental Research for logistical support and access to the field site.

Table 1. Summary of parameters used in the flow (upper section) and reactive transport model (lower section)

Parameter	Value	Unit	Reference
Flow parameters			
Hydraulic conductivity (K)	1~100	m/d	[*Sawyer et al.*, 2009]
Porosity	0.3		
Longitudinal Dispersivity (D_L)	0.5~2	m	
Residual water content (θ_r)	0.1		
van Genuchten (α)	10	1/m	
van Genuchten (n)	2		
Period (T)	24	h	[*Sawyer et al.*, 2009]
Amplitude (A)	0.1~0.5	m	[*Sawyer et al.*, 2009; *Briody et al.*, 2016]
Solute and biogeochemical parameters			
O_2 concentration in the river	9	mg/L	[*LCRA*, 2014]
DOC concentration in the river	6	mg/L	[*Briody et al.*, 2016]
NO_3 concentration in the river	20	mg/L	[*Briody et al.*, 2016]

Table 1 Continued

Parameter	Value	Unit	Reference
NH_4 concentration in the river	0.05	mg/L	[*LCRA*, 2014]
Oxygen inhibition constant (K_i)	1	mg/L	[*Gu et al.*, 2012]
Mass transfer coefficient (α)	5×10^{-5}	1/h	[*Gu et al.*, 2007]
Distribution coefficient of DOC (K_d)	50	L/kg	[*Gu et al.*, 2007]
Maximum specific uptake rate for AR (V_{AR})	2	1/h	[*Zarnetske et al.*, 2012]
Maximum specific uptake rate for NT (V_{NT})	1	1/h	[*Zarnetske et al.*, 2012]
Maximum specific uptake rate for DN (V_{DN})	4	1/h	[*Zarnetske et al.*, 2012]
Half saturation constant for O_2 (K_{O2})	1	mg/L	[*Gu et al.*, 2012]
Half saturation constant for DOC (K_{DOC})	2	mg/L	[*Gu et al.*, 2012]
Half saturation constant for NO_3 (K_{NO3})	1	mg/L	[*Gu et al.*, 2012]
Half saturation constant for NH_4 (K_{NH4})	0.5	mg/L	[*Zarnetske et al.*, 2012]

Table 1 Continued

Parameter	Value	Unit	Reference
Partition coefficient for O2 (y_{O2})	0.64		[*Zarnetske et al.*, 2012]

Table 2. Summary of simulation results for all scenarios

Scenario	**A (m)**	**D_L (m)**	**K (m/d)**	**M_{DN} (g)**	**M_{in} (g)**	**N_{RE} [%]**
Gaining	0.5	1	10	0.5	3.2	17.1
Neutral	0.5	1	10	0.7	13.4	5.4
Losing	0.5	1	10	0.9	26.3	3.5
Neutral	*0.1*	1	10	0.3	2.4	12.0
Neutral	*0.3*	1	10	0.6	8.1	7.0
Neutral	*0.5*	1	10	0.7	13.4	5.4
Neutral	0.5	*0.5*	10	0.5	13.6	4.0
Neutral	0.5	*1*	10	0.7	13.4	5.4
Neutral	0.5	*2*	10	1.0	13.6	7.5
Neutral	0.5	1	*10*	0.7	13.4	5.4
Neutral	0.5	1	*50*	1.5	43.7	3.4
Neutral	0.5	1	*100*	2.1	82.5	2.5

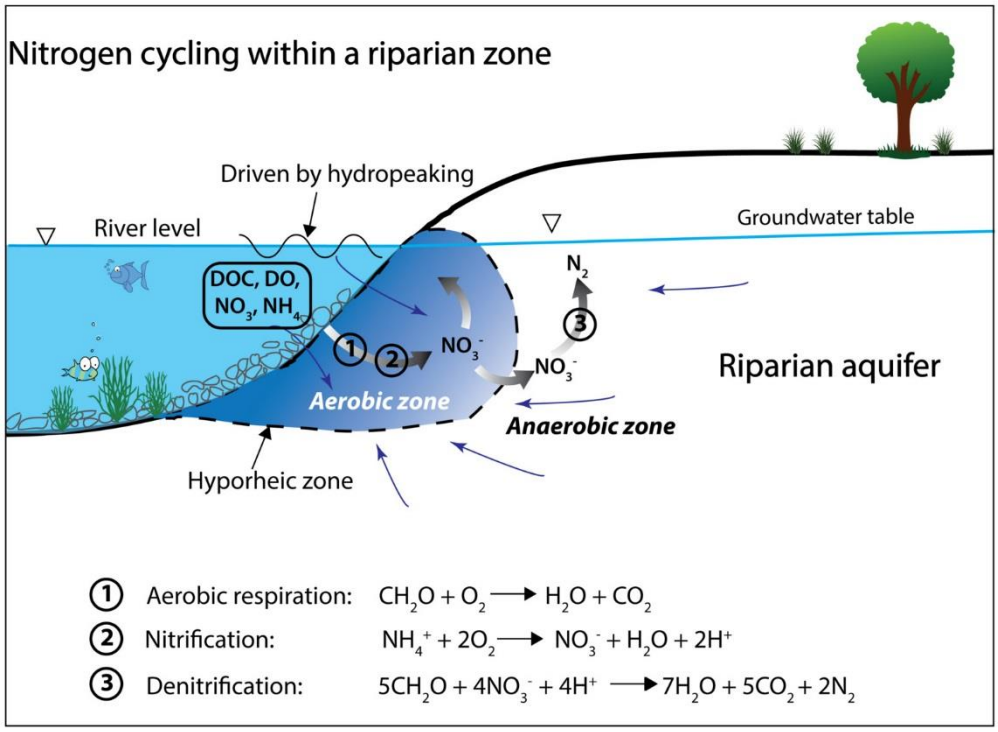

Figure 3. Simplified nitrogen cycling pathways within a riparian zone. River fluctuations are driven by dam release or "hydropeaking", resulting in a dynamic aerobic zone where aerobic respiration and nitrification occur. Dissolved oxygen reacts with ammonium via nitrification, producing additional nitrate. As nitrate goes deeper into the anaerobic zone, denitrification occurs which releases nitrogen gas into the atmosphere. Blue arrows indicate transient flow directions.

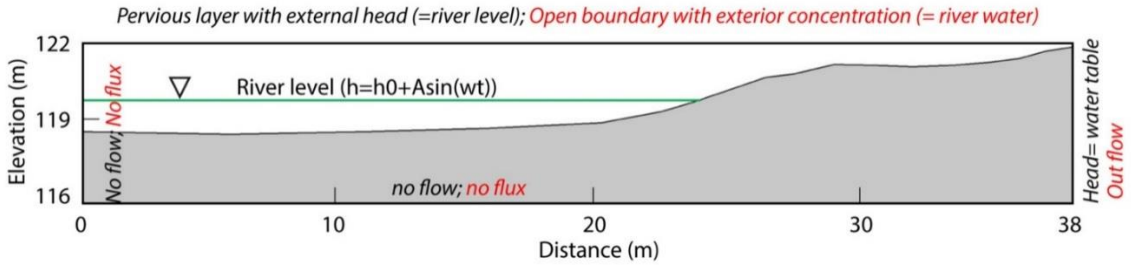

Figure 4. Model geometry and boundary configurations for flow (black italic) and solute transport (red italic). River stage (green) is simplified as a sine wave.

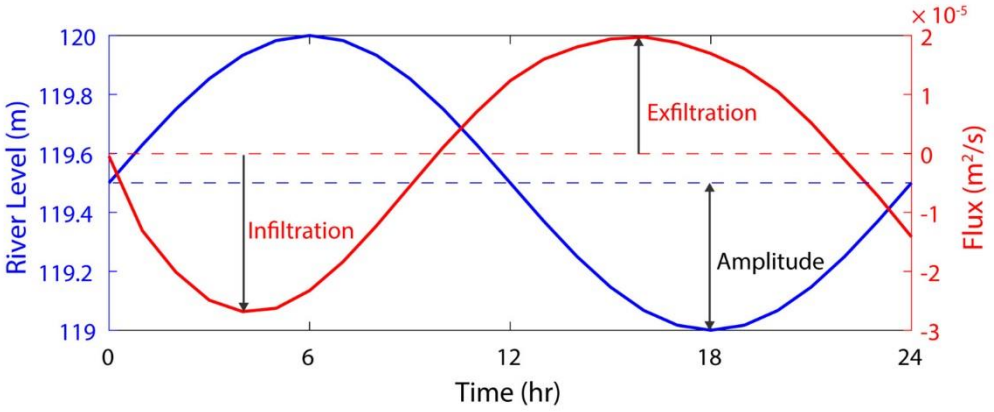

Figure 5. River stage fluctuation during a 24-hour cycle with an amplitude of 0.5 m (solid blue line) and integrated flux across the top boundary (solid red line). Positive values denote groundwater discharge into the river (exfiltration) and negative values indicate river water recharge to the bank (infiltration). Average river stage and zero flux are indicated by the dashed blue and red lines, respectively.

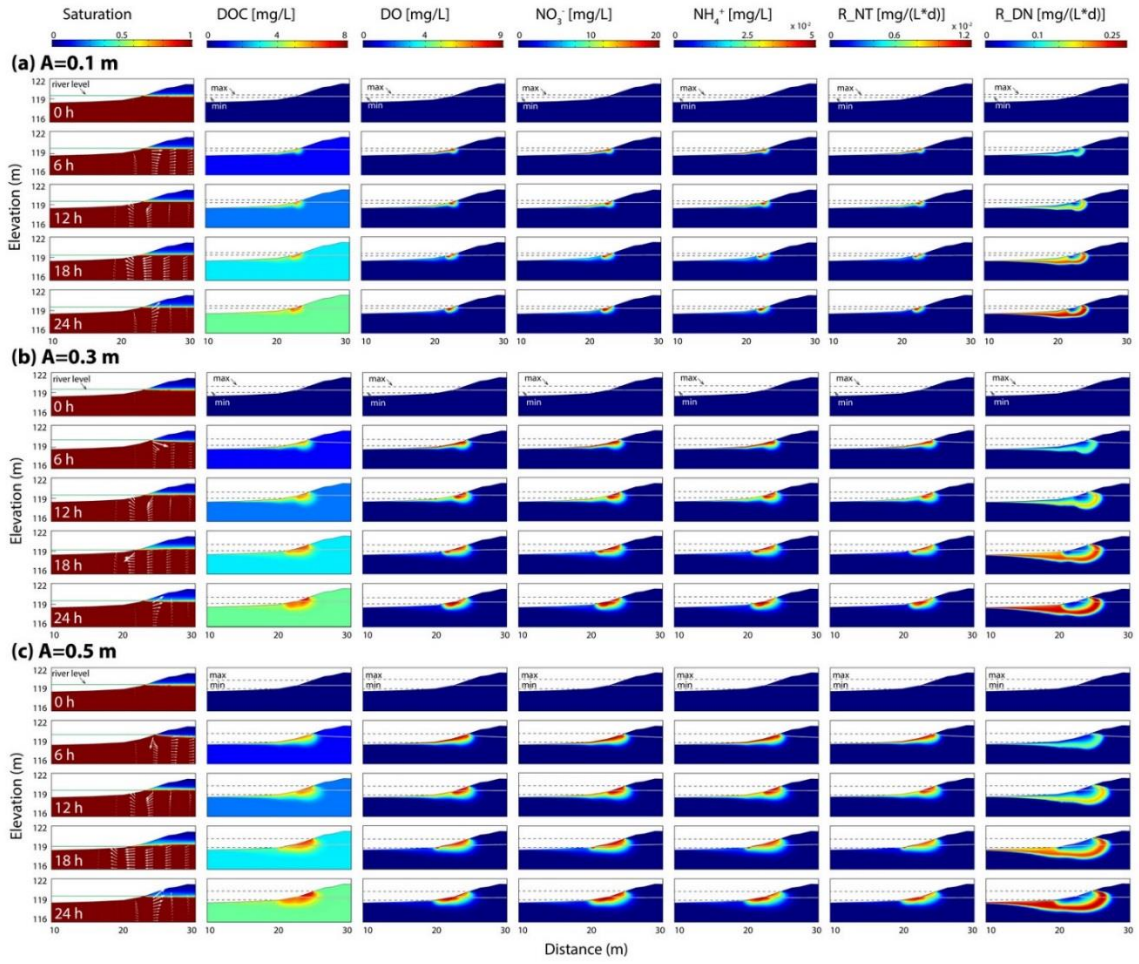

Figure 6. 2D snapshots of simulated water saturation, solute concentration (DOC, DO, NO_3^- and NH_4^+) and reaction rates under neutral conditions over a 24 hour period given (a) A=0.1 m, (b) A=0.3 m, (c) A=0.5 m. The green line outside the domain indicates river stage. The dashed line delineates the maximum and minimum river stage. The gray line inside the domain shows the groundwater table and white arrows indicate the direction of groundwater flow.

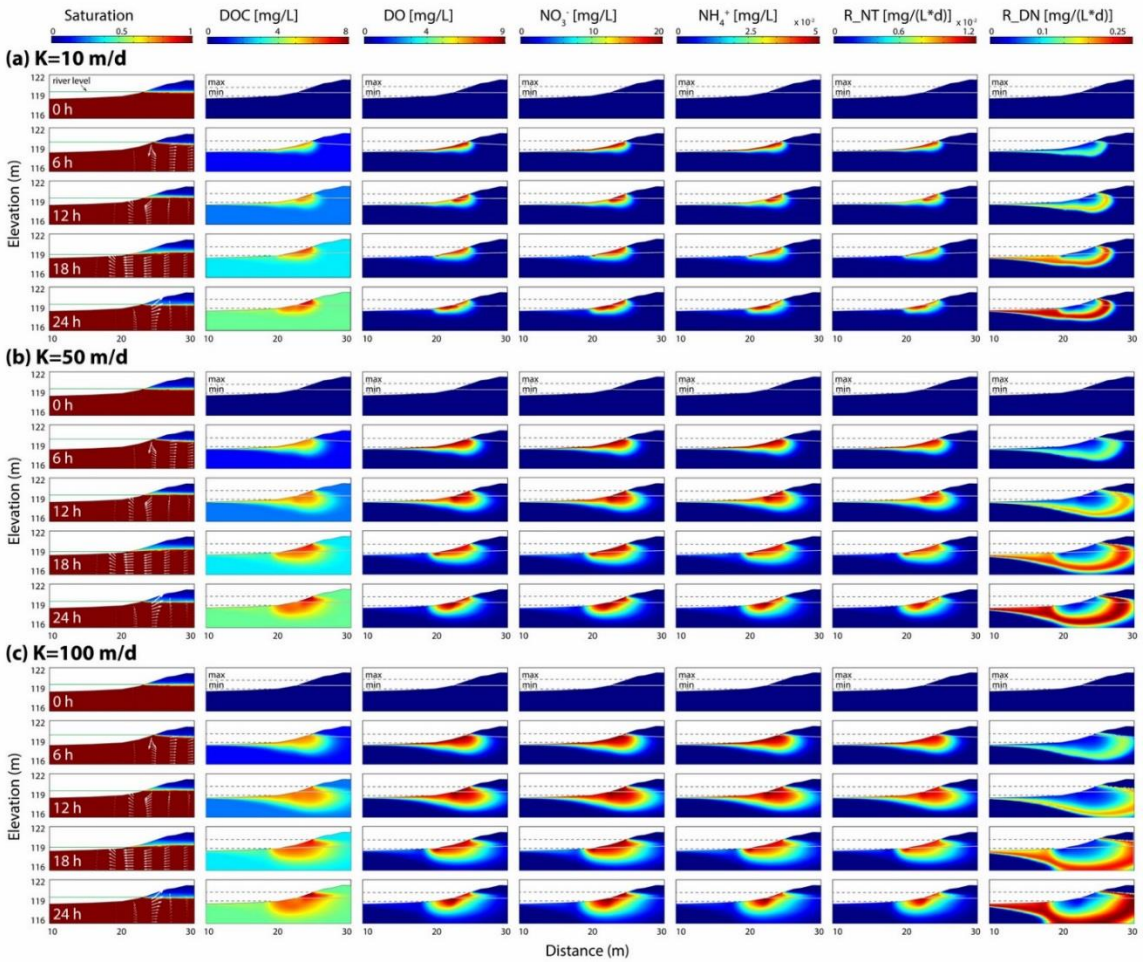

Figure 7. 2D snapshots of simulated water saturation, solute concentration (DOC, DO, NO_3^- and NH_4^+) and reaction rates under neutral conditions over a 24 hour period given (a) K=10 m/d, (b) K=50 m/d, (c) K=100 m/d. The green line outside the domain indicates river stage. The dashed line delineates the maximum and minimum river stage. The gray line inside the domain shows the groundwater table and white arrows indicate the direction of groundwater flow.

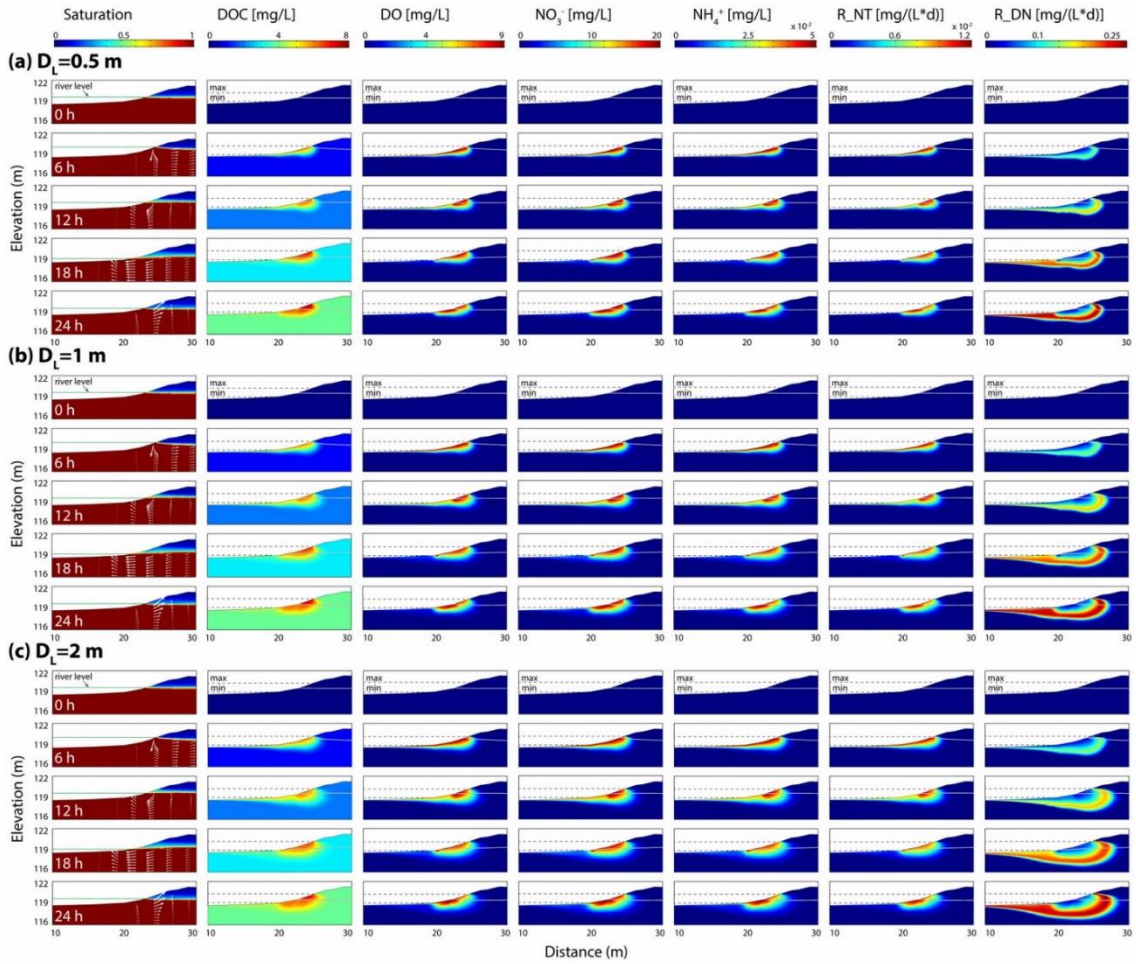

Figure 8. 2D snapshots of simulated water saturation, solute concentration (DOC, DO, NO_3^- and NH_4^+) and reaction rates under neutral conditions over a 24 hour period given (a) D_L=0.5 m (b) D_L =1 m, (c) D_L =2 m. The green line outside the domain indicates river stage. The dashed line delineates the maximum and minimum river stage. The gray line inside the domain shows the groundwater table and white arrows indicate the direction of groundwater flow.

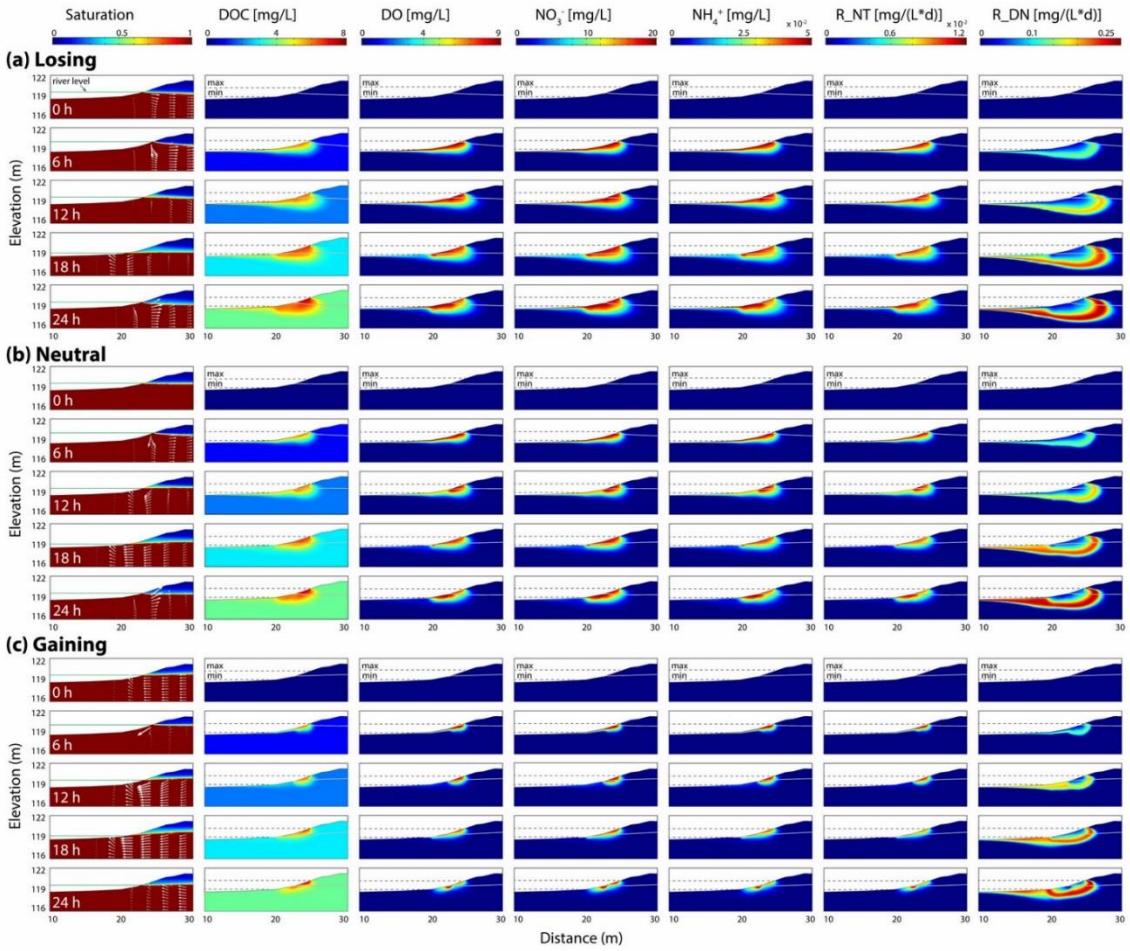

Figure 9. 2D snapshots of simulated water saturation, solute concentration (DOC, DO, NO_3^- and NH_4^+) and reaction rates under (a) Losing, (b) Neutral, (c) Gaining conditions over a 24 hour period. The green line outside the domain indicates river stage. The dashed line delineates the maximum and minimum range of river stage. The gray line inside the domain shows the groundwater table and white arrows indicate the direction of groundwater flow.

CHAPTER III

THE IMPACT OF THE DEGREE OF AQUIFER CONFINEMENT AND ANISOTROPY ON TIDAL PULSE PROPAGATION[*]

3.1 Summary

Oceanic tidal fluctuations which propagate long distances up coastal rivers can be exploited to constrain hydraulic properties of riverbank aquifers. These estimates, however, may be sensitive to degree of aquifer confinement and aquifer anisotropy. We analyzed the hydraulic properties of a tidally influenced aquifer along the Meghna River in Bangladesh using: 1) slug tests combined with drilling logs and surface resistivity to estimate Transmissivity (T); 2) a pumping test to estimate T and Storativity (S) and thus Aquifer Diffusivity (D_{PT}); and 3) the observed reduction in the amplitude and velocity of a tidal pulse to calculate D using the Jacob-Ferris analytical solution. Average Hydraulic Conductivity (K) and T estimated with slug tests and borehole lithology were 27.3 m/d and 564 m^2/d, respectively. Values of T and S determined from the pumping test ranged from 400 to 500 m^2/d and 1-5 × 10^{-4}, respectively with D_{PT} ranging from 9-40 × 10^5 m^2/d. In contrast, D estimated from the Jacob-Ferris model ranged from 0.5-9 × 10^4 m^2/d. We hypothesized this error resulted from deviations of the real aquifer conditions from those assumed by the Jacob-Ferris model. Tidal pulses were simulated across a

[*] Reprinted with permission from "The Impact of the Degree of Aquifer Confinement and Anisotropy on Tidal Pulse Propagation" by Shuai, P., P. S. K. Knappett, S. Hossain, A. Hosain, K. Rhodes, K. M. Ahmed, and M. B. Cardenas (2017b), *Groundwater*, doi:10.1111/gwat.12509.

range of conditions and D was calculated with the Jacob-Ferris model. This sensitivity analysis demonstrated that moderately confined ($K_{top}/K_{aquifer} < 0.01$) or anisotropic aquifers ($K_x/K_z > 10$) yielded D within a factor of 2 of the actual value. The order of magnitude difference in D between pumping test and Jacob-Ferris model at our site argues for little confinement or anisotropy.

3.2 Introduction

Characterizing aquifer hydraulic properties is important to managing groundwater resources including modeling the movement and transformation of contaminants and nutrients between rivers and aquifers. Aquifer hydraulic properties can be characterized at different scales. In order from small to large scale, these methods include grain size analyses [*Hazen*, 1911], slug tests [*Butler*, 1997] and pumping tests [*Fetter*, 2000]. Large scale (>100 m) estimates of Aquifer Diffusivity (D) can further be made using tidal methods when an aquifer is bordered by an oscillating surface water body. Aquifer Diffusivity (D) can be calculated using the observed time lag and amplitude attenuation of a tidal pulse with distance into the aquifer. Since D is equal to the ratio of Transmissivity (T) to Storativity (S) (T/S), it can be used to constrain the value of S when T can be estimated using less intrusive slug tests combined with observed lithology. This may be desirable in contaminated aquifers where a pumping test would produce a large volume of water that would need to be treated or where pumping could cause salt water intrusion. In a confined aquifer T is equal to Hydraulic Conductivity (K) multiplied by Aquifer Thickness (b), and S is equal to Specific Storage (S_s) multiplied by b. Therefore D also equals K/S_s. In tidal methods D is calculated by

analyzing the diffusive wave propagation of a tidal pulse into aquifers bounded by rivers, large lakes and oceans. Aquifer parameters (T, K, S, S_s) can be used to model the volumetric flux of water between river and aquifer under dynamically changing river stages and hydraulic gradients. The objective of this study is to compare the values of D and its components (T, S) estimated with pumping tests to D measured with a widely used 1D analytical model, explain the source of the discrepancy, and recommend optimal settings where the 1D analytical model or one of its similar derivations should be used.

Tidal methods are particularly useful in deltas and coastal rivers where ocean tides cause river stage fluctuations hundreds of kilometers inland [*Musial et al.*, 2016]. Shallow aquifers within the Ganges-Brahmaputra-Meghna (GBM) delta are widely contaminated with toxic concentrations of arsenic (As) [*Fendorf et al.*, 2010]. Here, under gaining stream conditions aquifer hydraulic properties likely control the rate of accumulation of arsenic (As) within near-river (<5 m) sediments [*Datta et al.*, 2009; *Jung et al.*, 2012, 2015]. Hydraulic properties may also determine how fast As is released from freshly deposited river sediments and moves into an aquifer under the influence of urban pumping causing localized losing stream conditions in the river [*Stahl et al.*, 2016]. Finally, aqueous-phase concentrations of As have been found to oscillate seasonally in riverbank aquifers with monsoonal climates [*Xie et al.*, 2015; *Schaefer et al.*, 2016]. Therefore, to accurately predict the volumetric and mass fluxes of water and dissolved metals within a riverbank aquifer, novel approaches are needed to accurately characterize the hydraulic properties of riverbank aquifers.

There are numerous analytical solutions describing water table fluctuations in response to tidal forcing in a neighboring surface water body. These were derived for confined aquifers [*Jacob*, 1950; *Ferris*, 1951; *Van, der Kamp*, 1972; *Song et al.*, 2007; *Rotzoll and El-Kadi*, 2008; *Guo et al.*, 2010], leaky confined aquifers [*Jiao and Tang*, 1999; *Jeng et al.*, 2002; *Chuang and Yeh*, 2007, 2008, 2011; *Xia et al.*, 2007; *Sun et al.*, 2008; *Chuang et al.*, 2010], and unconfined aquifers [*Li et al.*, 2000; *Teo et al.*, 2003; *Song et al.*, 2007; *Chang et al.*, 2010; *Yeh et al.*, 2010]. Although multi-dimensional sophisticated analytical solutions exist for complex aquifers, a simple one dimensional (1D) Jacob-Ferris model assuming a semi-infinite, homogeneous, isotropic and confined aquifer with a vertical bank submitted to sinusoidal wave variation has been widely used for estimating D [*Erskine*, 1991; *Millham and Howes*, 1995; *Trefry and Johnston*, 1998; *Schultz and Ruppel*, 2002; *Jha et al.*, 2003; *Trefry and Bekele*, 2004; *Rotzoll et al.*, 2008, 2013; *Zhou*, 2008]. The following equations have been modified to calculate diffusivity using either amplitude attenuation (D_{AAM}) or time lag (D_{TLM}) following the Jacob-Ferris approach:

Governing equation:

$$\frac{\partial^2 h}{\partial^2 x} = \frac{S}{T}\frac{\partial h}{\partial t} \quad \left(h = h_0 \sin\left(\frac{2\pi t}{t_0}\right) at\ x = 0\ and\ h = 0\ at\ x = \infty\right) \tag{3.1}$$

1D simple solution:

$$h = h_0 e^{-x\sqrt{\left(\frac{\pi S}{t_0 T}\right)}} \sin\left(\frac{2\pi t}{t_0} - x\sqrt{\left(\frac{\pi S}{t_0 T}\right)}\right) \tag{3.2}$$

Amplitude attenuation method (AAM):

$$D_{AAM} = \frac{T}{S} = \left(\frac{x}{\ln\left(\frac{h}{h_0}\right)}\right)^2 \frac{\pi}{t_0} \tag{3.3}$$

Time lag method (TLM):

$$D_{TLM} = \frac{T}{S} = (\frac{x}{t_L})^2 \frac{t_0}{4\pi} \quad (3.4)$$

where x is the distance from monitoring well to shoreline, h is the diffusive wave amplitude observed at the monitoring well, h_0 is wave amplitude in the river or surface water body, t_0 is wave period, t_L is time lag.

Previous studies have applied the above simple 1D expressions (Equation (3.3) and (4)) to estimate D for coastal aquifers [*Schultz and Ruppel*, 2002; *Zhou*, 2008], riverbank aquifers [*Trefry and Johnston*, 1998], island aquifers [*Trefry and Bekele*, 2004; *Rotzoll and El-Kadi*, 2008] and atoll aquifers [*Chattopadhyay et al.*, 2015]. To further constrain T and S (or K and S_s), independent measurements including slug tests and pumping tests are often conducted in conjunction with tidal methods [*Erskine*, 1991; *Millham and Howes*, 1995; *Trefry and Johnston*, 1998]. Erskine [1991] estimated S using both D_{AAM} and D_{TLM} after measuring T using a pumping test within an unconfined, coastal aquifer. Millham and Howes [1995] estimated K using D_{TLM} and S from reported pumping tests within a shallow, highly permeable costal unconfined aquifer. Similarly, Trefry and Johnston [1998] obtained K by combining pumping tests analysis and the Jacob-Ferris model within a shallow, sandy riverbank unconfined aquifer.

Few studies have directly compared D obtained from pumping tests (D_{PT}) with D estimated from tidal methods (D_{TLM} or D_{AAM}) to verify aquifer properties and validate the 1D Jacob-Ferris model in the specific aquifer under study. Pumping tests and analytical tidal methods, such as the Jacob-Ferris 1D model, provide independent and

complimentary information on aquifer properties across a scale on the order of tens to hundreds of meters. Both methods yield independent estimates for D and therefore pumping tests can empirically validate the Jacob-Ferris model.

Although the 1D Jacob-Ferris model is promising because of its ease of application, large discrepancies frequently emerge between D estimated from observed time lag and decreased amplitude of the pulse with distance. For example, Erskine (1991) found that D_{TLM} was approximately one order of magnitude larger than D_{AAM} in an unconfined, coastal aquifer. Accordingly, when they estimated S (using T from a pumping test) from D_{AAM} they found that S_{AAM} was an order of magnitude larger than S_{TLM}. Similarly, Jha et al. (2008) found D_{TLM} was consistently larger than D_{AAM} in both unconfined and confined aquifers.

In contrast, other studies found larger D_{AAM} values than D_{TLM}. Working in an unconfined aquifer Schultz and Ruppel (2002) found that D_{AAM} was 16 times larger than D_{TLM}. Accordingly their estimate of T derived using D_{AAM} (T_{AAM}) was also 16 times larger than that estimated using D_{TLM} (T_{TLM}). These inconsistencies in D_{AAM} and D_{TLM} may be explained by the presence of a phreatic surface. As to whether D_{AAM} or D_{TLM} is more reliable, conventional methods like pumping tests and slug tests may provide useful constraints. Schultz and Ruppel (2002) found that values of K derived from D_{AAM} assuming S and b were more consistent with estimates from grain size distribution, slug tests and pumping tests than values of K derived with D_{TLM}. To quantify the differences between D_{AAM} and D_{TLM}, a slope factor is used where [*Trefry and Bekele*, 2004]:

$$Slope\ Factor = \sqrt{\frac{D_{AAM}}{D_{TLM}}} \tag{3.5}$$

This is a measure of the internal inconsistency of a 1D tidal pulse propagation model. A slope factor of close to one suggests the tidal pulse propagation through the aquifer is described well by the Jacob-Ferris model.

The objective of this study is to compare the values of D and its components (T, S) estimated with pumping tests and the Jacob-Ferris tidal pulse propagation model, explain the source of the discrepancy, and determine optimal settings where the 1D analytical model or one of its similar derivations should be used. This was accomplished by measuring T, using slug tests and borehole data, and measuring T and S using a pumping test. From these D_{PT} could be calculated and compared to D obtained from the 1D Jacob-Ferris tidal pulse model. The value of T obtained from the slug test and borehole lithology was used to confirm the value of T obtained with the pumping test. We hypothesized the error in D was caused by multi-dimensional factors (i.e. aquifer geometry, aquifer anisotropy and heterogeneity) not included in the 1D model. Thus, we tested the sensitivity of D_{AAM}, D_{TLM} and Slope Factor to aquifer geometry (sloping banks), aquifer anisotropy, and aquifer heterogeneity.

3.3 Study Site

The Meghna River is one of three major rivers forming the GBM delta. The river stage fluctuates with 12 hour (semi-diurnal) and 14 day (neap-spring) periods driven by ocean tides in the Bay of Bengal which propagate 200 km north to the field site. The river also fluctuates seasonally peaking (~7 masl) during the late monsoon (August-October) and falling to its nadir (~3 masl) during the dry season (November-April).

Much of the land surface across the delta is flooded during the late monsoon [*Steckler et al.*, 2010].

The aquifers of the GBM delta are composed of sandy unconsolidated Pleistocene to Holocene fluvial and deltaic sediments. Holocene aquifer pore waters contain elevated As whereas the pore waters of deeper older Pleistocene aquifers contain little As [*Fendorf et al.*, 2010]. Our study site (Veast) is located on the eastern bank of the Meghna River (Figure 10). To investigate the extent of surface water intrusion into the riparian aquifer, a monitoring well transect consisting of six 15 m deep wells (T1-T6) was installed orthogonal to the eastern bank, spaced 15 m apart (Figure 11). An irrigation well was located at the end of the transect furthest from the river. One additional shallow well (T6a) with a depth of 7 m was installed next to T6 directly adjacent to the shoreline of the river during the dry season. During the monsoon the river rises to inundate several of the wells closest to the river. The river stage was measured using a gage located 3 km south of the well transect. Approximately 4 m of silt lie on top of the aquifer at the end of the transect furthest away from the river (T1), and thins to less than 0.3 m near the shoreline (T6). The hydraulic conductivity of this layer was estimated using a drive point piezometer (DP2a) installed along the riverbank to 1 m depth next to well T6 (Figure 11). Underneath this silt layer lies a 25 m thick layer of fine, grey, sand of Holocene age. The average concentration of As in this shallow aquifer is 350 μg/L. This shallow aquifer is underlain by a laterally continuous 7 m thick clay layer. Underlying this clay layer is a low-As (<10 μg/L), red-brown sand (Pleistocene) aquifer.

3.4 Methodology

3.4.1 Borehole Lithology and Well Installation

Monitoring wells were installed using the traditional hand flapper method which is a reverse circulation percussion drilling method that produces high quality lithology [*Horneman et al.*, 2004]. Sediments were logged every 30 cm and the relative quantities of clay, silt and sand were recorded by visual inspection.

3.4.2 Electrical resistivity tomography survey

Electrical resistivity tomography (ERT) was utilized to interpolate lithology between boreholes and confirm the dimensions of the aquifer and aquitards were relatively consistent both orthogonal and parallel to the river. This allowed us to control for substantial upstream or downstream changes in T or K which might impact the interpretation of the modeling results. Thus, the dimensions of the aquifer and its overlying and underlying fine layers were mapped using a combination of observed borehole lithology and ERT (Supersting, Advanced Geosciences Institute, Austin, TX). Electrical resistivity tomography was performed along two 581 m arrays parallel and perpendicular to the monitoring well transect. Eighty-four electrodes were spaced 7 m apart and the dipole-dipole method was used (Figure 12) [*Slater et al.*, 2010]. The electrical resistivity field was solved by numerical inversion using the software Earth Imager 2D (Advanced Geosciences Institute, Austin, TX).

3.4.3 Slug tests

Slug tests were performed on the Veast transect monitoring wells to measure the spatial variability in K across the aquifer. Hydraulic Conductivities were compared with

the distribution of subsurface resistivity. Pneumatic rising head slug tests were performed at each piezometer using a pressure transducer (Levelogger Edge, Solinst Canada Ltd., Georgetown, Ontario, Canada) and a pneumatic slug test device [*Knappett et al.*, 2012]. This method is described here briefly. A pressure transducer was suspended below the water level and sealed inside the well to measure water level changes. A volume of air was added into the well to displace the water level downward approximately 50 cm using a bicycle pump. Once the valve on the top of the piezometer was released, the transducer recorded the pressure changes every 0.5 second to capture the recovery curve of the water table. Horizontal K values were calculated using the Hvorslev method [*Hvorslev*, 1951]. Each test was performed in triplicate. The average coefficient of variation (CV) in K for a given well was less than 5%. Finally, duplicate manual falling head slug tests were performed on a drive-point piezometer (DP2a) (Solinst model 615, Solinst Canada Ltd., Georgetown, Ontario, Canada) to estimate K of the top confining layer (K_{top}). The drive-point piezometer was developed by extensive flushing of water before performing the slug test [*Bouwer and Rice*, 1976]. The outer diameter of the drive-point head is 30 mm and the inner diameter of the pipe that connected to the head was 26 mm. The equivalent screen length is 10 cm.

3.4.4 Pumping test

A pumping test was conducted by pumping the irrigation well for 7 hours at a rate of 1,377 m^3/day on January 12, 2016. This yielded a range of T and S values from which a range of D_{PT} could be calculated and compared to a range of D values obtained from 1D analytical modeling of the tidal pulse (D_{AAM} and D_{TLM}). The mean value of D_{PT}

was then applied in the later sensitivity analysis using a 2D numerical model to determine the cause of the deviation of D_{AAM} and D_{TLM} from D_{PT}. During the pumping test water levels in three monitoring wells (T1, T2 and T4) were recorded manually using an electric water-level meter (Model 101 Water Level Meter, Solinst Canada Ltd., Georgetown, Ontario, Canada). Manual water level measurements were taken every 5-10 minutes during early time at the start of pumping to characterize the exponential shape of the drawdown curves for each well. The obtained drawdown curves were corrected for tidal influence using the observed amplitude attenuations and time lags. This is an empirical correction only and does not assume an underlying theoretical model. Aquifer T and S were then estimated by manually fitting the tide-corrected drawdown curves to standard analytical transient pumping test models using Theis [*Theis*, 1935] and Hantush-Jacob [*Hantush and Jacob*, 1955] well functions, respectively. A different value of T and S was calculated for each drawdown curve from each well and the average of these were used.

3.4.5 Modeling Tidal Pulse with a 1D Analytical Model

Aquifer diffusivity was calculated using 1D tidal methods (Jacob-Ferris) by estimating time lag and amplitude attenuation of a tidal pulse between the river and a given monitoring well. Synchronized pressure transducers recorded the river stage and the hydraulic heads in the wells. The raw pressure readings were corrected for atmospheric pressure fluctuations, which was recorded by a Barologger (Barologger Edge, Solinst Canada Ltd., Georgetown, Canada) located 18 km to the west. The method for correcting the water levels can be found in full detail in Knappett et al. (2016).

Other studies have used one of two techniques to empirically measure time lags and amplitude attenuation of a tidal pulse arriving at a well. The first technique is the least-square method. This method uses the lumped tidal component approach wherein river stage and water levels in the wells are fitted to sinusoidal waves using least-squares regression and the lag time and amplitude is then taken from the fitted parameters [*Erskine*, 1991; *Trefry and Johnston*, 1998; *Jha et al.*, 2008; *Jha and Singh*, 2014]. The second approach is spectral analysis which uses the standard Fast Fourier transform (FFT) to identify the major tidal modes. This is also known as the multi-tidal component approach. It considers each of the simple harmonic components as a perfect sinusoidal wave [*Schultz and Ruppel*, 2002; *Trefry and Bekele*, 2004; *Jha et al.*, 2008]. Our study used spectral analysis to determine the phase and amplitude of each tidal mode over one year. These were then used to estimate time lags and amplitude attenuations respectively. Aquifer diffusivity was then calculated using the 1D Jacob-Ferris analytical model (Equation (3.3) and (3.4)).

3.4.6 Numerical simulations

Water flow across the river-aquifer boundary was modeled in 2D with a finite-element code (COMSOL Multiphysics) to test the sensitivity of bank morphology, aquifer anisotropy and heterogeneity on tidal pulse propagation. To validate the model in a simple setting, a 1D numerical model was first developed to confirm the similarity to the Jacob-Ferris analytical solution [*Ferris*, 1951] for a confined, 1D aquifer. A 2D flow model was then developed to evaluate the impact different physical scenarios would have on the D calculated with the 1D Jacob-Ferris model (D_{AAM} or D_{TLM}). The 2D

model domain was 250-m-wide and 20-m-thick with a no-flow boundary on the top and bottom. The no-flow boundaries on the top and bottom were justified by the capping silt layer and the laterally continuous 7 m thick clay layer. Thus evapotranspiration and precipitation were not considered across the top boundary during our simulations. A specific head boundary was set on the left side of the model and a constant head boundary was set on the right hand side (Figure 13). The initial river condition was neutral. The mesh was refined within the seepage face area and along the upper boundary with an element size as small as 0.1 m. A coarser mesh of 1 m was applied uniformly to the rest of domain.

To model the tidal pulse propagation accurately, Richards equation was solved to account for variably saturated flow. In addition, a stress source term was implemented to include total stress changes within the modeled aquifer domain directly underlying the river due to river stage fluctuations [*Reeves et al.*, 2000; *Cardenas et al.*, 2015]. A simple harmonic wave was imposed on the left hand boundary to represent river stage fluctuations. A seepage face boundary condition was assigned at the interface between river and aquifer, which splits the boundary into zero-pressure for the nodes along the seepage face and zero-flux for the nodes above the seepage face using a conditional statement (see details in Chui and Freyberg (2009)). The nodes below seepage face are given specified heads equal to river stage. This approach of implementing the seepage face in the model was successful in matching observed seepage face length [*Chui and Freyberg*, 2009]. Other authors have followed this same approach [*Abarca et al.*, 2013; *Cardenas et al.*, 2015]. To facilitate convergence, a smoothing function is used to

switch between the Dirichlet condition (i.e. zero-pressure) and Neumann condition (i.e. zero-flux) during river stage fluctuations. The initial distributions of hydraulic heads were obtained by running a steady-state model with a constant river stage and groundwater level. A maximum time step of 50 seconds was used to ensure accuracy and convergence of the transient model. River stage and soil hydraulic properties used in the model are reported in Table S1.

A series of different scenarios were simulated including: 1) varying bank slopes from 10° to 90°; 2) changing hydraulic anisotropy from 10 to 1000; and 3) adding a confining layer on top. The K of this layer (K_{top}) was then varied over three orders of magnitude. The simulated pressure pulses were fitted with the Jacob-Ferris solution to determine the sensitivity of D_{AAM} and D_{TLM} to deviations from the aquifer properties and dimensions assumed by the 1D model. These deviations represent realistic riverbank and coastal aquifers.

3.5 Results

3.5.1 Estimating Aquifer Transmissivity from slug tests and borehole lithology

Aquifer T was measured with slug tests to calculate K multiplied by aquifer thickness (b) observed in the borehole lithology. This b was confirmed to be consistent 581 m inland and 290 m north and south of the well transect by the ERT survey. Resistivity values correlated closely with observed lithology within 30 m beneath surface. Below this depth the ERT failed to pick up the bottom of the 7 m thick clay layer and the top of the lower sand aquifer due to its limitations (Figure 12). The ERT did however, pick up the top of the 7 m thick clay aquitard bounding the bottom of the

shallow sand aquifer. Resistivity values ranged from 5.4 to 104 Ohm-m. The ERT results indicated the lower confining clay layer and the upper semi-confining silt layer both had resistivity values between 20 and 30 Ohm-m. The resistivity values in the sand aquifer ranged from 40 to 104 Ohm-m. This was consistent with reported resistivity values of 38, 51 and 246 Ohm-m for clay, sandy-clay loam and coarse gravel, respectively [*Nyquist et al.*, 2008].

Hydraulic conductivities determined from slug tests ranged from 18.4 to 34.1 m/d between the eight monitoring wells screened within the shallow aquifer (Table S2, supporting information). This represented an average of 27.3 m/d with a standard deviation of 5.5 m/d. The K values agreed with observed resistivity values within the aquifer with high K coinciding with high resistivity values (Figure 12). Aquifer thickness (b) was informed from the drill cutting to be 20 m. Therefore, average T from the slug tests was estimated as 546 m^2/d.

Estimating Aquifer Diffusivity at the Field Site Using 1D Analytical Jacob-Ferris Model

Hydraulic heads and river stage were measured every 20 minutes throughout 2015 (Figure 14). Only 267 days (19 April, 2015 to 10 January, 2016), however, were analyzed to exclude irrigation pumping noise occurring in the late dry season from February to April each year [*Harvey et al.*, 2006; *Knappett et al.*, 2016]. The K1 (Lunar-solar diurnal constituent), O1 (Main lunar diurnal constituent), M2 (Main lunar semidiurnal constituent), S2 (Main solar semidiurnal constituent) and M4 (Shallow water constituent) modes were well resolved in all four hydrographs from the river and three monitoring wells, with M2 as the most prominent mode [*Hicks et al.*, 2000]. This

represented the semi-diurnal tide generated in the Bay of Bengal. The M2 signal was used to calculate amplitude attenuation and time lag since it had the maximum signal-to-noise ratio. Generally the pulse amplitude decreased and time lag increased with distance from river (Table 3). D_{AAM} was consistently larger than D_{TLM} by a factor of 1.32 to 2.33. Slope factors varied from 1.15 to 1.53. Larger values of D_{AAM} are consistent with Schultz and Ruppel (2002). Erskine (1991), however, found D_{AAM} was smaller than D_{TLM}. Both authors were working in unconfined coastal aquifers.

3.5.2 Estimating T and S with a Tidally-corrected Pumping test

Optimal T and S values were obtained by minimizing the root-mean-squared-error (RMSE) between simulated and observed drawdown curves (Figure 15). Several analytical solutions were tested on the observed drawdown data to measure T and S and to diagnose the aquifer type. These included the Theis confined model [*Theis*, 1935], the Theis unconfined model where S is replaced by specific yield (S_y), and the Hantush-Jacob leaky aquitard solution [*Hantush and Jacob*, 1955]. The optimal RMSE for each of these methods was 0.21 m, 0.21 m and 0.11 m, respectively. This implies water leaked into the drawdown cone area from the fine layers above or below the aquifer during pumping. The model captured the initial drawdown from elastic storage. However, the observed hydraulic heads only reached a quasi-steady state due to a short pumping duration of 7 hours. A longer pumping test would have provided more confirmation of the aquifer type. We estimated T and S of 400 m^2/d and 1.0×10^{-4}, 450 m^2/d and 5.0×10^{-4}, and 500 m^2/d and 5.0×10^{-4}, for T1, T2 and T4, respectively. These values of T compared closely to that estimated with slug tests. The subtle changes in best

fit T and S values between the observation wells likely reflected heterogeneity in the aquifer. Furthermore, well T1 was likely located too close to the pumping well at a lateral distance of only 1.5 m resulting in a smaller and, perhaps less representative estimate for T and S. Therefore, the T and S values calculated for T4 should be the most representative of the aquifer since the drawdown at T4 represents the average properties of the aquifer over the largest distance. The values of T and S were averaged over the 3 wells to produce values of 450 m^2/d and 5.0×10^{-4}, respectively. This corresponds to D_{PT} of 9.0×10^5 m^2/d.

3.5.3 Evaluating the Sensitivity of D Calculated Using the 1D Jacob-Ferris method to Multi-Dimensional Aquifer Properties

Aquifer diffusivity calculated from the 1D Jacob-Ferris tidal methods ranged from 5.1×10^3 m^2/d to 9.8×10^4 m^2/d with an average value of 5.0×10^4 m^2/d. This value was approximately one order of magnitude smaller than from the pumping test (9.0×10^5 m^2/d). We hypothesized this disagreement was partly caused by the oversimplification of the Jacob-Ferris model compared to an anisotropic, heterogeneous aquifer where the contact between the aquifer and the river is not a vertical boundary, but a sloped bank. To investigate the effects of river bank slope, the presence of an unsaturated zone, aquifer anisotropy and varying degrees of confinement on wave propagation, 2D numerical simulations were performed.

River stage was simulated as a sinusoidal wave pulse at the left boundary with amplitude of 1 m and period of 12 h. Aquifer diffusivity, T and S estimated from the pumping test ($D_{PT}=9.0 \times 10^5$ m^2/d, $T_{PT}=450$ m^2/d, $S_{PT}=5.0 \times 10^{-4}$) were input into the

model. A preliminary 1D numerical model showed good agreement with the Jacob-Ferris analytical solution at increasing distance (10 m, 30 m and 50 m) from shoreline (Figure S1, supporting information). We then extended our numerical studies to 2D.

Changing the aquifer type from confined to unconfined resulted in calculated average D_{TLM} and D_{AAM} values 64 and 305 times lower, respectively, than the value of D input into the 2D model (D_{PT}) (**Table 4**). The average slope factor was 0.46. Thus the existence of phreatic surface had greater damping effect on amplitude attenuation than time lag [*Erskine*, 1991].

Next the bank slope of the 2D unconfined aquifer model was varied from 90° to 10° (Figure 16 (a)-(c)). The estimated D_{AAM} and D_{TLM} did not vary substantially with slope angle. As bank slope was decreased pulse amplitudes were slightly damped with more delayed arrivals. More gentle slopes resulted in more pronounced propagation bias with slope factors ranging from 0.46 for the 90° bank slope to 0.28 for the 10° bank slope. Even a model with a 1° bank slope resulted in no significant difference in estimated D (results not shown). Bank slope, however, is unlikely to explain the error in D estimated in the field. This finding is consistent with Trefry and Bekele (2004).

Next we imposed vertical hydraulic anisotropy (K_x/K_z=10, 100 and 1000) in the aquifer assuming a 30° bank slope (Figure 16 (d)-(f)). In general, with increasing aquifer anisotropy pulse amplitudes were less damped and their arrival was less delayed. D_{TLM} was only 2 times smaller than D_{input} while D_{AAM} was about 65 times smaller. Thus, when applying 1D analytical tidal methods in anisotropic aquifers, it is best to use TLM rather

than AAM since D_{TLM} was very close to the D input into the model, especially when anisotropy is greater than 10 (**Table 4**).

Finally, we investigated the effect of varying degrees of confinement on wave propagation by imposing a confining layer on top (K_{top}) with various hydraulic conductivities ($K_{top}/K_{aquifer}$=0.1, 0.01 and 0.001, $K_{aquifer}$=22.5 m/d) (Figure 16 (g)-(i)). As the top layer becomes finer, pulse amplitudes are less damped and their arrival are less delayed. On average, D_{TLM} is 4 times smaller than D_{input} whereas D_{AAM} was about 119 times smaller. The ratio of D_{AAM} over D_{TLM} ranged from 30 to 50 with an average of 26. This resulted in the slope factor ranging from 0.21 to 0.48. Thus, as in an anisotropic aquifer, these simulations suggest that D_{TLM} will be more accurate than D_{AAM} when a semi-confining layer is present.

3.6 Discussions

3.6.1 Factors that Impact Tidal Pulse Propagation

Our simulations demonstrated that aquifer anisotropy and degrees of confinement had significant impact on wave propagation, while the effect of bank slope was negligible. The application of Jacob-Ferris solution works better when anisotropy ratio is larger than 10 or with a confining layer on top (for example, $K_{top}/K_{aquifer}$ = 0.01). This is an important finding since many alluvial aquifers along rivers often have vertical hydraulic anisotropies close to 10 [*Johnson and Morris*, 1962]. In contrast beach aquifers are extensively mixed by wave action resulting in relatively isotropic aquifers (anisotropy < 3) [*Li et al.*, 2010]. Thus in general the Jacob-Ferris 1D solution may be more appropriate for calculating D along tidally influenced rivers and estuaries, and less

accurate along beach aquifers. Unfortunately, vertical hydraulic anisotropy is often ignored in modeling studies partly because it is difficult to measure [*Mohanty et al.*, 1994; *Chen*, 2000]. In addition, fine layers lining the banks of coastal rivers are very common and are known as levee deposits [*Slingerland and Smith*, 2004]. They represent the annual accumulation of sediment during flood stage [*Weinman et al.*, 2008]. In contrast to the riverine setting, these layers are not usually present along beaches. Thus, the Jacob-Ferris 1D model may be more appropriate in river environments with well-developed natural levees.

Our experimental scenarios were not exhaustive. Other hydrogeologic and geometric parameters, not considered here, could affect propagation bias. For example, river fluctuation amplitude and frequency, groundwater flow direction within the aquifer, recharge, evapotranspiration and multiple layers in the aquifer may impact tidal pulse propagation. Trefry and Bekele (2004) showed that tidal pulse propagation was highly sensitive to horizontal layering in unconfined aquifer. The propagation bias increased with decreasing K ratio between upper layer and lower layer in field studies. In the same study, they found that recharge on top had negligible effect on propagation bias.

Even a limited number of realistic 2D simulations, however, provided useful information about wave propagation bias and how that translated to errors in estimating D_{TLM} and D_{AAM} ranging from 500 times too small to nearly accurate. The presence of phreatic surface create the greatest errors in the estimation of D using 1D Jacob-Ferris model. In contrast, modest levels of aquifer anisotropy and confinement greatly

improved the accuracy of D using the 1D Jacob-Ferris model. The results suggest that for a riverbank aquifer with an anisotropy ratio larger than 10 or confining layer with K smaller than 0.2 m/d (assuming aquifer K >20 m/d), the 1D Jacob-Ferris model produces reasonably accurate results with the D_{TLM} being more accurate than D_{AAM}.

3.6.2 Constraining Riverbank Aquifer Properties Using Field and Modeling Approaches

Characterizing the physical properties of aquifers requires knowing T and S at meaningful scales which can then be used to calculate the flow field. Electrical resistivity tomography is attractive in that it does not disturb the aquifer [*Slater*, 2002]. Furthermore, when ERT is combined with slug tests results and borehole lithology these can, in some cases provide a 3D interpolation of the permeability field in the subsurface. This is particularly useful for studying heterogeneous systems. At our study site, ERT performed excellent in mapping the thickness and continuity of the shallow aquifer (<25 m), and the depth and continuity of the top of the clay layer (25 m). The resistivity values modeled through inversion below 25 m depth, however, were not reliable. A borehole drilled to 70 m depth at the Veast1a location (**Figure 11**) revealed the shallow clay layer is 7 m thick. Underlying this clay layer is a low-As (<10 µg/L), red-brown sand (Pleistocene) aquifer which contrasts with the grey sand high-As (>300 µg/L) aquifer above. The fact that ERT did not resolve the bottom of the clay layer or the transition to another sandy aquifer is a caution that the accuracy of this method decays rapidly with depth. All ERT results should be checked with borehole lithologies.

When the dimensions of the aquifer are known through borehole lithology, slug tests can be used to estimate T. Transmissivity estimated from slug tests was very close

to that estimated from the pumping test. When S (5×10^{-4}) obtained from the pumping test and the average D (5×10^4 m^2/d) estimated from tidal methods was combined to estimate T, it was only 25 m^2/d which was an order of magnitude less than T estimated from the other methods. This error stemmed from the order of magnitude lower D estimated from the Jacob-Ferris model compared to the pumping test. Considering the cost and labor involved in performing a pumping test, tidal methods together with known borehole lithology and slug tests can provide an alternative approach to estimation of T and S values. This approach may prove to be useful for estimating physical properties of coastal aquifers where seawater intrusion or contaminated water is a concern or where a pumping well is not available [*Chattopadhyay et al.*, 2015]. Even when T is accurately known, however, the accuracy of the derived value of S using the 1D Jacob-Ferris model, will depend on aquifer anisotropy and degree of confinement.

The aquifer at the Veast site consisted of a shallow bank slope of less than 5 degrees and a silty layer on top. Given the results of the sensitivity analysis, tidal methods may have provided reasonable estimates of aquifer properties. Borehole lithology at this particular site indicates little variation in grain size which indicates a relatively isotropic aquifer. We measured K by duplicate falling head slug tests with drive point piezometers installed in the upper silt layer. There values ranged from 1.0 to 1.5 m/day, which is only 1 order of magnitude less than K in the aquifer (27.3 m/day). Thus, low anisotropy and lack of sufficient confinement may explain the order of magnitude difference between D estimated using the 1D Jacob-Ferris model and the pumping test at our site. The Jacob-Ferris model, however, suggested that D_{AAM} is

slightly larger than D_{TLM} which contradicts our simulation results. It is, however, consistent with Schultz and Rappel (2002). The reason might be that we used time series data from a river gauge that is located 3 km downstream, which created small additional (<3 min) lags in the measured lag times. This additional lag time could lower the value of D_{TLM} by as much as 7%. It is, further possible that this lag time changes with different river discharge rates and stage during other times of the year. Similarly, the river amplitude manually measured at Veast site was found to be approximately 0.024 m larger than the river amplitude measured by the river gauge 3 km downstream during one 48 hour period in the dry season. Although it seems small, this difference can increase D_{AAM} by 40-50%. It is always preferable to measure river stage fluctuations as close to the groundwater investigation site as possible.

3.7 Conclusions

This study set out to compare the values of D estimated with a pumping test and the Jacob-Ferris tidal pulse propagation model, explain the source of the discrepancy, and determine optimal settings where the 1D analytical model should be used. An order magnitude of difference in estimated D were observed between the pumping test analysis and the Jacob-Ferris 1D model. Numerical simulations showed that the presence of a phreatic surface cause the greatest errors in the estimation of D using 1D Jacob-Ferris model. Modest levels of aquifer anisotropy and confinement, however, tend to compensate, resulting in more accurate estimates of D using the 1D Jacob-Ferris model. The effect of bank slope is negligible. The Jacob-Ferris model should perform well within a riverbank unconfined aquifer with an anisotropy ratio larger than 10 or a top

confining layer K that is smaller than 0.2 m/d (assuming the aquifer K is greater than 20 m/d) with the D_{TLM} being more accurate than D_{AAM}. In all simulations, D estimated from TLM was generally larger, and more accurate than estimated from AAM. The existence of phreatic surface or a weakly confining layer combined with low aquifer anisotropy all result in low values of D calculated with the 1D Jacob-Ferris model. When pumping tests are not feasible in some coastal areas due to cost, contaminated water, or the risk of seawater intrusion, the 1D Jacob-Ferris model combined with slug tests, borehole lithology and ERT survey is a viable alternative approach for obtaining T and S. This will work best in aquifers with modest anisotropy (>10) or a strong confining layer ($K_{top}/K_{aquifer} = 0.01$).

Acknowledgement

This research was supported by a Geological Society of America student research grant. M. Bayani Cardenas is supported by the National Science Foundation (EAR-1344547). The authors would like to thank two anonymous reviewers who provided useful suggestions that greatly improved the manuscript.

Table 3. Diffusivities calculated from 1D Jacob-Ferris model

Well ID	Distance from shore (m)	Amplitude of M2 (m)	Phase of M2 (rad)	D_{AAM} (m^2/d)	D_{TLM} (m^2/d)	Slope factor ($\sqrt{D_{AAM}/D_{TLM}}$)
VeastT1	80	0.064	1.563	9.75E+04	7.36E+04	1.15
Veast1a	75	0.066	1.468	9.47E+04	4.07E+04	1.53
VeastT5	20	0.076	1.581	1.15E+04	5.08E+03	1.51
River	0	0.120	1.928			

Table 4. Diffusivities and slope factors calculated from numerical simulations under various boundary conditions and aquifer characteristics K_{top} is the hydraulic conductivity for the top confining layer. K_{input} equals 22.5 m/d and D_{input} equals 9E+05 m^2/d.

*value in parentheses represents deviation from model input (D_{input}/D_{AAM} or D_{input}/D_{TLM})

Model Setup				D_{AAM} (D_{input}/D_{AAM})			D_{TLM} (D_{input}/D_{TLM})			Slope Factor		
Confined/Unconfined	Bank slope (°)	Anisotropy (Kx/Kz)	Degree of confinement (K_{top}/K_{input})	10 m	30 m	50 m	10 m	30 m	50 m	10 m	30 m	50 m
Confined	90	1	1	9.00E+05 (1)	9.00E+05 (1)	9.00E+05 (1)	9.00E+05 (1)	9.00E+05 (1)	9.00E+05 (1)	1.00	1.00	1.00
Unconfined	90	1	1	3.15E+03 (285.46)	2.88E+03 (311.99)	2.81E+03 (319.85)	1.70E+04 (52.82)	1.48E+04 (61.00)	1.15E+04 (78.53)	0.43	0.44	0.50

Table 4 Continued

Model Setup				D_{AAM} (D_{input}/D_{AAM})			D_{TLM} (D_{input}/D_{TLM})			Slope Factor		
Unconfined	60	1	1	2.13E+03 (421.61)	2.55E+03 (352.52)	2.60E+03 (346.76)	1.04E+04 (86.28)	1.25E+04 (71.98)	1.02E+04 (88.37)	0.45	0.45	0.50
Unconfined	45	1	1	1.85E+03 (487.35)	2.41E+03 (374.07)	2.52E+03 (356.59)	1.04E+04 (86.28)	1.02E+04 (88.02)	1.02E+04 (88.37)	0.42	0.49	0.50
Unconfined	30	1	1	1.74E+03 (518.31)	2.36E+03 (380.85)	2.45E+03 (366.91)	1.04E+04 (86.28)	1.25E+04 (71.98)	1.02E+04 (88.37)	0.41	0.43	0.49
Unconfined	10	1	1	1.60E+03	2.27E+03	2.29E+03	2.07E+04	1.56E+04	1.15E+04	0.28	0.38	0.45

Table 4 Continued

Model Setup				D_{AAM} (D_{input}/D_{AAM})			D_{TLM} (D_{input}/D_{TLM})			Slope Factor		
				(560.88)	(397.29)	(393.15)	(43.49)	(57.54)	(78.53)			
Unconfined	30	10	1	4.05E+03 (222.37)	6.38E+03 (141.00)	6.64E+03 (135.47)	2.20E+05 (4.08)	3.64E+05 (2.46)	4.10E+05 (2.19)	0.14	0.13	0.13
Unconfined	30	100	1	3.00E+04 (29.96)	5.47E+04 (16.45)	5.96E+04 (15.10)	4.59E+05 (1.96)	8.90E+05 (1.01)	1.05E+06 (0.85)	0.26	0.25	0.24
Unconfined	30	1000	1	8.44E+04 (10.66)	1.58E+05 (5.69)	1.77E+05 (5.08)	2.94E+05 (3.06)	5.31E+05 (1.69)	6.71E+05 (1.34)	0.54	0.55	0.51

Table 4 Continued

Model Setup				D_{AAM} (D_{input}/D_{AAM})			D_{TLM} (D_{input}/D_{TLM})			Slope Factor		
Semi-confined	30	1	0.1	2.16E+03 (416.23)	3.68E+03 (244.84)	4.15E+03 (216.76)	7.94E+04 (11.33)	1.12E+05 (8.00)	1.32E+05 (6.82)	0.38	0.40	0.43
Semi-confined	30	1	0.01	1.14E+04 (78.68)	2.20E+04 (40.85)	2.58E+04 (34.86)	4.96E+05 (1.81)	9.22E+05 (0.97)	9.57E+05 (0.94)	0.33	0.21	0.28
Semi-confined	30	1	0.001	5.09E+04 (17.66)	9.96E+04 (9.03)	1.14E+05 (7.91)	2.23E+05 (4.03)	4.67E+05 (1.92)	5.63E+05 (1.59)	0.48	0.46	0.45

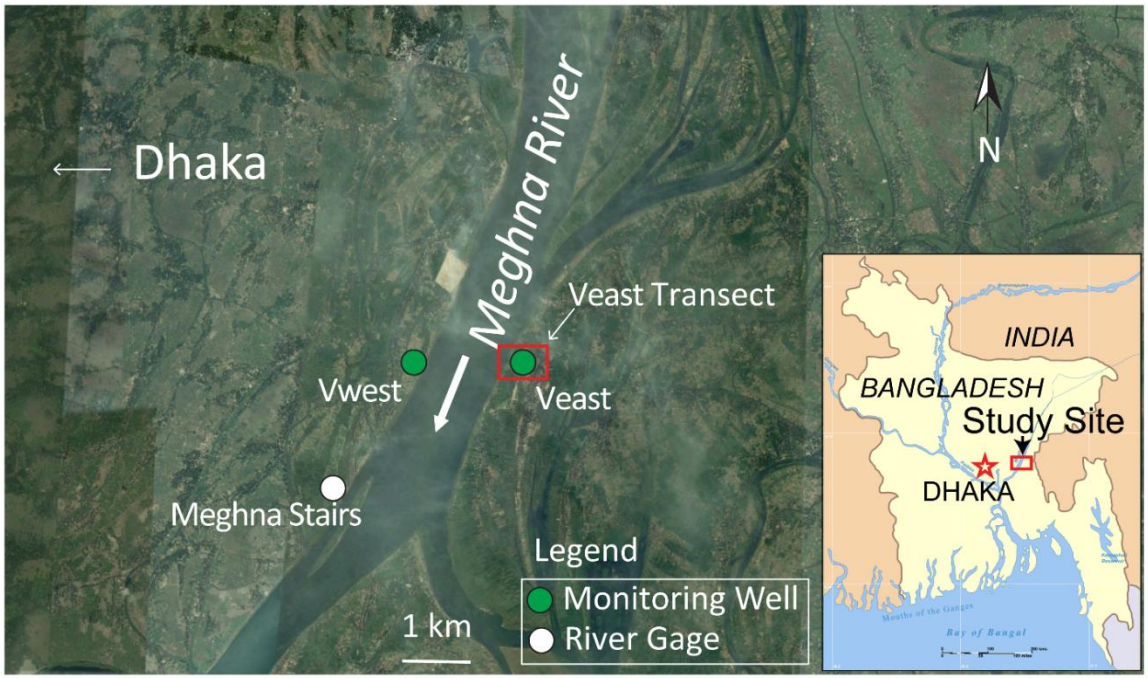

Figure 10. Location of study site including the Meghna River and relative location of the site within the country of Bangladesh.

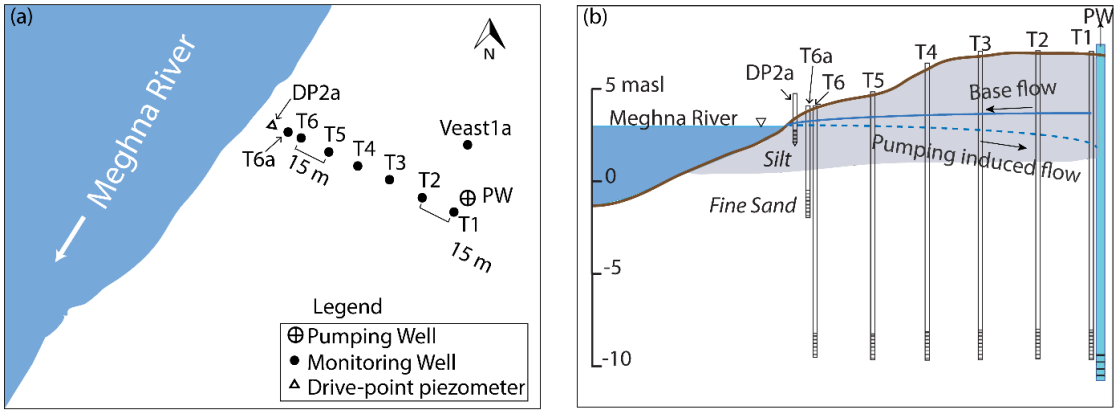

Figure 11. Geologic setting of the Veast monitoring well transect along the Meghna River. (a) Plan view; (b) Vertical profile.

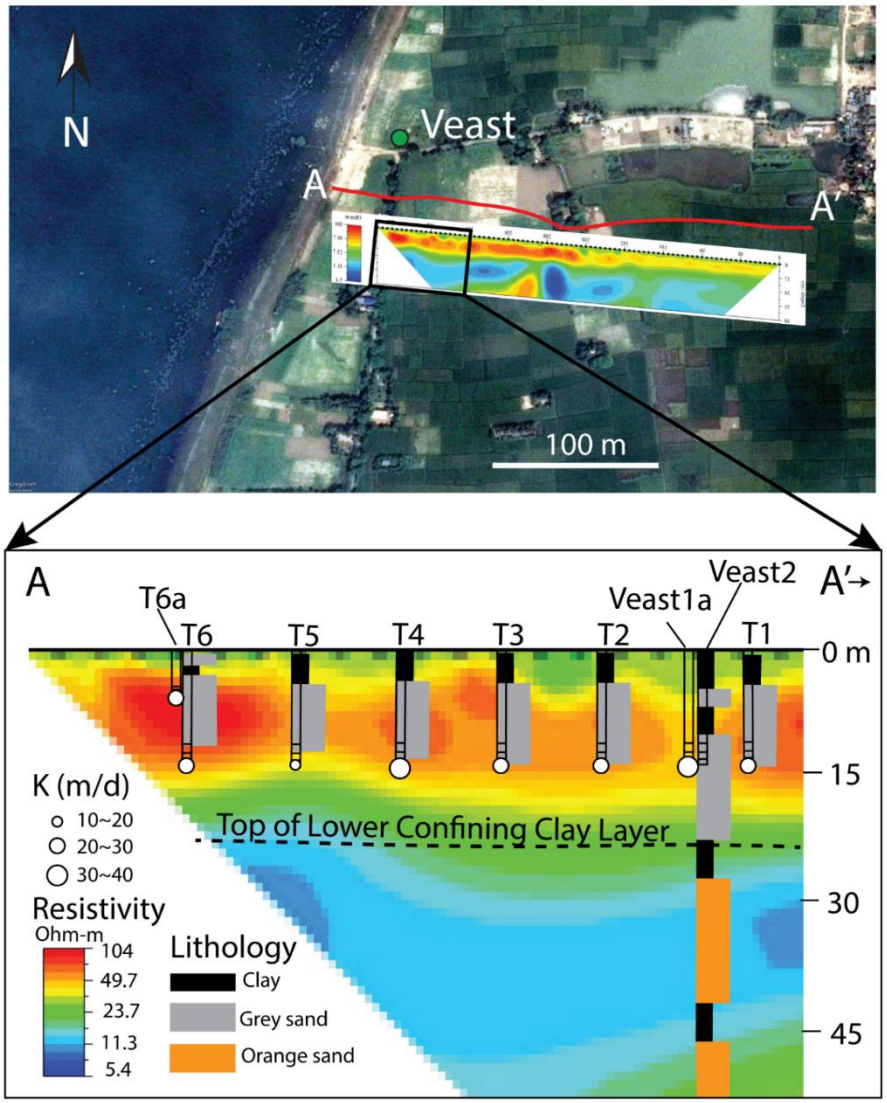

Figure 12. Subsurface resistivity, measured K and borehole lithology at Veast transact. The locations of monitoring wells (grey, vertical bars) and their screened intervals (horizontal lines) are shown. The size of white circle corresponds to K. Lithology is shown as a series of rectangular box with different color representing soil types. Resistivity is indicated by using color bar. Only a portion of the resistivity profile (A-A') is shown here.

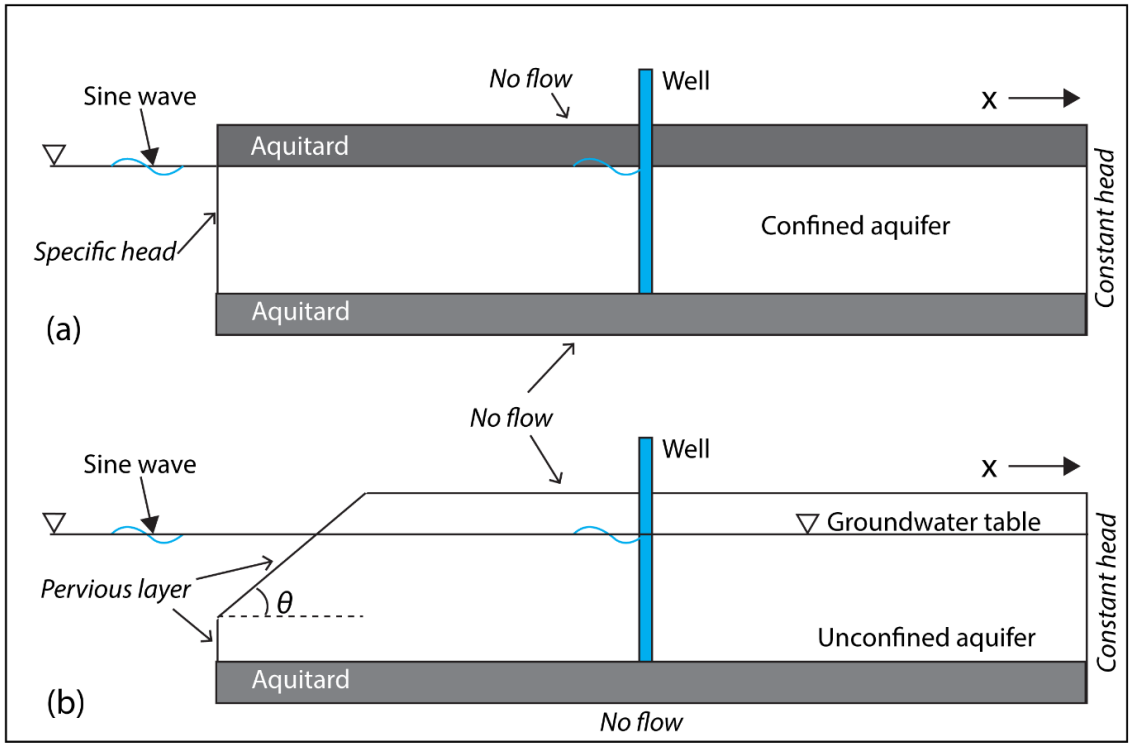

Figure 13. Conceptual models of sinusoidal wave propagation. (a) Jacob-Ferris confined model; (b) Sloping bank unconfined model. The x-z dimension is 250 m by 20 m. Also shown is the model boundary conditions in italics.

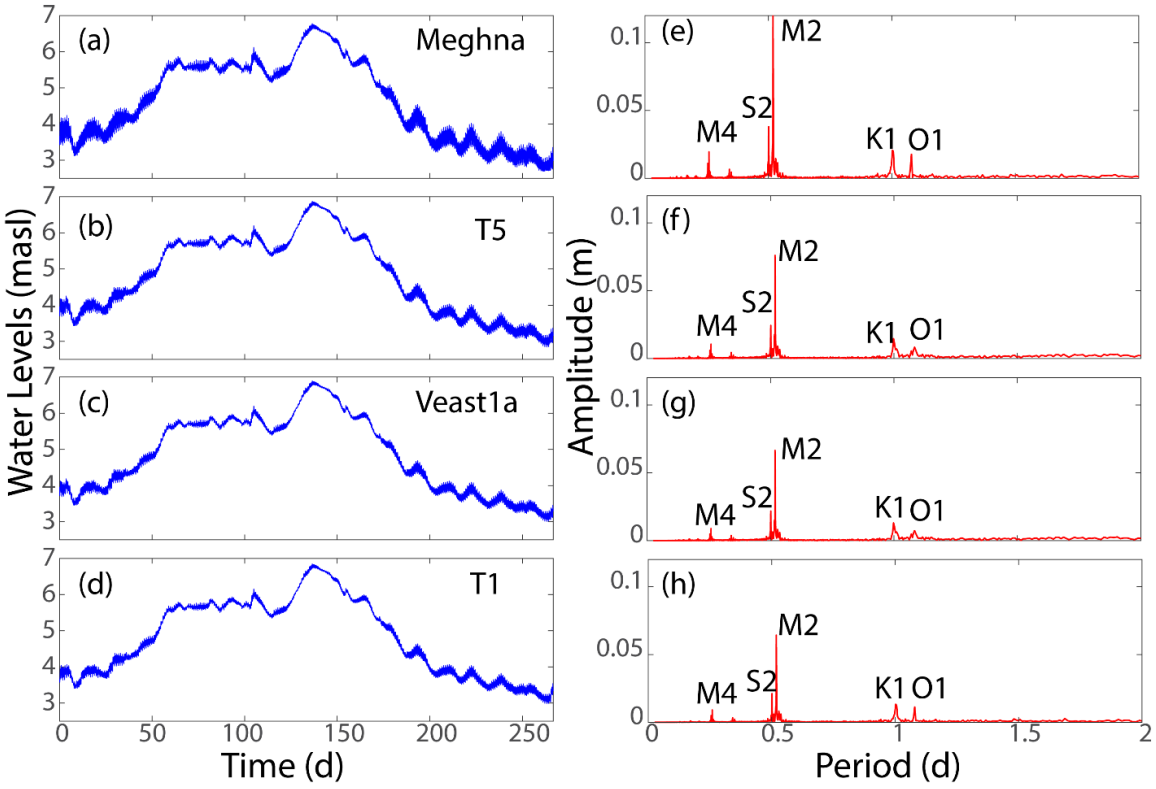

Figure 14. Spectral analysis of river and groundwater hydrographs. Fast Fourier transforms were applied to each time series to extract amplitude and period information. (a-d) river and groundwater hydrograph; (e-h) Periodogram of harmonic frequencies for each tidal signal.

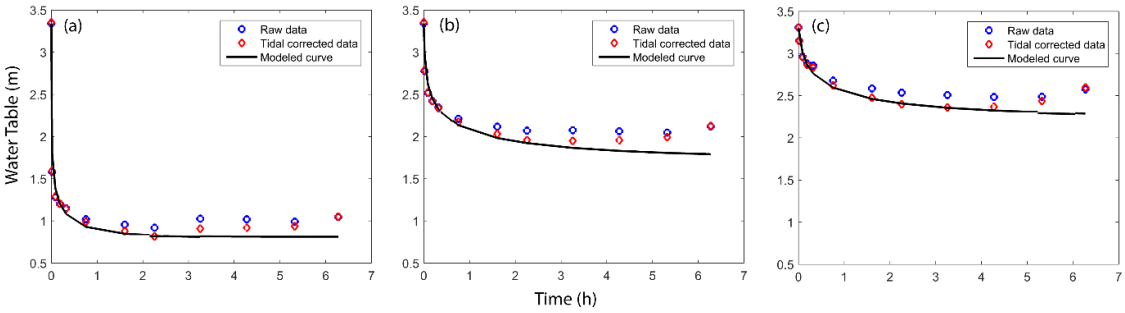

Figure 15. Pumping test modeling for three monitoring wells: (a) T1 (T=400 m^2/d and S=1.0 × 10^{-4}; RMSE=0.11); (b) T2 (T=450 m^2/d and S=5.0 × 10^{-4}; RMSE=0.13); (c) T4 (T=500 m^2/d and S=5.0 × 10^{-4}; RMSE=0.10). The water table was manually measured (blue circle) and was corrected for tidal influence (red circle). Different analytical transient pumping test models are applied to fit the data. Only the best fit drawdown curve is shown here [*Hantush and Jacob*, 1955].

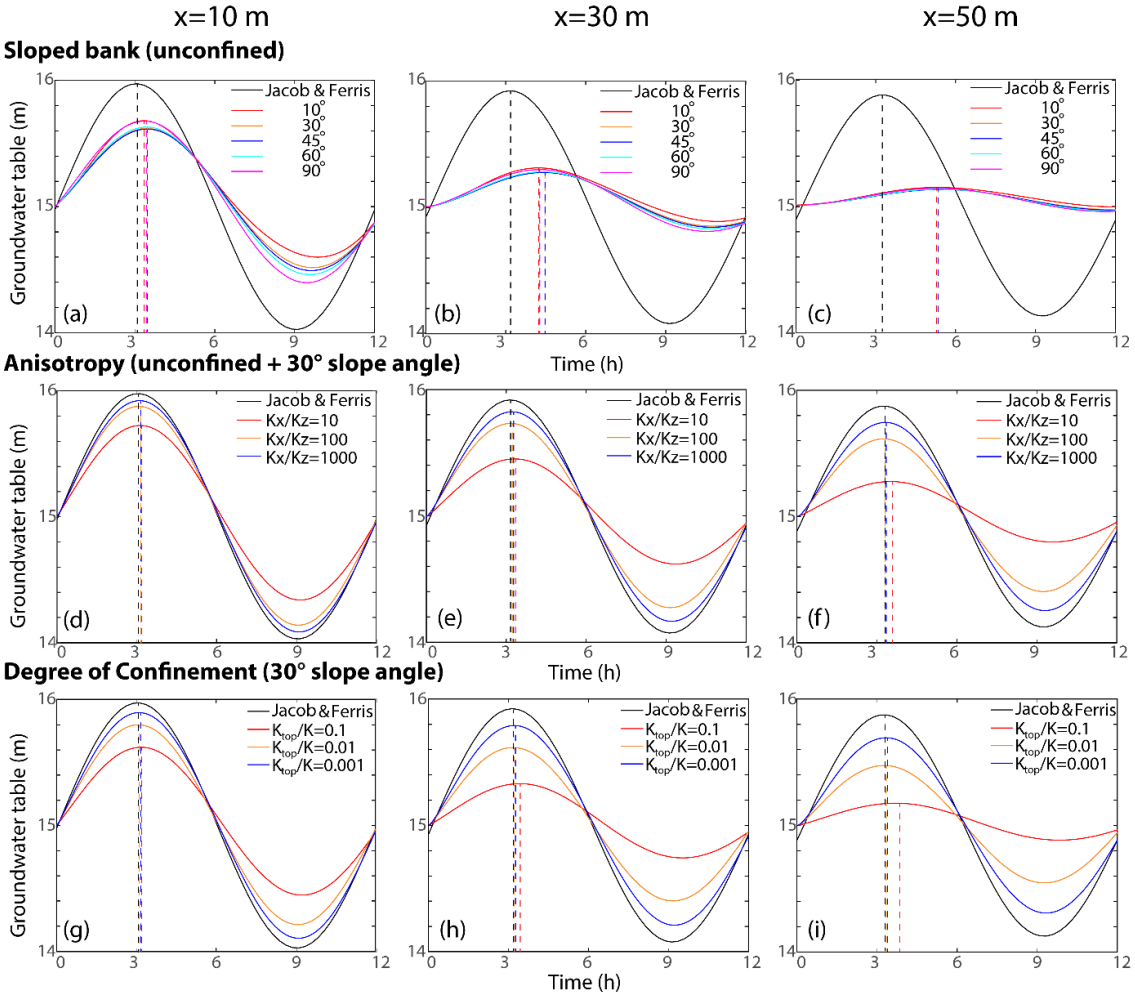

Figure 16. Two dimensional numerical models with various boundary conditions and aquifer characteristics to test wave propagation bias between 1D Jacob-Ferris analytical model and 2D realistic numerical model. (a-c) sloping bank; (d-f) aquifer anisotropy; (g-i) aquifer heterogeneity. X is the distance from mean shoreline. The dashed lines represent peaks of pulse propagation.

Supporting Information

Additional Supporting Information may be found in the online version of this article:

Table S1. Model parameters input for 2D numerical model

Parameters	Units	Value
Hydraulic conductivity (K)	md^{-1}	22.5
Specific Storage (S_s)	m^{-1}	2.50E-05
Effective Porosity		0.3
Residual Water Content		0.1
van Genuchten (α)	m^{-1}	10
van Genuchten (n)		2
Wave amplitude	m	1
Wave period	h	12

Table S2. Hydraulic conductivities (K) estimated from slug tests at eight monitoring wells along Veast transect. Also shown is its distance from shoreline.

Well ID	Distance from shore (m)	K (md^{-1})
T6a	4.5	30.0
T6	5.0	29.1
T5	20.0	18.4
T4	35.0	34.1
T3	50.0	26.3
T2	65.0	23.6
T1	80.0	23.2
Veast1a	75.0	34.0

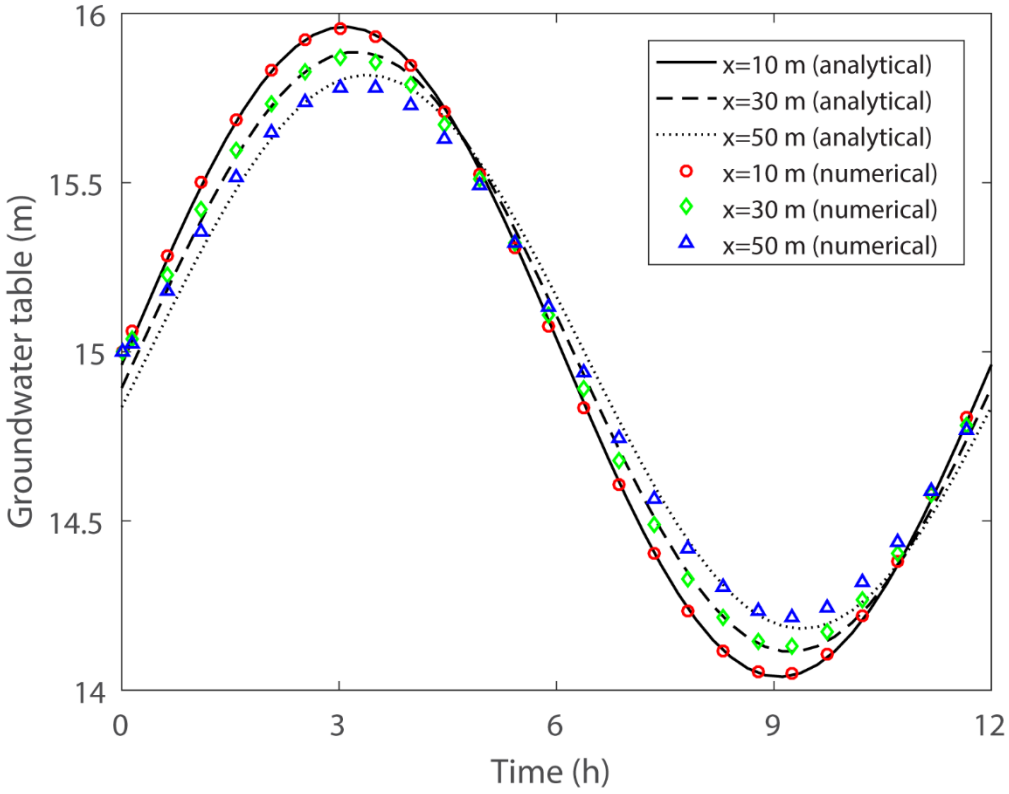

Figure S1. One dimensional (1D) numerical model compared with the 1D Jacob-Ferris analytical solution at three different distances (x=10, 30, 50 m). Colored symbols represent numerical solution and 2D solid and dashed lines represent the analytical solution.

CHAPTER IV

THE IMPACTS OF TIDAL AND SEASONAL RIVER STAGE FLUCTUATIONS AND GROUNDWATER PUMPING ON THE FORMATION AND FATE OF ARSENIC WITHIN PERMEABLE NATURAL REACTIVE BARRIERS

4.1 Summary

River stage fluctuations induced by ocean tides and rainfall enhance the exchange between oxic river water and reducing groundwater. When this mixing occurs within riverbank aquifers high in dissolved iron (Fe) and arsenic (As), the timing and extent of mixing may control the accumulation and mobility of arsenic (As) within the hyporheic zone (HZ). A two-dimensional, variably saturated, flow and reactive transport model was developed to simulate the impacts of tidal and seasonal fluctuations on the formation of a Permeable Natural Reactive Barrier (PNRB) and As mobility in an aquifer adjacent to the Meghna River in Bangladesh. River stage fluctuation period and amplitude strongly controls the spatial and temporal distribution of the PNRB. The PNRB forms much faster and denser under semi-diurnal tidal fluctuations compared to that under the less-frequent neap-spring tides. As tidal amplitude increase,s the PNRB expands horizontally because of a larger contact area between river and groundwater. Seasonal fluctuations along a sloping riverbank expands the PNRB up to 60 m horizontally and 5 m vertically. Even the smallest tidal fluctuations simulated in this study with an amplitude of only 0.07 m greatly impacts the lateral extent and density of Fe and As within PNRB. Lastly, simulations indicated that under a reversal from gaining to losing river conditions the As attached to FeOOH within a PNRB, at molar

ratios (As:Fe = 0.089) observed in the field, can contaminate vast areas of the adjacent aquifer. The findings of this study have broad implications to regulated rivers and stake-holders using shallow aquifers adjacent to rivers for drinking water supply and irrigation.

4.2 Introduction

Coastal rivers fluctuate with semi-diurnal, diurnal and neap-spring tides, which drives surface water in and out of aquifers over short time periods. In areas with monsoonal climates or temperate regions with spring snowmelts, seasonal changes in the river stage will drive surface water into and out of the aquifers over a longer term. The exchange between oxygen-rich surface water and groundwater is known to alter local redox conditions and stimulate biogeochemical reactions within the hyporheic zone (HZ) [*Gu et al.*, 2012; *Zarnetske et al.*, 2012]. The role of nested frequencies of periodic river stages at short-and-seasonal periods, however, and their influence on the release or trapping of heavy metals in aquifer sediments, has not been widely explored [*Berube et al.*, 2017].

Within the Ganges-Brahmaputra-Meghna Delta (GBMD) in Bangladesh, tidally induced river stage fluctuations introduce oxygen- and nutrient-rich river water into the reducing, ferrous iron (Fe(II))-rich aquifers [*Zheng et al.*, 2005], forming amorphous, reactive ferric (Fe(III)) oxide (FeOOH) minerals during infiltration of the oxidized river water [*Jung et al.*, 2015]. Existing and actively forming FeOOH minerals can adsorb and sequester dissolved oxyanions such as arsenic (As(III) as $H_3AsO_3^0$ and As(V) as $H_XAsO_4^{X-3}$), which are also found at locally elevated concentrations in most shallow aquifers in the GBMD [*van Geen et al.*, 2003; *Fendorf et al.*, 2010]. Therefore, oxidized

Fe(III) may form a permeable natural reactive barrier (PNRB) along the river bed and bank, especially when a river is strongly gaining [*Jung et al.*, 2009, 2012, 2015; *Lee et al.*, 2014; *MacKay et al.*, 2014; *Baken et al.*, 2015]. The earliest observation on As in groundwater in the GBMD noted a strong correlation between dissolved Fe(II) and As in shallow aquifers [*Nickson et al.*, 1998]. On the other hand, once attached to FeOOH, tAs oxyanions may be released from FeOOH minerals within aquifer sediments in the presence of labile organic carbon [*Nickson et al.*, 1998; *Harvey et al.*, 2002; *McArthur et al.*, 2008]. Thus if hydrological conditions change, an established PNRB may release its accumulated metals and elements to the aquifer. This process will be limited by the supply of electron donors such as fresh river water DOC or DOC produced from particulate organic matter (POC) in the riverbank sediments. Terminal electron acceptors, especially O_2 and NO_3^-, will also infiltrate into the riverbank aquifer from the river under a losing stream scenario [*Postma et al.*, 2010; *Stahl et al.*, 2016].

Elevated solid-phase As concentrations have been found in the riverbank sediments along areas of the Meghna River that are subject to daily tides and seasonal flooding (Datta et al., 2009). This enrichment of As has previously been attributed to redox trapping by FeOOH during groundwater discharge over decadal to centennial timescales. Previous work by *Datta et al.* [2009] found extremely high solid-phase As concentrations in the sediments lining the entire length of the Meghna River (between 22.5°N and 25°N) from 1-to-3-m-depth below the riverbed, with levels ranging from 1 to 23,000 mg/kg with an average of 4,000 mg/kg (n=14). Downstream of the Meghna River (23.6°N), *Jung et al.* [2012] also found high concentration of As (46~600 mg/kg)

at depth shallower than 2 m or deeper than 5 m in the river sediments. In a further study, *Jung et al.* [2015] concluded that the elevated HCl leachable As in the riverbank sediment (up to ~700 mg/kg) was a result of trapping groundwater As that was discharging to the river by PNRB with Darcy flux of 10 m/yr over hundreds of years. In calculating the time to accumulate the observed solid-phase concentrations of As, the authors did not explicitly account for the impacts of the frequent mixing of river water and groundwater, driven by river stage fluctuations from tides and seasonal flooding on As trapping and mobilization in the riverbank aquifer.

Recently, efforts have been focused on studying seasonal variations in As concentrations in groundwater and its implications on the potential risks for drinking water [*Polizzotto et al.*, 2008; *Duan et al.*, 2014; *Postma et al.*, 2016b; *Schaefer et al.*, 2016; 2017]. In the Mekong River floodplain of Cambodia, *Polizzotto et al.* [2008] observed a sharp As concentration gradient, from <10 µg/L in near surface sediments to ~600 µg/L at 4 m depth from the surface. They found the strongest temporal variations in As concentration near the bank of Mekong River. These were caused by the changes in hydraulic gradient induced by seasonal river stage fluctuations (~8 m). In New England, *Ayotte et al.* [2015] found that As concentrations in the wells were higher in the fourth quarter (October through December) than in the first quarter (January through March). Most of the wells had As concentration that varied by a small amount (< 4 µg/L), whereas some wells had As concentration that varied by more than 30 µg/L. In China, *Schaefer et al.* [2016] observed a dramatic seasonal change in dissolved As concentration (100~1,200 µg/L) in groundwater with increasing As concentrations

observed during groundwater discharge and decreasing As concentration during groundwater recharge over a one year period within the Jianghan Plain of the Yangtze River. They hypothesized that surface water intrusion during the dry season under the influence of irrigation pumping drew in water rich in oxygen and nitrate, thus promoting the oxidation of As(III) and adsorption of As, which lowered As concentrations in groundwater. Whereas field measurements can suggest natural and anthropogenic causes of the spatial and temporal distribution of As in riverbank aquifers, measurements alone cannot unravel the coupled hydro-geochemical mechanisms causing that distribution. Under dynamically changing flow directions within riverbank aquifers, using numerical model is critical to explore the coupling of physical and biogeochemical processes and to predict how river stage regulation and seasonal groundwater pumping in aquifers bordering rivers will impact the trapping and mobilization of metals and toxic elements.

Models assuming steady-state flow regimes, ranging in complexity from simple 1-D to complex 3-D numerical models have been applied to improve our understanding of the sources and fate of As in aquifers in the GBMD [*Nakaya et al.*, 2011; *van Geen et al.*, 2013; *Desbarats et al.*, 2014]. These models have also been applied to predict future movement of As from a high-As to a low-As aquifer [*McArthur et al.*, 2008; *van Geen et al.*, 2013]. In systems with spatially complex flow fields, many studies assume steady-state flow while emphasizing a wide range of reactions within a reactive transport model [*Postma et al.*, 2007, 2016a; *Jung et al.*, 2012]. *Postma et al.* [2016a] used a 1-D reactive transport model to study the evolution of groundwater chemistry over 6,000 years in a 20-m-thick aquifer within the Red River flood plain. They showed that groundwater As

reached a maximum of 600 µg/L at a simulation time of 1,200 years. *Kocar et al.* [2014] developed steady-state 1- and 2-D reactive flow and transport models coupled with Monod kinetics reactions to study the impact of subsurface physical factors on the distribution of As on the Mekong River delta in Cambodia. They showed that the rate of As release and physical properties, hydraulic conductivity (K) in particular, significantly changed the subsurface distribution of As.

Other studies have focused on modeling the dynamic subsurface flow system and its implications on As mobilizations, however the reactions considered in these models were typically limited to the inclusion of a retardation coefficient for As [*Benner et al.*, 2008; *Nakaya et al.*, 2011; *Khan et al.*, 2016; *Knappett et al.*, 2016]. *Khan et al.* [2016] used a large regional scale flow model to address the vulnerability of deep, low-As groundwater to mega-city pumping in Dhaka, Bangladesh. Their simulations predicted that intensive groundwater pumping induced preferential flowpaths that may contaminate deep (>150 m) aquifer within a decade. *Nakaya et al.* [2011] developed a transient, 3-D model to to study the relationship between pore water residence time and As concentrations in a shallow, Holocene aquifer in Bangladesh. They found that the release of As from Holocene aquifer in their study area is likely to occur in vertically infiltrating water. Most of the aforementioned steady-state and transient models examine groundwater flow paths with pore-water residence times ranging in age from decades to centuries.

Few models have fully coupled transient flow with biogeochemical reactions to study As mobilization within aquifers which have very young pore waters of less than a

year. This is critical because flow paths with short pore-water residence times re-order which chemical reactions predominate according to their reaction kinetics. The Damkohler number was developed to describe this process [*Jennings*, 1987]. It is equal to the rate of desorption of a chemical times the pore-water residence time [*Bearup et al.*, 2012]. Reactions with large Damkohler numbers (>100) will dominate bulk pore-water chemistry, whereas those with small values (<0.01) will be unimportant. This framework, however, is insufficient to describe the number and relative rates and direction of reactions occurring within a dynamically changing riverbank aquifer. Thus any model that assume steady state will likely be oversimplified and make poor predictions with respect to the order and direction redox reactions occurring across aqueous and solid phases. For example, aqueous Fe(II) precipitates rapidly in hydrous amorphous iron oxides (FeOOH) in the presence of oxygen or directly as ferrihydrite ($Fe(OH)_3$) during microbially-mediated precipitation [*Hohmann et al.*, 2010]. These rapidly precipitated minerals and also rapidly dissolves in the presence of organic matter [*Postma et al.*, 2010]. Therefore, reactions like these will tend to dominate Fe cycling in parts of a riverbank aquifer subject to rapid turnover in redox conditions with a regular supply of incoming dissolved Fe from the aquifer towards the river.

Our study is the first-of-its-kind with the objective to investigate the role of tidally-induced river stage fluctuations on short-term PNRB formation and implications for the release of As from these PNRB under intensive groundwater pumping scenarios. Here, we developed a 2-D (vertical slice) model, developed along an 85-m well-transect perpendicular to the east bank of the Meghna River, to examine the quantify the roles of

coupled hydro-(bio)geochemical processes producing observed spatial and temporal variations of As in the hyporheic zones within a tidally-influenced regions of the GBMD [*Berube et al.*, 2017]. A sensitivity analysis was performed to examine the impacts of aquifer hydraulic conductivity (K), and river stage fluctuation period and amplitude, on the density, kinetics, and spatial extent of Fe-oxides precipitating within the PNRB. A secondary objective was to evaluate the fate of As associated with Fe-oxides under strongly losing river conditions induced by local groundwater pumping.

4.3 Methodology

4.3.1 Study Site

The numerical model presented here is based on water levels, hydraulic properties and chemistry of a shallow aquifer along Meghna River in central Bangladesh, located approximately 35 km east of Dhaka [*Berube et al.*, 2017]. In a previous study by [*Shuai et al.*, 2017b], a transect consisting of six deep (~15 m) monitoring wells and one shallow well (~7 m) were installed perpendicular to the river on the eastern bank of Meghna River, at 15 m spacing. An irrigation well was located at the end of well transect farthest from the river which was screened across the entire shallow aquifer. The aquifers of the GBMD are comprised of sandy, unconsolidated Pleistocene to Holocene fluvial and deltaic sediments [*Goodbred et al.*, 2014]. Groundwater in the shallow Holocene aquifer (<25 m) is generally reducing with high dissolved Fe (~ 30 mg/L) and As concentration (~ 300 µg/L) in the pore water, while the deeper Pleistocene aquifer contains little dissolved As [*McArthur et al.*, 2008]. A thin silt layer overlies the top of the sandy Holocene aquifer. The aquifer is underlain by a 7-

m-thick clay layer. Hydraulic conductivities (K) were measured using slug tests and pumping tests: within the overlying silt layer and the shallow aquifer, K is ~ 1 and ~ 22.5 m/d, respectively [*Shuai et al.*, 2017b]. Pressure transducers, installed in 15-m-deep monitoring wells and a river gauge located 3 km downstream, were used to record water table and river stage fluctuations, respectively [*Berube et al.*, 2017; *Shuai et al.*, 2017b]. The Meghna River stage fluctuates with semi-diurnal (12 h) and neap-spring (14 d) ocean tides and is further influenced by seasonal monsoon flooding causing the river to fluctuate with an amplitude of 1.8 m annually. The river stage reaches its maximum of ~7 masl and minimum of ~3 masl during the late monsoon (August to October) and dry season (November to April), respectively [*Berube et al.*, 2017]. The groundwater table within the monitored riverbank aquifer is strongly influenced by river stage fluctuations which decrease in amplitude with distance from the riverbank [*Shuai et al.*, 2017b]. The hydraulic gradient between the river and the aquifer reverses annually with the gradient trending towards the river (losing) as river stage rises during early monsoon and away from the river (gaining) as river stage falls during late monsoon. Under natural conditions within this part of the GBMD, the Meghna would be gaining throughout the dry season (Berube et al., 2017), however at our study site, irrigation pumping in the late dry season (February to April), causes the river to be locally losing with a head difference of ~0.5 m between the river and groundwater table 85 m from the river's edge. This produces an average lateral hydraulic gradient of ~0.005 m/m. The influence of this seasonal irrigation pumping is not explicitly modeled in this study, but in our previous study it was shown that such an average lateral hydraulic gradient would move

river water twice as far laterally and vertically into the riverbank aquifer over 2 months of late dry season pumping compared to under base flow condition [*Berube et al.*, 2017]. The impact of seasonal irrigation pumping on PNRB formation and seasonal As mobilization into aquifers was not explicitly modeled in the present study. Instead this study focusses on the natural development of the PNRBs under a range of rive level fluctuation periods and amplitudes and the fate of As within an already-formed PNRB under sustained groundwater pumping conditions. In this scenario, year-round groundwater pumping would be increased for municipal or industrial uses (Stahl et al., 2016).

4.3.2 Model Development

A 2-D finite element model was developed using COMSOL Multiphysics to study coupled variably saturated flow and biogeochemical reactions under the influence of ocean tides and seasonal flooding. Similar models were implemented to simulate nitrogen cycling in a riparian zone subject to dam regulations [*Shuai et al.*, 2017a]. The governing flow and solute transport equations of this model were fully described in *Shuai et al.* [2017a]. The model considered both unsaturated and saturated flow by solving Richards' Equations. Solute transport was solved by the advection-dispersion-reaction equation. Before transport or reactions were calculated, the velocity field was first generated in the flow model. This was then used in the transport model using a segregated solver in COMSOL.

4.3.2.1 Flow Model

The model domain is 120 m (x direction) by 20 m (z direction) with bank morphology taken from a 2-D transect at eastern bank of Meghna River. The bank slope is less than 5 degrees with a silty layer on top [*Shuai et al.*, 2017b]. To simplify our model, however, the domain was treated as homogeneous and isotropic with no recharge or evaporation on top, which is reasonable given the presence of a ~1-m-thick clay layer in the upper 2 m of the aquifer near the river's edge. The average K was estimated to be 22.5 m/d (n=3) using pumping test during our previous study [*Shuai et al.*, 2017b]. The longitudinal dispersivity value used in our study was 1 m with transversal dispersivity of 0.1 m, which was typical as dispersivity correlates to the dimension of the aquifer [*Gelhar et al.*, 1992]. The bottom and river side of the domain were treated as no flow boundaries. The landward side was treated as a specific head boundary. This boundary was based on observations in the monitoring well at the end of the transect farthest from the river. The model domain was discretized uniformly with refinement towards the sloping bank interface (Figure 17).

The upper interface was assigned a seepage face boundary (see details in *Shuai et al.* [2017b]), which splits the boundary into zero-pressure for the nodes along the seepage face and zero-flux for the nodes above the seepage face using a conditional statement. The nodes below the seepage face are given specified heads equal to river stage. The river stage was approximated as a sine function below:

$$RL = H_0 + \sum_{i=1}^{n} A_i sin(\omega_i t) \quad (4.1)$$

where RL is river stage (m), H_0 is mean river stage (m), A_i is the amplitude (m) and ω_i is the angular frequency (1/d) of ith river stage fluctuation signal. The dominant tidal frequencies are semi-diurnal and neap-spring with amplitude of 0.14 m and period ($1/\omega$) of 0.52 d and 14.8 d, respectively (Table 5). Seasonal monsoon fluctuation was also approximated using a sine wave with amplitude of 1.8 m and period of 360 d. In addition, a stress term has been implemented in the model to account for the total stress changes induced by river fluctuations [*Reeves et al.*, 2000]. The maximum time step was set to 0.1 d to ensure the convergence of the model.

A set of particles uniformly located along the interface were released at time t=0 as river water infiltrated into the aquifer to show the flowpath of a river water molecule entering the aquifer. For each particle, the pore water residence time was calculated. This is the time a particle spends in the subsurface traveling along a particular flow path. Particle tracking was conducted using Darcy velocity output from flow equation.

4.3.2.2 Biogeochemical Model

The modeled biogeochemical reactions were aerobic respiration, iron (Fe(II)) oxidation, iron oxide (FeOOH) reduction and particulate organic carbon (POC) dissolution (Table 6). Under a sustained, losing river scenario with groundwater pumping, As was assumed to release only through reductive dissolution of Fe-oxides with a fixed As/Fe molar ratio of 89 mmol/mol. This As/Fe ratio was based on measurement made on riverbank sediments within 1 to 2 km of our field site [*Datta et al.*, 2009]. The approach of introducing As into the system as a product of Fe-oxide reduction has been used by serval other studies [*Postma et al.*, 2007, 2016a; *Kocar et al.*,

2014]. Our ratio is 74 times and 445 times larger compared to 1.2 mmol/mol in Red River floodplain, Vietnam and 0.2 mmol/mol in Mekong Delta, Cambodia, respectively [*Kocar et al.*, 2014; *Postma et al.*, 2016a]. This is, however, consistent with elevated As concentration (~4,000 mg/kg) found in the PNRB along the Meghna River [*Datta et al.*, 2009].

The aquifer is initially assumed to have uniformly distributed Fe(II) (30 mg/L) and zero FeOOH. The DOC is released to the pore water through POC dissolution with initial concentration of 6.5 mg/L. River fluctuations deliver repeated pulses of oxidized substrates such as dissolved oxygen into the Fe(II)-rich aquifer, fueling the formation of Fe(III)-oxides. At the back end of tidal pulses through the HZ, reducing conditions are induced to varying degrees across the PNRB. During reductive dissolution, local geochemical conditions across the PNRB may lead to As release into the aquifer; simultaneously, local geochemical conditions in other zones of the PNRB may promote active As sequestration in secondary Fe(II/III) or other phases.

Four aqueous species (DOC, O_2, Fe(II) and As) and two solid species (FeOOH and POC) were considered in the model. The reaction network and rate constants were adopted from literature [*Gu et al.*, 2007, 2012; *Kocar et al.*, 2014; *Liu et al.*, 2017]. The concentration for each species in river and groundwater were based on field measurements. Flow and biogeochemical parameters were listed in Table 7.

Multiple Monod kinetics was used for O_2 and DOC consumption during aerobic respiration [*Gu et al.*, 2012; *Zarnetske et al.*, 2012]:

$$R_1 = -\theta k_1 \left(\frac{C_{DOC}}{K_{DOC}+C_{DOC}}\right)\left(\frac{C_{O_2}}{K_{O_2}+C_{O_2}}\right) \quad (4.2)$$

where θ is volumetric water content, R_1 and k_1 are reaction rate and rate constant, K_{DOC} and K_{O_2} are half saturation constants for DOC and O_2 respectively, C_{DOC} and C_{O_2} are concentration for DOC and O_2 respectively. Monod kinetics is chosen because it does not assume a biological reaction is instantaneous and the biological reactions were limited by the availability of species [*Zarnetske et al.*, 2012].

The kinetics of Fe^{2+} oxidation was assumed to follow a second-order rate expression with respect to Fe^{2+} and O_2 [*Liu et al.*, 2017]:

$$R_2 = -\theta k_2 C_{Fe^{2+}} C_{O_2} \quad (4.3)$$

where R_2 and k_2 are reaction rate and rate constant for iron oxidation, and $C_{Fe^{2+}}$ and C_{O_2} are concentration for Fe^{2+} and O_2 respectively.

Microbially meditated reductive dissolution of Fe-oxide was assumed to follow a first-order rate expression with respect to Fe(III) and a Monod-type expression with respect to DOC:

$$R_3 = -\theta k_3 I_{O_2} C_{Fe(III)} \left(\frac{C_{DOC}}{K_{DOC}+C_{DOC}}\right) \quad (4.4)$$

where $I_{O_2} = \left(K_I/K_I + C_{O_2}\right)$ is inhibition term for O_2 and K_I is inhibition constant. Inhibition term is used to represent inhibition of Fe-oxide reduction given O_2 availability.

POC dissolution was simulated by a first-order mass transfer process [*Jardine et al.*, 1992; *Gu et al.*, 2007; *Zarnetske et al.*, 2012; *Sawyer*, 2015]:

$$R_4 = \alpha(k_d C_{DOC} - C_{POC}) \quad (4.5)$$

where α is a first-order mass transfer coefficient, and k_d is a linear distribution coefficient for the hyporheic sediment. The POC content is 0.2 % of sediments, typical in sandy aquifer [*Gu et al.*, 2007]. The DOC concentration generated through POC dissolution is not allowed to exceed the maximum groundwater DOC concentration (i.e. 6.5 mg/L). In areas of low DOC with active DOC consumption, POC will rapidly degrade to maintain a DOC concentration of 6.5 mg/L so that DOC becomes abundant. Whereas in areas of high DOC, the transformation from POC to DOC is negligible.

For the sustained, losing river scenario, a Langmuir sorption model was used to describe As sorption to aquifer solids (Fe-oxides):

$$C_p = \frac{k_l C_{p_{max}} C}{1 + k_l C} \quad (4.6)$$

where C_p and C are sorbed and dissolved As concentrations, respectively, k_l is the Langmuir constant, $C_{p_{max}}$ is maximum sorption concentration of As. *Harvey et al.* [2002] showed that the Langmuir isotherm fit As sorption to Fe-oxides better than a linear isotherm since the data indicated a limited number of attachment sites.

Where a species may be involved in several reactions, as a reactant or a product, the net reaction rates of these major species were expressed as the sum of production and consumption rates, taking into account of the stoichiometric coefficient (see Table 6).

$$R_{O_2} = -R_1 - R_2 \quad (4.7a)$$

$$R_{DOC} = -R_1 - R_3 \quad (4.7b)$$

$$R_{Fe(II)} = 4R_3 - 4R_2 \quad (4.7c)$$

$$R_{FeOOH} = 4R_2 - 4R_3 \quad (4.7d)$$

$$R_{As} = 4xR_3 \quad (4.7e)$$

where *x* is the molar ratio between FeOOH and As (i.e. 0.089 in our study). A negative sign indicates a reactant species was consumed whereas a positive sign indicates a species was produced.

We started with a base case scenario (Case 1) with combined tidal fluctuations (semi-diurnal and neap-spring tides) and a K of 22.5 m/d (Table 8). Further, the tidal signal was deconstructed into its components: semi-diurnal (Case 2) and neap-spring tide (Case 3) to study the different tidal frequencies on the rate of iron oxidation and thus PNRB formation. Water levels at river gauge and inland well were approximated using sine wave and used as boundary conditions to simulate seasonal accumulation of PNRB (Case 4). A sensitivity analysis was also performed using only neap-spring tides to examine the impacts of tidal amplitude and K (Case 5~8). Finally, a steady-state model with constant river stage (18 m) and groundwater table (16.2 m) was used to simulate a losing river condition due to sustained groundwater pumping (Case 9). The PNRB formed during the duration of the Case 4 simulation was used to describe the initial condition of Fe-oxide. This was assumed to be a mature PNRB. The bound As was released through FeOOH reductive dissolution in the presence of DOC, after which As was retarded by adsorption onto the sediments as As migrated into the aquifer. For Cases 1-3 and 5-8, the inland groundwater boundary was set at a constant 18.14 m compared to the mean river stage 18 m, indicating gaining river conditions. The model was simulated for 14.8 days spanning one neap-spring tidal cycle. For Case 4, both river and

groundwater boundaries were approximated using one simple harmonic wave with the same fluctuation amplitude (1.8 m) and period (360 d). The time lag between those two was estimated to be 0.1 rad (equal to 5.7 d) based on separate spectral analysis of river and groundwater hydrograph over 3 years. The total simulation time is 360 d.

The total mass of FeOOH accumulated in the HZ at given time t could be calculated using the following equation:

$$M_i(t) = \int_{\Omega} \theta C_i(t) d\Omega \tag{4.8}$$

where M_i is the total mass of FeOOH or As, C_i is the concentration of solid phase FeOOH or aqueous As, Ω is the domain area and t is time.

The key assumptions in our model are as follows. (1) Tidal and seasonal fluctuations can be approximated using sine waves with known amplitude and frequency; (2) All dissolved Fe(II) that precipitates as Fe-oxides does so as ferrihydrite; (2) Initial As concentration is assumed to be zero and As(III) is dominant in the aqueous phase; (3) All soluble DOC is bioavailable; (4) The composition of the iron oxides was redefined to contain a trace of As based on a known molar As to Fe ratio; (5) Reductive dissolution of iron oxides is the main mechanism for As release at our site; (6) The reduction of As(V) to As(III) can be combined with Fe-oxide reduction using one simple reaction (see Table 6) [*Kocar et al.*, 2014].

4.4 Results

4.4.1 Impact of Frequency of Tidally Induced River Stage Fluctuations on PNRB Formation

Both cumulative influx (water recharge into the aquifer) of the river water across the riverbank and efflux (water discharge into the river) of pore water increased as river fluctuation frequency increased (Figure 18). However, the net groundwater discharge (efflux minus influx) across Case 1-3 did not change substantially (Table 9).

For case 1, the combined tidal frequency (semi-diurnal plus neap-spring) showed more variability. The maximum instantaneous influx (37×10^{-6} $m^3/(m\cdot s)$) occurred when both semi-diurnal and neap-spring tides reached their combined maximum river stages (~ 4 d). In contrast, the maximum instantaneous efflux (47×10^{-6} $m^3/(m\cdot s)$) coincided with the minimum river stage (~ 11 d) (Figure 18 (a)). The cumulative influx and efflux was 9.0 and 18.6 m^3/m, respectively (Table 9).

Under only semi-diurnal fluctuations (Case 2), the flow direction across the upper boundary switched every12 h. The maximum instantaneous influx and efflux was 25×10^{-6} $m^3/(m\cdot s)$ and 39×10^{-6} $m^3/(m\cdot s)$, respectively. The cumulative influx and efflux was 8.7 m^3/m and 18.2 m^3/m, respectively.

Under only neap-spring tidal fluctuations (Case 3), infiltration began after 2 days when the river stage was approaching its maximum. The period of infiltration only lasted for approximately 3 days. The maximum instantaneous influx reached 2×10^{-6} $m^3/(m\cdot s)$ and the maximum efflux reached 18×10^{-6} $m^3/(m\cdot s)$. The cumulative influx and efflux were 0.4 and 10.7 m^3/m, respectively.

Flow paths as indicated by a conservative particle tracking were significantly altered by frequent river fluctuations (Figure 19). Under the combined tidal fluctuations (Case 1), particles released along the riverbank moved further into the aquifer with maximum depth of 2 m and width of 8 m. The particles zig-zagged back and forth caused by short-term (12 h) river-stage fluctuations. This elongated flow paths indicates relatively long pore-water residence time and mixing between river water and groundwater compared to short flow paths. Similarly, under only semi-diurnal tidal fluctuations (Case 2), particles penetrated 2 m deep into the aquifer with a maximum width of 7 m. In contrast, under just neap-spring tidal fluctuations (Case 3), the majority of the particles that were released along the riverbank infiltrated less than 1 m below the sediment and exited from upper interface within 7 days. Only a few flow paths were able to penetrate deep into the aquifer.

The temporal distribution of flow velocity and FeOOH concentration were illustrated for the neap-spring fluctuation simulation (Case 3) (Figure 20). River water started infiltrating as stage approached high tide (t=3.7 d) (Figure 18 (c)). The intrusion of oxygen from the river fueled the rapid oxidation of Fe(II) and thus the formation of Fe-oxides. Therefore the extent of the nascent PNRB during rising river stage coincided with the oxic boundary, which is defined herein as 10% of the oxygen concentration measured in the river (0.7 mg/L). As river stage dropped and eventually reached low tide (t=11.1 d), maximum groundwater discharge occurred (Figure 18 (c)) and new Fe-oxides precipitated below mean river stage line.

The size of PNRB was strongly impacted by the extent of oxic zone induced by different river stage fluctuation frequencies and combinations of frequencies (Figure 21). Similar to the particle tracking results, the distribution of all solutes were broadened and deepened as the frequency of river stage fluctuations increase. Case 1, with combined semi-diurnal and neap-spring tides, exhibited slightly shallower and wider formation (Figure 21 (j)) of a PNRB compared to Case 2 (Figure 21 (k)) and Case 3 (Figure 21 (l)). For Case 2 with semi-diurnal fluctuations only, the concentration of FeOOH was unevenly distributed (Figure 21 (k)). Dense FeOOH (~ 50 mg/kg) occurred both along the upper interface and further inland. In comparison, for the neap-spring tide fluctuations only (Case 3), the high solid-phase concentration (> 50 mg/kg) of FeOOH appeared at the junction between the mean river stage and the riverbank where large influxes occurred. The zone of depleted Fe(II) was much larger than the oxic zone. This is caused by the combined effects of dilution from mixing between iron free river water (as indicated by the conservative tracer (see Figure 21 (a-c)) and Fe(II) oxidation in the groundwater.

The mass of FeOOH accumulated within the aquifer at much faster rates with higher river fluctuation frequency (Figure 22). In fact, high frequency, semi-diurnal fluctuations combined with neap-spring tidal fluctuations (Case 3) are predicted to have a synergistic effect on accumulation rate, during the first 7 days of simulation. After the first 7 days of simulation, however, these nested frequencies had an antagonistic effect, allowing the sum of the individual accumulation rates for each frequency (Case 2 rate +

Case 3 rate) top catch up (Fig. 22). The final FeOOH mass for both Case 1 and the sum of Case 2 and Case 3 reached around 3 kg per meter river length.

Total accumulated FeOOH mass over the 14.8 day simulation period was the highest for the combined frequency Case 1 (3 kg/m), followed by semi-diurnal fluctuations only (Case 2) (1.8 kg/m) and lastly, neap-spring fluctuations only (Case 3) (1.1 kg/m). Both of the simulations using semi-diurnal tidal signals in the river stage (Case 1 and 2) indicated small 12 h fluctuations in accumulated FeOOH mass. Both Case 1 and 3 predicted a slowdown in the rate of FeOOH accumulation as groundwater discharge predominated within the shallow riverbank aquifer at the end of the neap-spring tidal cycle.

4.4.2 Impact of Hydraulic Conductivity on PNRB Formation

To examine the impact of K on PNRB formation, simulations were performed by varying K from 11.25 m/d (Case 5) to 45 m/d (Case 6) compared to the neap-spring tide only case (Case 3) (22.5 m/d). Each model was run for one neap-spring tidal cycle (Figure 23). Higher K increased the Darcy flux (as indicated by the size of the arrows) and solute fluxes within the aquifer. These increases greatly expanded the spatial distribution of FeOOH. Similarly, the oxygen plume penetrated much deeper and wider with larger K (data not shown). As a result, the horizontal and vertical expansion of the PNRB increased accordingly (Figure 7). However, the maximum concentration (~ 50 mg/kg) of FeOOH was always found where the mean river stage intercepted the riverbank.

Consistent with the distribution of FeOOH within the aquifer and the flow rate, the rate of increase in FeOOH mass was faster and attained higher overall amounts with larger K (Figure 24). After 14.8 d, the accumulated FeOOH mass increased from 0.8 to 1.4 kg/m as K increased from 11.25 (Case 5) to 45 m/d (Case 6). Among all Cases, the accumulation rate for FeOOH leveled off after rising for 12 days as increasing groundwater discharge inhibited river water intrusion during neap tide levels.

4.4.3 Impact of Tidal Amplitude on PNRB Formation

Starting with Case 3 as the base scenario, the tidal amplitude was varied from 0.07 m (Case 8) to 0.28 m (Case 7) to evaluate its impact on rates of FeOOH accumulation within the PNRB (Figure 25). The magnitude of amplitude did not significantly changed the flow field, however, the spatial and temporal distribution of solutes were altered. Given the same bank slope, a larger amplitude results in a longer seepage face resulting in more oxygen and DOC entering the aquifer. Consequently, the oxic zone was much wider horizontally with larger amplitude although the depth of the oxic boundary did not change substantially. Similarly, the distribution of FeOOH spanned almost 12 m horizontally for Case 7 (A=0.28) compared to 8 m for Case 8 (0.07).

The accumulated FeOOH mass after one neap-spring tidal cycle was greater for larger amplitude fluctuations with a maximum of 1.6 kg/m attained for Case 7 with the highest amplitude fluctuations, followed by 1.1 and 0.9 kg/m for Case 3 (A=0.14) and Case 8 (A=0.07), respectively (Figure 26). This finding suggests that the much greater amplitude in seasonal fluctuations at the field site along the Meghna River (~1.8 m)

compared to tidal fluctuations (~0.14 m), may exert much greater influence on PNRB formation than.

4.4.4 Impact of oxidation rate on PNRB Formation

Iron oxidation rate constant (k2) (Equation (4.3)) was varied by a factor of 10 (from 4.2e-6 to 4.2e-4 m3/(s·mol)) for Case 3 to test the sensitivity of k2 to the rate of FeOOH accumulation (Figure 27). Larger k2 induced faster precipitation rate of FeOOH and denser concentration of FeOOH mass near the mean river stage line and elsewhere. The maximum mass of FeOOH per meter river length after 14.8 d simulation was 0.6 kg, 0.8 kg and 1.1 kg for k2 equaled 4.2e-6 m3/(s·mol), 4.2e-5 m3/(s·mol) and 4.2e-4 m3/(s·mol), respectively (Figure 28).

4.4.5 Impact of Seasonal River Stage Fluctuations on PNRB Formation

The instantaneous water flux across the river-aquifer interface depends on the head difference between river stage and the groundwater table (Figure 29). The river stage was initially higher than the groundwater table during the rising limb of the hydrograph in the early monsoon, but the head difference decreased as the river stage reached its maximum in September (t=~90 d). Meanwhile, flux across the river-aquifer interface started with maximum instantaneous influx (17×10^{-6} $m^3/(m\cdot s)$) and then approached zero as the river stage approached the groundwater table. As the river stage fell below the groundwater table, groundwater started discharging to the river and continued for the next 180 days until the river stage reached its nadir. The highest instantaneous efflux (12×10^{-6} $m^3/(m\cdot s)$) occurred in November when the head difference between river stage and groundwater table was the largest. As the river stage rose above

the groundwater table in March (t=~270 d), river water began to infiltrate into the aquifer again, completing the seasonal cycle. The cumulative influx of river water and efflux of pore waters over one year of seasonal fluctuations only, is 185.5 and 108.2 m^3/m, respectively. The net efflux is negative (-77.3 m^3/m) indicating net river infiltration (Table 9).

Seasonal fluctuations have the greatest impact on the temporal and spatial distribution of solutes (Figure 30) compared to the short-term tidal fluctuations. Regardless of river stage, the greatest solute flux centered on the junction of river surface and riverbank. There was almost zero oxygen remaining in the vadose zone after the water table fell. This indicates that aerobic respiration and iron oxidation easily consumed the oxygen. Since the aquifer is capped by a silt layer which likely remained saturated, the vadose zone above the water table was assumed to not be connected to the atmosphere.

The Fe(II) concentration was greatly depleted adjacent to the bank under the combined influence of iron oxidation and dilution from river. The precipitated FeOOH followed the oxygen plume as river water infiltrated into the aquifer. The PNRB reached its maximum landward horizontal extent at maximum river stage in September (t=90 d) (Figure 29 (a)). At this time, a substantial influx of water occurred in response to the large hydraulic gradient. Following this peak river stage fell faster than the groundwater table. This resulted in groundwater displacing the fresh river water. As river stage continued to fall, the PNRB gradually contracted laterally towards the river due to

reductive dissolution of the newly formed FeOOH below river as well as in the unsaturated zone near upper part of the bank.

The PNRB reached its maximum riverward horizontal extent at the river stage nadir in March (t=270 d). As river recovered to its initial stage, some of the reduced FeOOH re-precipitated along the bank. The total lateral extent of the of PNRB formed by one year of seasonal fluctuations in the Meghna River stage is approximately 60 m across the aquifer. The average depth was approximately 3 m. The faster precipitation and slower reduction of FeOOH is caused by the magnitude difference in the kinetic rates (Table 7).

The accumulated FeOOH mass showed seasonal fluctuations as river stage rose and fell (Figure 31). The mass reached its maximum of 3.2 kg/m in August (t=70 d) and slowly decreased and stabilized to around 2.0 kg/m after a year.

4.4.6 Arsenic Mobilization from PNRBs under Sustained Groundwater Pumping

River recharge induced by groundwater pumping strongly mobilized As into the aquifer (Case 9) (Figure 32). The average flow velocity towards aquifer was 220 m/yr. A retardation factor of 20 was calculated from the model, which is typical for grey sand aquifer in Bangladesh [*Radloff et al.*, 2011]. After 360 d simulations, the arsenic plume with concentration of 10 µg/L moved 50 m across the aquifer. The highest concentration of As (55 µg/L) was found at the mean river stage line. In comparison, using a retardation factor of 1 results in most of the aquifer contaminated with As concentration over 50 µg/L within two month (data not shown). Dissolved Fe(II) was entirely flushed out the aquifer. Although the accumulated mass of FeOOH continued to drop, a

significant amount of PNRB was still forming along the bank. In addition, the extent of oxygen plume was limited by aerobic respiration with *in situ* DOC in the aquifer.

4.5 Discussion

4.5.1 The roles of tidal and seasonal fluctuations on PNRB formation

Within a homogeneous, isotropic riverbank aquifer, tidally- and seasonally-induced fluctuations in river stage lead to complex and highly dynamic groundwater flowpaths and solute distribution patterns. These greatly altered the redox conditions in the aquifer and caused alternating precipitation and dissolution of reactive FeOOH minerals. In shallow aquifers in Bangladesh, As concentrations are strongly controlled by redox conditions and correlated with iron content [*Nickson et al.*, 1998]. The modeling performed in our study predicts that during periods of groundwater discharge in the dry season, reducing conditions prevail and only a thin PNRB forms along the bank which traps the discharging As in the groundwater. As river stage rises rapidly in the early monsoon [*Knappett et al.*, 2016] or during periods of irrigation pumping [*Berube et al.*, 2017], river water recharging the aquifer brings oxygen and precipitates more Fe-oxide which may locally, lower As concentration in the aquifer [*Schaefer et al.*, 2016]. As river stage falls in late monsoon, discharging groundwater resumes and the newly-formed Fe-oxide may be reduced in the presence of reductants (DOC) and release As subsequently (Figure 34). [*Fendorf et al.*, 2010] reported that low-As concentrations in pore waters are consistently associated with orange sand where Fe(III) oxides are present, whereas elevated As concentrations are often, though not always, associated with grey sand indicative of coatings of reduced or mixed-valence Fe(II+III) oxides .

Therefore, it is important to understand the processes creating PNRBs to predict the spatial distribution of As along riverbanks lining rivers around the world. However, no previous studies has reconstructed the formation of PNRBs using a transient, reactive flow and transport model, under tidal and seasonal fluctuations.

Our study showed that with tidal fluctuations alone, the combined semi-diurnal and neap-spring tides, even the smallest amplitude (i.e. 0.07 m) used in this study would rapidly increase the solid-phase FeOOH concentrations to over 50 mg/kg. The total mass of Fe-oxide reaches around 3 kg per river length within 15 days simulation period. Under the influence of annual, seasonal river stage fluctuations alone, the accumulated Fe-oxide mass across the whole aquifer reached around 2kg per river length after one year simulation. As expected, the combined tidal and seasonal fluctuations would further increase the buildup of PNRB (data not shown).

4.5.2 Implication of modeling As mobilization

Without detailed field mapping, the distribution of PNRB and the concentration of Fe-oxides (and, hence As source) could not be determined a priori. In simulating the mobilization of As from distributed sources above shallow aquifers, *Kocar et al.* [2014] assumed an infinite source of As bearing Fe-oxides within surficial (0-12 m) wetland sediments to simulate As release driven by the oxidation of organic matter. Within a riverbank aquifer, however, the spatiotemporal distribution of Fe-oxides is highly influenced by tidal and seasonal fluctuations, resulting in the same part of the aquifer reverting between an As source and sink. To model As mobilization, it is important to know the location of well-developed or “mature” PNRBs and the timing of seasonal or

long-term As release. The modeling approach presented here is helpful to predict the possible locations of a PNRB in a riverbank.

A multi-dimensional model was necessary to reveal the complex flow field, particularly along a sloped bank. As the river stage rises and falls, the inundation area above the aquifer is highly variable and groundwater flows in both horizontal and vertical directions. A 1-D tube flow model is too simplified to represent such dynamic flowpath. [*Postma et al.*, 2016a] showed that it would take 1,200 years to accumulate the maximum observed dissolved As concentrations of 600 µg/L by assuming a 1-D tube model with a constant infiltration rate of 0.5 m/year. However, Fe-oxide precipitated much faster at the intercept between river stage and bank where larger influx was observed compared to the rest of the aquifer. Thus it may take shorter amount of time for the PNRB to build up adjacent to the bank and release As under reducing condition.

4.5.3 Limitations of this study

Homogeneous and isotropic aquifer were assumed in our model for simplification purposes, however, this commonly will not reflect field conditions. Confining layers (i.e. silt or clay sediment) along riverbanks limit mixing between river water and groundwater. Based on their observations from multiple sites 5-20 km south of our study area along the Meghna River [*Jung et al.*, 2015] proposed a conceptual model wherein the presence of silty-clay surficial deposits limited the infiltration of oxic surface water and the formation of an PNRB. In our field site, a silty layer was observed on top of the sandy aquifer with K an order of magnitude lower than the aquifer [*Shuai et al.*, 2017b], indicating that our simulation of the size of PNRB predicted for our field

site might be overestimated. Indeed, the mapped FeOOH and MnOOH layers at our field site indicated the PNRB was confined to the supper 2 m of the riverbank sediment [*Berube et al.*, 2017].

In addition to oxygen, other electron acceptors such as nitrate and manganese (Mn(IV)) may contribute to the oxidation of Fe(II) within the aquifer which can then trap dissolved As [*Harvey et al.*, 2002; *Burgin and Hamilton*, 2007]. [*Harvey et al.*, 2002] found that As concentration declined within hours after injection of nitrate into the aquifer. They suspected As was adsorbed on Fe-oxides precipitated by microbial reduction of nitrate coupled to iron oxidation. Abundant nitrate concentrations were found in the river (~2 mg/L) and riverbank aquifer (4 ~ 12 mg/L) at our site which may suggest additional supply of oxidant.

Adsorption of Fe(II) onto sediments and precipitation through other compounds such as siderite ($FeCO_3$) was not considered in the model. [*Postma et al.*, 2016a] found that 90% of Fe(II) released from Fe-oxide reduction had been re-precipitated and siderite was believed to be the major component of sedimentary Fe(II). In our field site, coring samples taken from riverbed directly adjacent to low tide line was found sign of presence of siderite [*Berube et al.*, 2017]. Additionally, precipitation of Fe(II) favored Fe-oxide reduction by removing carbonate ions and dissolved Fe(II) from solution (Table 6). Siderite precipitation and dissolution of Fe-oxides thus have buffering effect on the concentration of Fe(II) in the solution [*Kocar et al.*, 2014; *Postma et al.*, 2016a]. Therefore, our model may overestimate the mass of FeOOH by ignoring adsorption of Fe(II) and precipitation of Fe(II) through other sinks.

4.6 Conclusions

A 2-D, variably saturated, transient, biogeochemical reactive flow and transport model was developed to evaluate the impact of tidal and seasonal river stage fluctuations on PNRB formation within riverbank aquifers. Simulations showed that the volumes of water exchanged between river and aquifer, flow velocities, and flowpath lengths, and solute transformation rates were strongly affected by the frequency of tidal fluctuations. Semi-diurnal tides drove more water exchange across the river-aquifer interface compared to neap-spring tides over the same 14 day simulation period. Particle tracking revealed longer flowpaths and prolonged pore-water residence times with more frequent river fluctuations. The lateral extent of PNRBs greatly exceed the anoxic-oxic boundary when the river stage is low. At any given point in time, the highest rate of FeOOH precipitation occurred at the junction between the mean river stage and the riverbank. More frequent river stage fluctuations increase the biogeochemical reaction rates resulting in faster accumulation of Fe-oxides within the PNRB.

Sensitivity analyses were conducted varying K and tidal fluctuation amplitude. Higher K induced a greater penetration depth of solutes and the formation of a deeper PNRB whereas higher river stage fluctuation amplitude caused a greater lateral expansion of the PNRB. Increasing either amplitude or K led to faster accumulation of FeOOH mass. Seasonal fluctuations greatly altered the spatial distribution of PNRB as it has larger contact area between river and aquifer compared to tidal fluctuations. As a result, the horizontal length for PNRB span almost 60 m across the aquifer. The spatial

distribution of the PNRB showed seasonal fluctuations as a result of interplay between iron oxidation and reductive dissolution of FeOOH.

Our simulations showed that even the smallest tidal fluctuations (i.e. amplitude of 0.07 m) has significant effect on PNRB formation. These PNRBs are known to trap As. Our modeling suggested that under a reversal of conditions from naturally gaining to artificially losing, the As trapped within the PNRB can be mobilized to rapidly contaminate shallow aquifers. This mobilization of As from FeOOH-enriched river sediments caused by groundwater pumping has been observed in a field study near Hanoi, Vietnam [*Stahl et al.*, 2016]. In the absence of an PNRB, the intrusion of river water into shallow aquifers under the influence of groundwater pumping may present little threat to groundwater quality [*Postma et al.*, 2016b].

Our study found that tidal and seasonal river stage fluctuations accelerate the formation of PNRBs and broadened their spatial extent. This knowledge can be used to predict where they are forming along rivers and even inform river and aquifer management strategies that will either minimize their formation in the first place, or stabilize them.

Table 5. Tidal amplitude and period

	Amplitude (m)	Period (d)
Semi-diurnal	0.14	0.52
neap-spring	0.14	14.8
seasonal	1.8	360

Table 6. Reactions used in the reactive transport model

Reaction process	Reaction equation	
Aerobic respiration	$CH_2O + O_2 \rightarrow CO_2 + H_2O$	(1)
Fe(II) oxidation	$4Fe^{2+} + O_2 + 6\ H_2O \rightarrow 4FeOOH + 8\ H^+$	(2)
FeOOH reduction	$CH_2O + 4FeOOH{\cdot}(H_3AsO_3)_x + 6H^+ \rightarrow CO_3^{2-} + 4Fe^{2+} + 6H_2O + 4x\ H_3AsO_3$	(3)
POC dissolution	$POC \rightarrow DOC$	(4)
As adsorption to aquifer solids	$H_3AsO_3 + \equiv Sediment = Sediment{\cdot}(H_3AsO_3)$	(5)

Note: x is the As/Fe molar ratio, i.e. 0.089

Table 7. Model flow and biogeochemical parameters

Parameter	Value	Unit	Reference
Flow parameters			
Hydraulic conductivity (K)	22.5	m/d	[*Shuai et al.*, 2017b]
Porosity	0.35		
Longitudinal Dispersivity (DL)	1	m	
Transversal Dispersivity (DL)	0.1	m	
Residual water content ()	0.1		
van Genutchen (α)	1	1/m	
van Genutchen (n)	2		
Diffusivity	1.00E-10	m^2/s	
Bulk density	1.60E+03	kg/m^3	
Solute and biogeochemical parameters			
O2 concentration in the river	7.4	mg/L	Field
DOC concentration in the river	3	mg/L	Field
DOC concentration in the aquifer	6.5	mg/L	Field
Fe(II) concentration in the aquifer	30	mg/L	Field

Table 7 Continued

Parameter	Value	Unit	Reference
Oxygen inhibition constant (Ki)	1	mg/L	[*Gu et al.*, 2012]
Mass transfer coefficient (alpha)	5.0E-05	1/h	[*Gu et al.*, 2007]
Distribution coefficient of DOC (Kd)	50	L/kg	[*Gu et al.*, 2007]
aerobic respiration rate constant (k1)	1.1E-06	mol/(m^3*s)	[*Gu et al.*, 2012]
Iron oxidation rate constant (k2)	4.2E-04	m^3/(s*mol)	[*Liu et al.*, 2017]
Reductive dissolution rate constant (k3)	2.8E-08	1/s	[*Liu et al.*, 2017]
Half saturation constant for O2 (KO2)	1	mg/L	[*Gu et al.*, 2012]
Half saturation constant for DOC (KDOC)	2	mg/L	[*Gu et al.*, 2012]
Langmuir sorption K	5.4	L/kg	[*Kocar et al.*, 2014]
Langmuir sorption C	1.5	mg/kg	[*Kocar et al.*, 2014]
As-Fe mmol/mol ratio	0.089		[*Datta et al.*, 2009]

Table 8. Characteristic of the numerical experiments

Case	River BC	Inland BC	Simulation time (d)	K (m/d)	Amplitude (m)	As release
1 (base case)	semi-diurnal and neap-spring	constant (+)	14	22.5	0.14/0.14*	No
2	semi-diurnal only	constant (+)	14	22.5	0.14	No
3	neap-spring only	constant (+)	14	22.5	0.14	No
4	seasonal	seasonal	360	22.5	1.8/1.8	No
5	neap-spring only	constant (+)	14	11.25	0.14	No
6	neap-spring only	constant (+)	14	45	0.14	No
7	neap-spring only	constant (+)	14	22.5	0.28	No
8	neap-spring only	constant (+)	14	22.5	0.07	No

Note: + sign indicates gaining river condition with constant groundwater table 0.14 m higher above mean river stage (18 m);

* River fluctuation amplitude/groundwater fluctuation amplitude

Table 9. Calculated influx and efflux across river-aquifer interface

Case	Influx (m^3/m)	Efflux (m^3/m)	Net Efflux (m^3/m)
1	9	18.6	9.6
2	8.7	18.2	9.5
3	0.4	10.7	10.3
4	185.5	108.2	-77.3

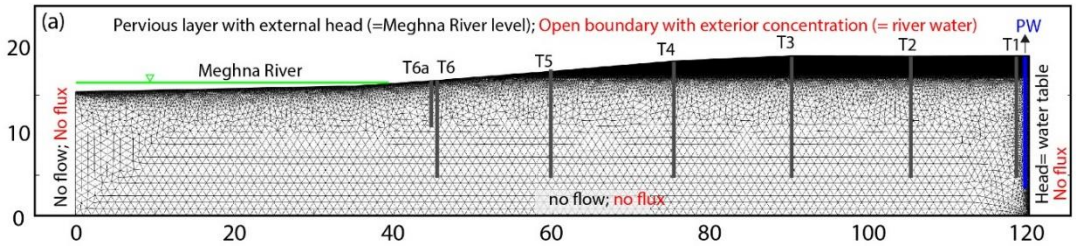

Figure 17. Model domain and flow (black) and solute (red) boundary conditions. The relative locations of the monitoring wells (gray line) overlapped with the aquifer. Mean river stage is indicated using a green line and the location of pumping well (blue line) is at the farthest end of the well transect. The mesh grids are uniform across the aquifer with finer mesh in the unsaturated zone.

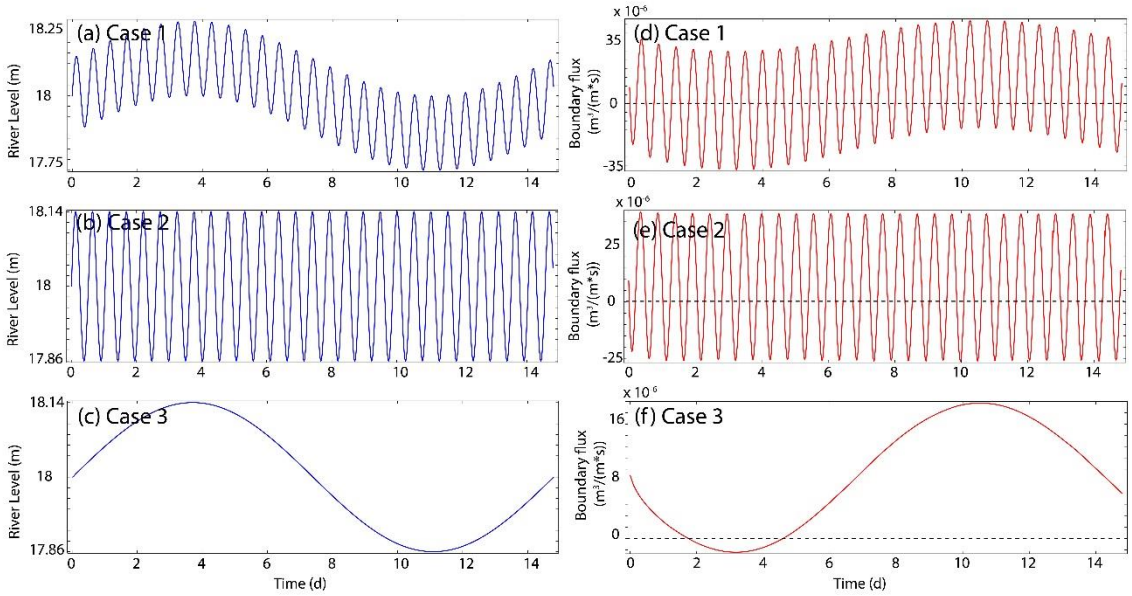

Figure 18. Tidal fluctuations (blue line) and boundary flux (red line). (a-c) River stage for Case 1 (combined tides), Case 2 (semi-diurnal tide only) and Case 3 (neap-spring tide only); (d-f) Boundary flux for Case 1-3. The dashed line represents zero boundary flux. Negative values indicate influx and positive values indicate efflux.

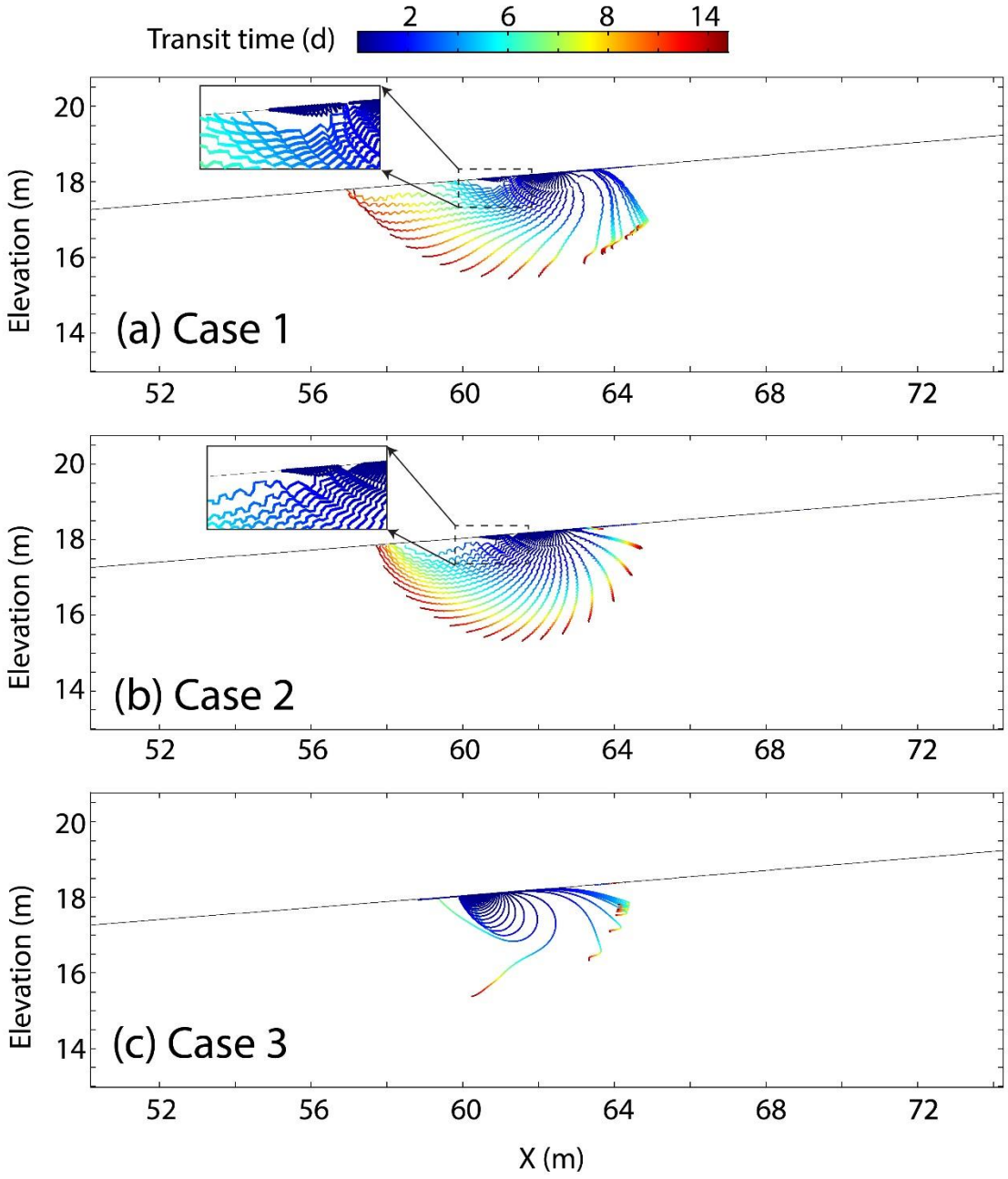

Figure 19. Particle tracking and its transit time. (a) Case 1 (combined tides); (b) Case 2 (semi-diurnal tide); (c) Case 3 (neap-spring tide). The black boxes in Case 1 and Case 2 zoom in the particle pathway. The color associated with each line represents the particle transit time.

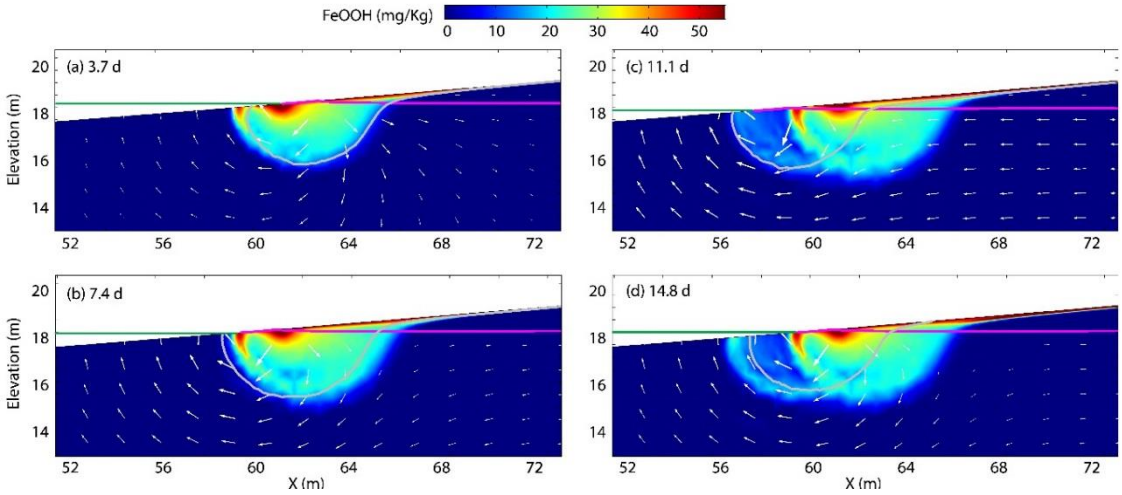

Figure 20. Time snapshots of FeOOH plume during neap-spring tide (Case 3). White arrows represent the relative magnitude and direction of groundwater flow. Green line indicates river stage and purple line indicates groundwater table. Grey contour shows the oxic-anoxic boundary.

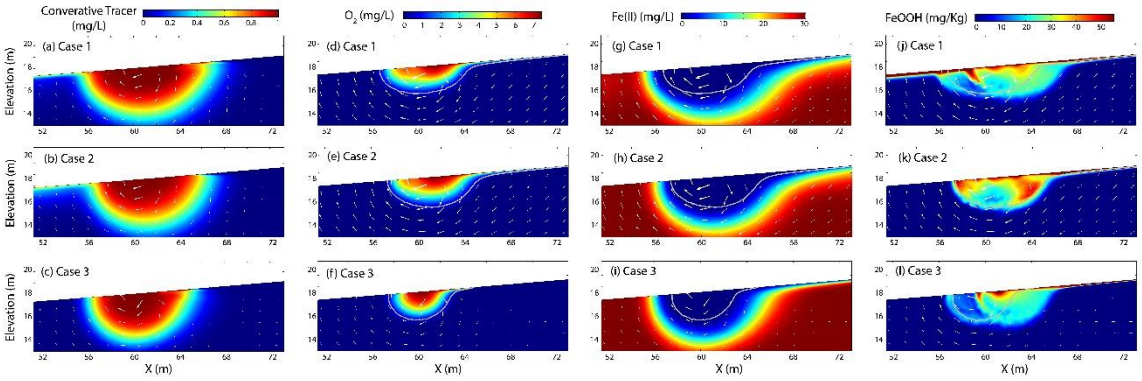

Figure 21. Solute concentration after 14.8 d simulations for (a) Case 1 (combined neap-spring and semi-diurnal), (b) Case 2 (semi-diurnal tide only), (c) Case 3 (neap-spring tide only). The gray contour line indicates the oxic-anoxic boundary.

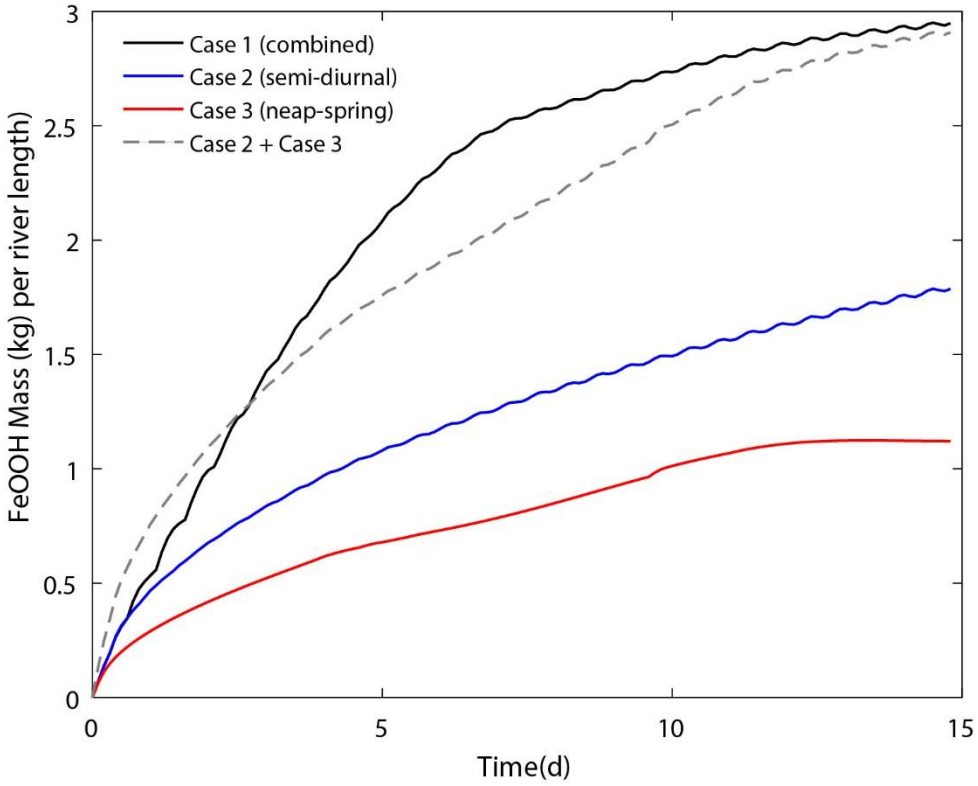

Figure 22. The mass of FeOOH accumulated in the aquifer during 14.8 d simulation period under Case 1~3. The dashed gray line is the sum of the blue line (Case 2) and red line (Case 3).

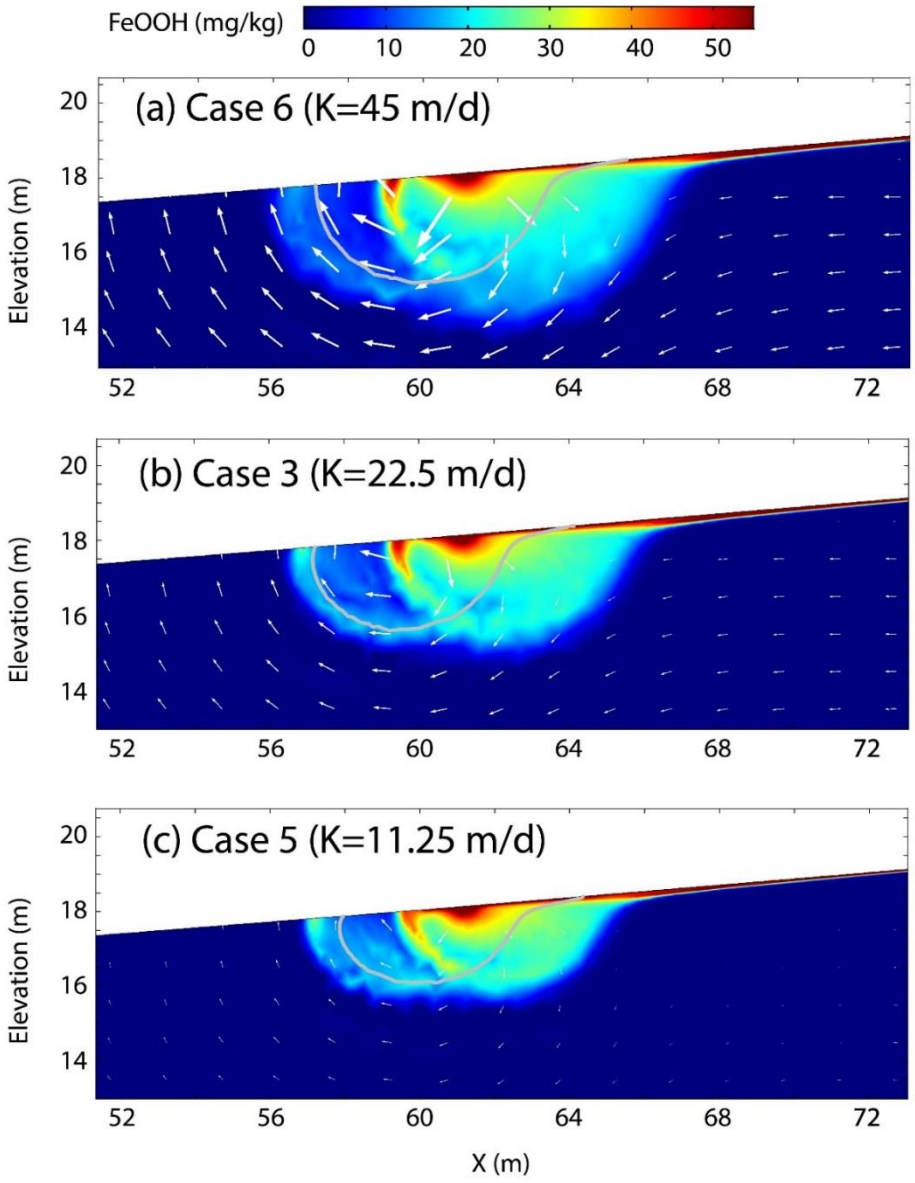

Figure 23. Concentration of FeOOH after 14.8 d simulation by varying hydraulic conductivity (K) using Case 3 as the base scenario. (a) Case 6 (K=45 m/d), (b) Case 3 (K=22.5 m/d) and (c) Case 5 (K=11.25 m/d). The gray contour line indicates the oxic-anoxic boundary.

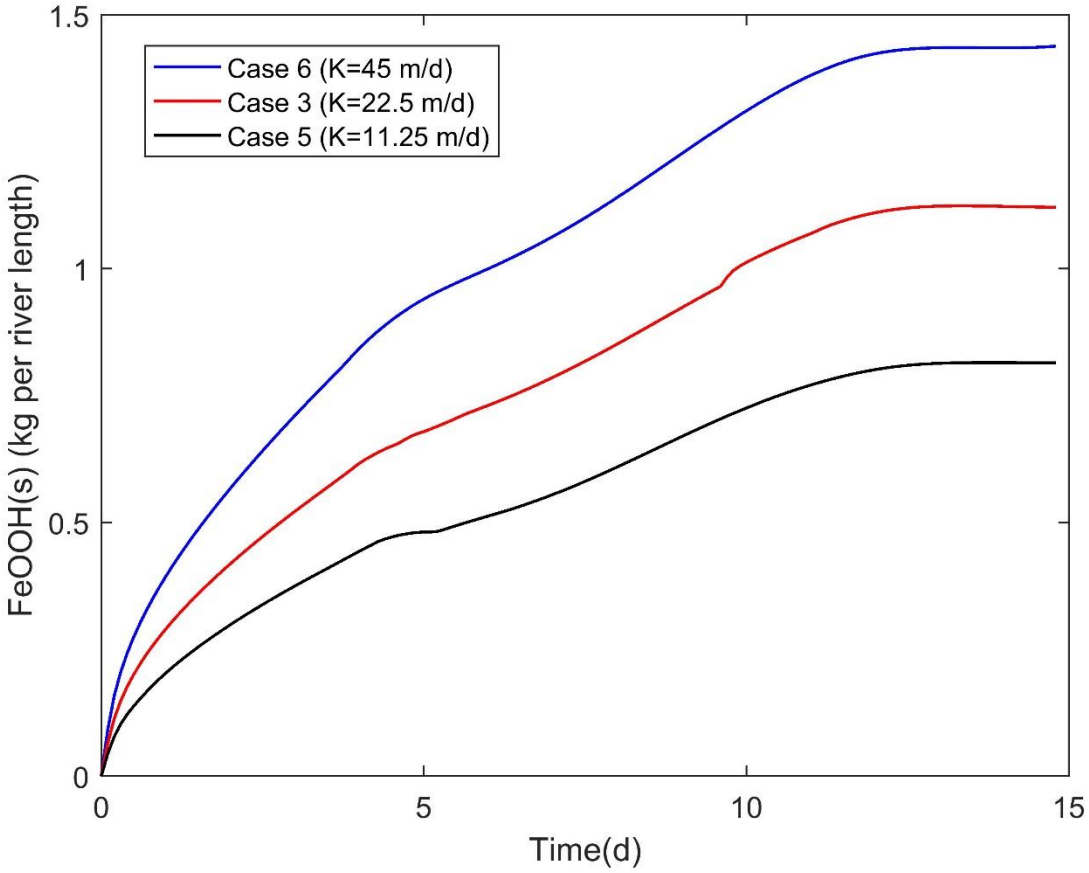

Figure 24. The mass of FeOOH accumulated in the aquifer during 14.8 d simulation period with varying hydraulic conductivities under Case 3, 5 and 6.

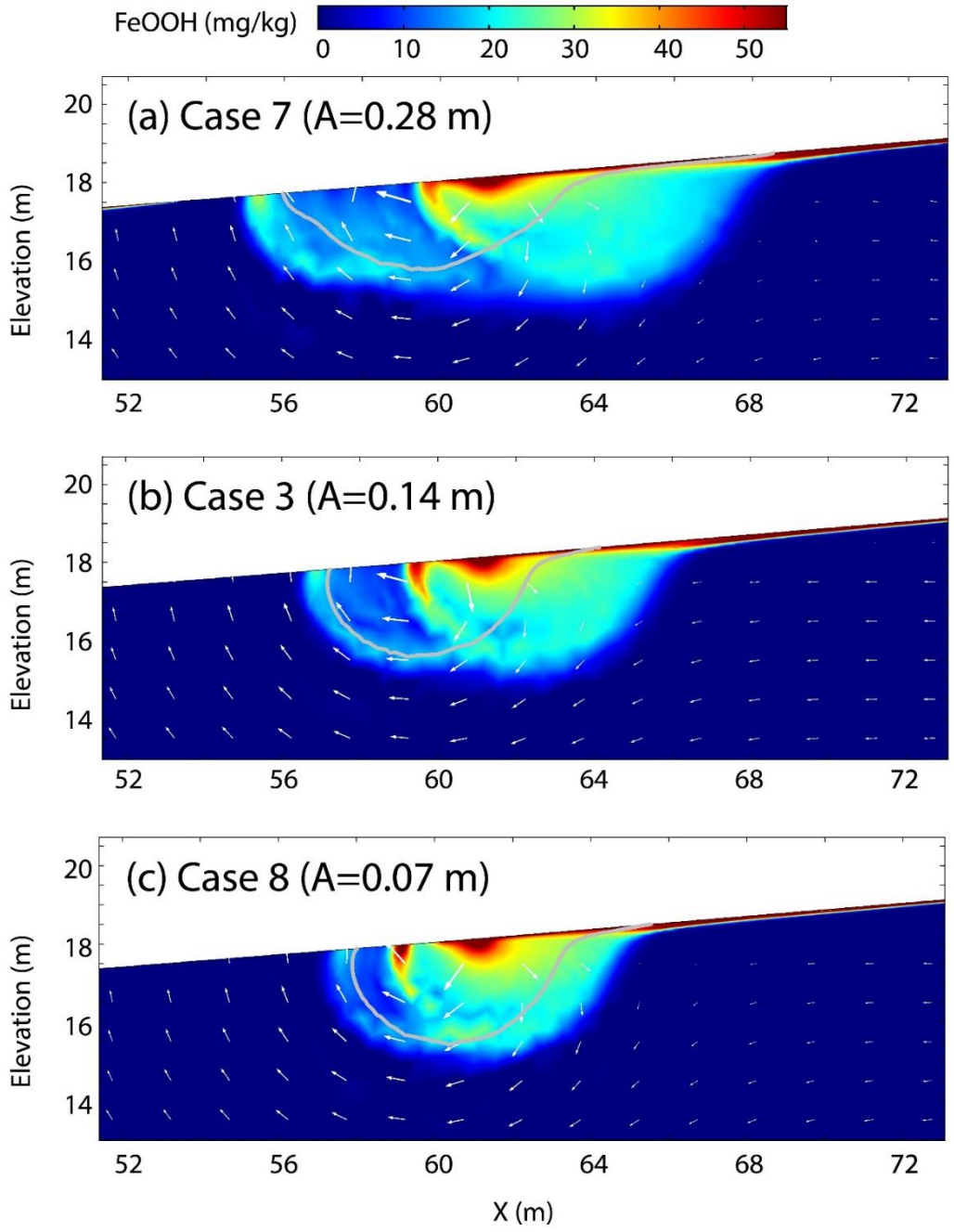

Figure 25. Concentration of FeOOH after 14.8 d simulation for (a) Case 7 (A=0.28 m), (b) Case 3 (A=0.14 m) and (c) Case 8 (A=0.07 m). The gray contour line indicates the oxic-anoxic boundary.

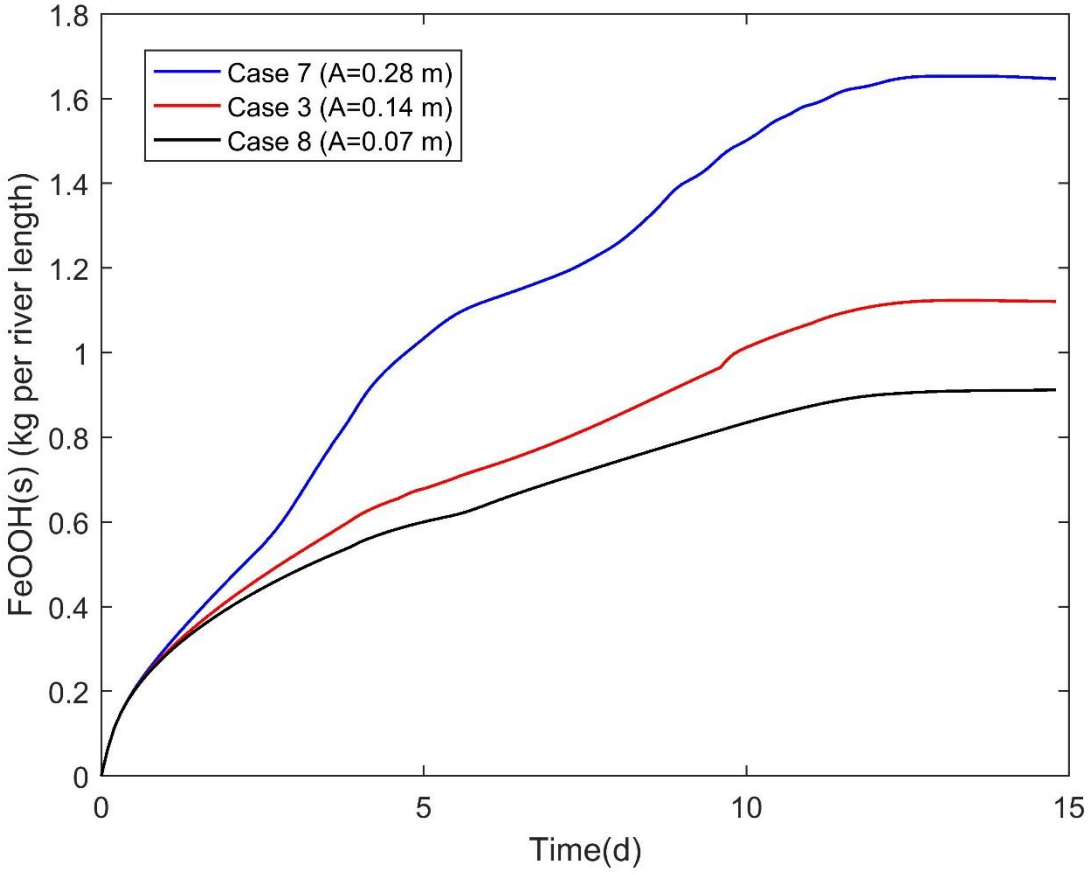

Figure 26. The mass of FeOOH accumulated in the aquifer during 14.8 d simulation period with varying tidal amplitudes under Case 3, 7 and 8.

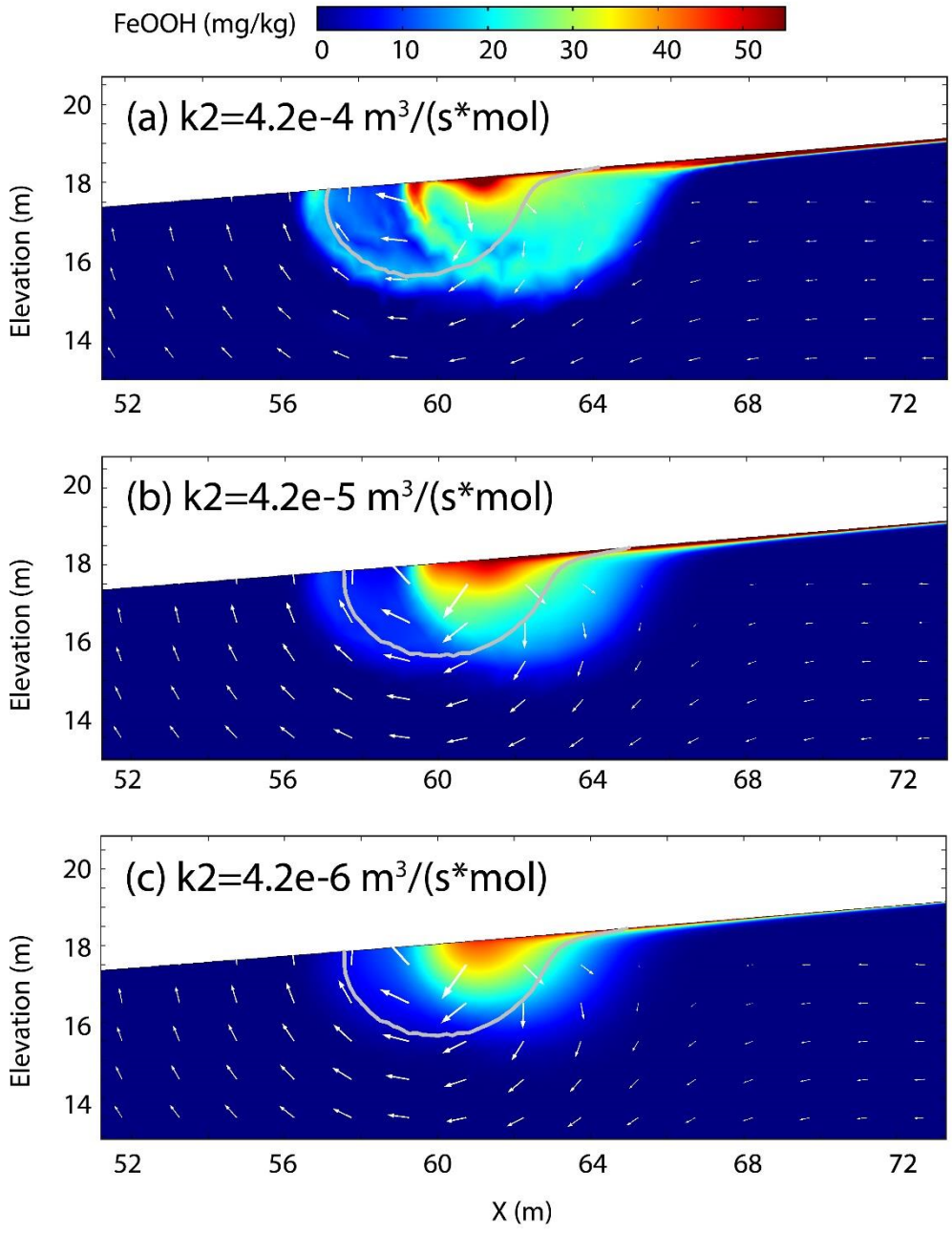

Figure 27. The mass of FeOOH accumulated in the aquifer after 14.8 d simulation period with different iron oxidation rate constants (k2). (a) rate constant of 4.2e-4 m^3/(s*mol), (b) rate constant of 4.2e-4 m^3/(s*mol), (c) rate constant of 4.2e-4 m^3/(s*mol). The gray contour line indicates the oxic-anoxic boundary.

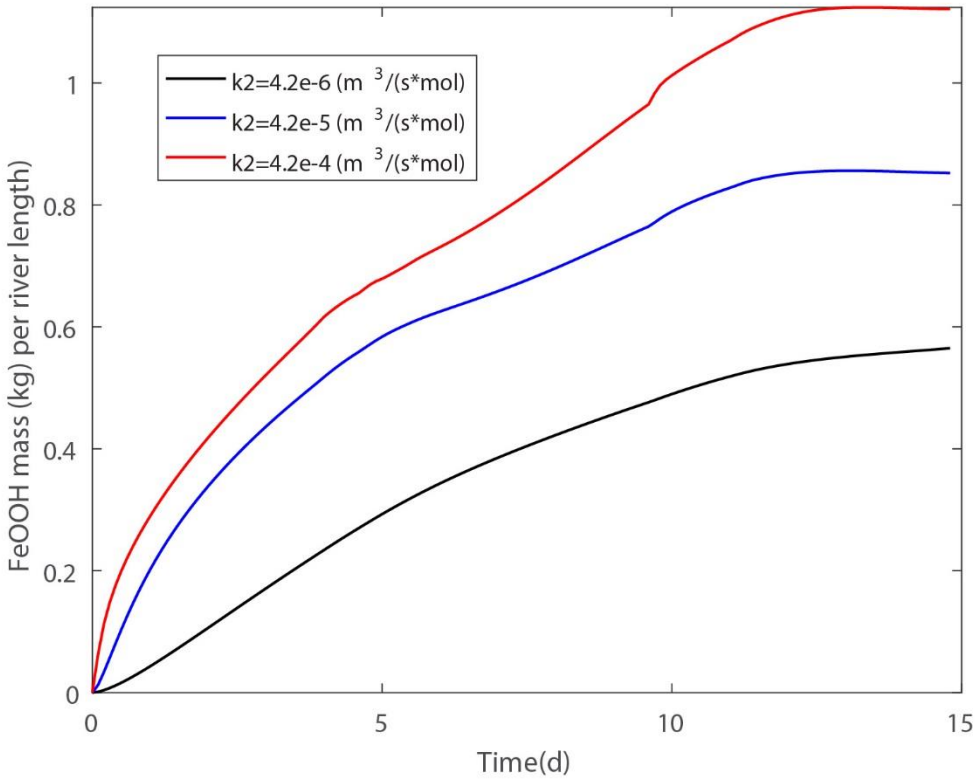

Figure 28. The mass of FeOOH accumulated in the aquifer during 14.8 d simulation period under different iron oxidation rate constants (k2).

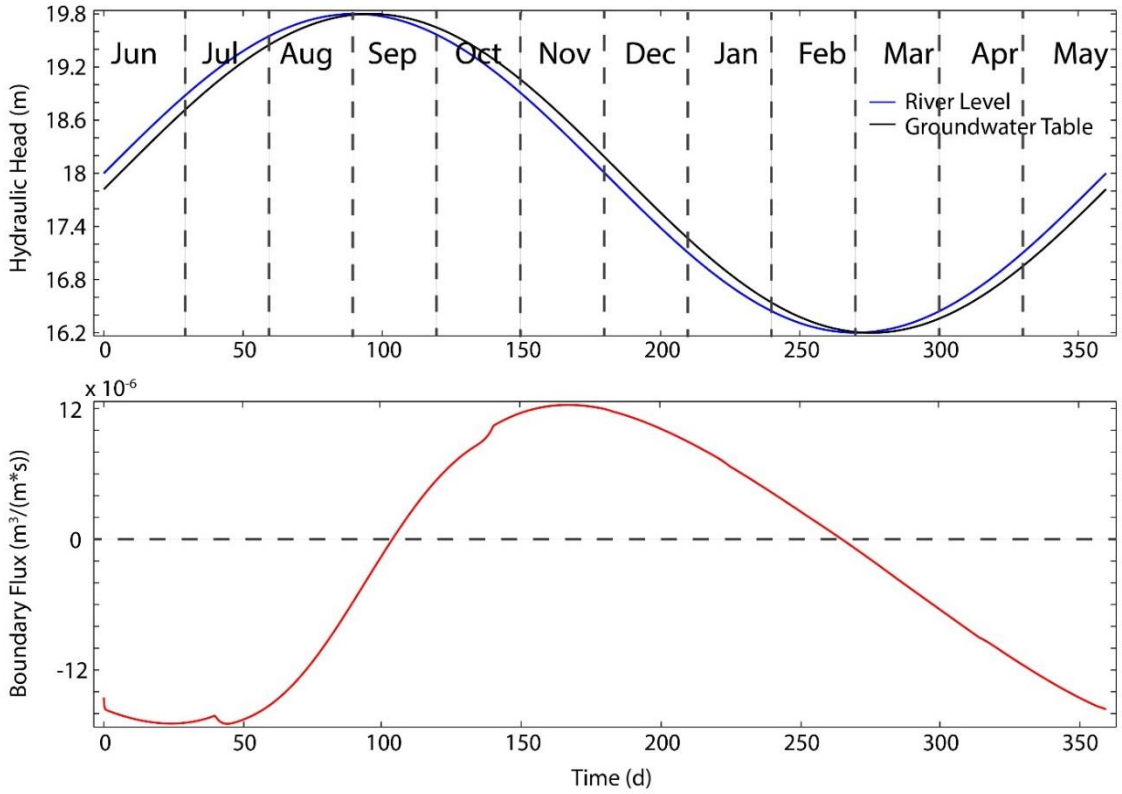

Figure 29. Seasonal river (blue line) and groundwater (black line) boundary along with its boundary flux (red line). The months are shown along with days as reference.

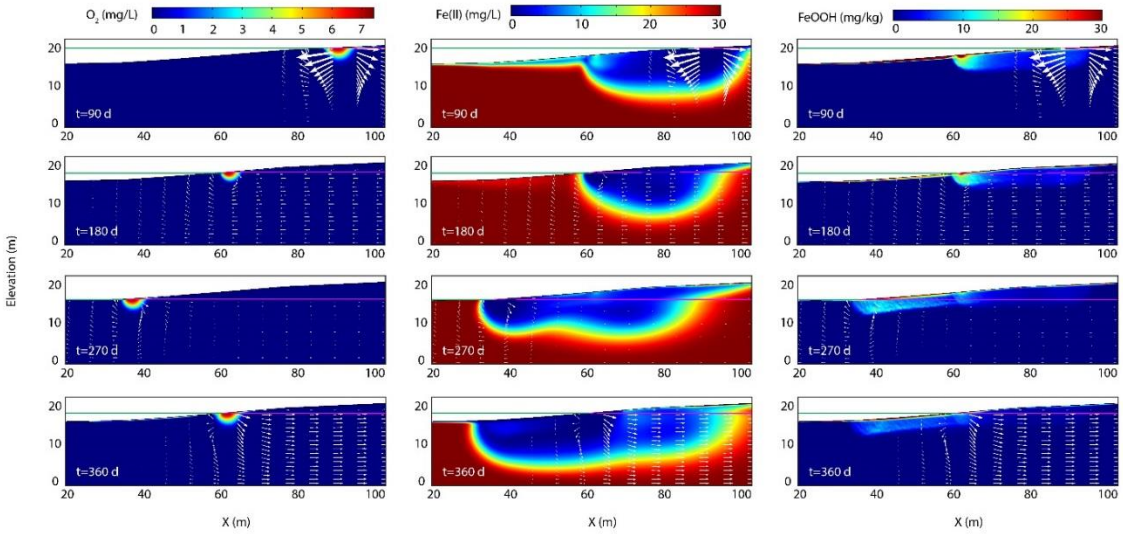

Figure 30. Snapshots showing the concentration of O2, Fe(II) and FeOOH over one year simulation with seasonal fluctuation. White arrows represent the relative magnitude and direction of groundwater flow. Green line indicates river stage and purple line indicates groundwater table.

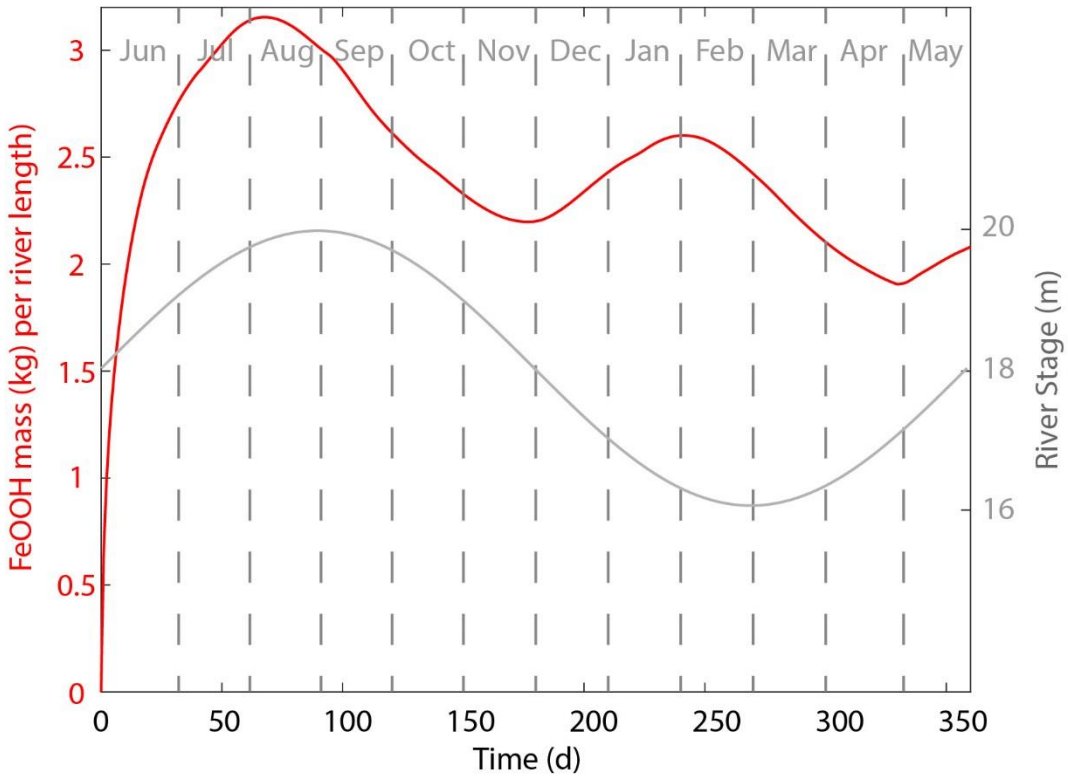

Figure 31. The mass of FeOOH accumulated in the aquifer during one year simulation period under the influence of seasonal fluctuation. Also shown are the months and the seasonal river stage.

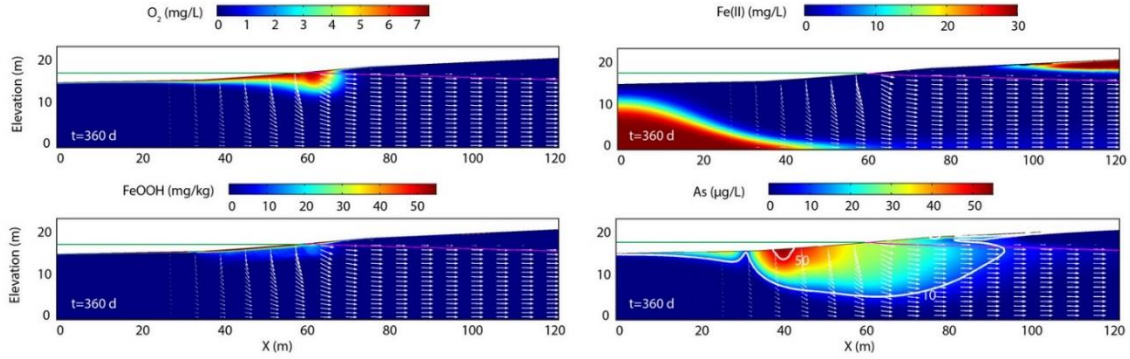

Figure 32. Solutes concentration after steady losing (360 d). White arrows represent the relative magnitude and direction of groundwater flow. Green line indicates river stage and purple line indicates groundwater table. The white contour line shows As concentration of 10 and 50 µg/L, respectively.

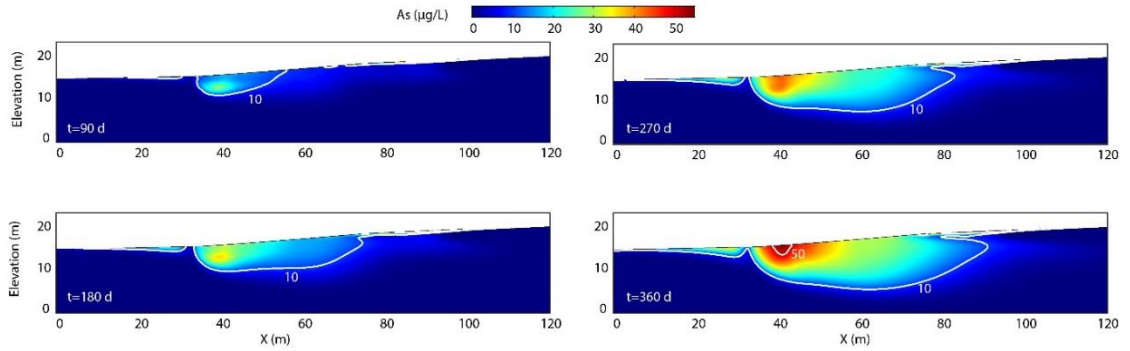

Figure 33. Snapshots of As concentration under steady losing river condition. The white contour line shows As concentration of 10 and 50 µg/L, respectively.

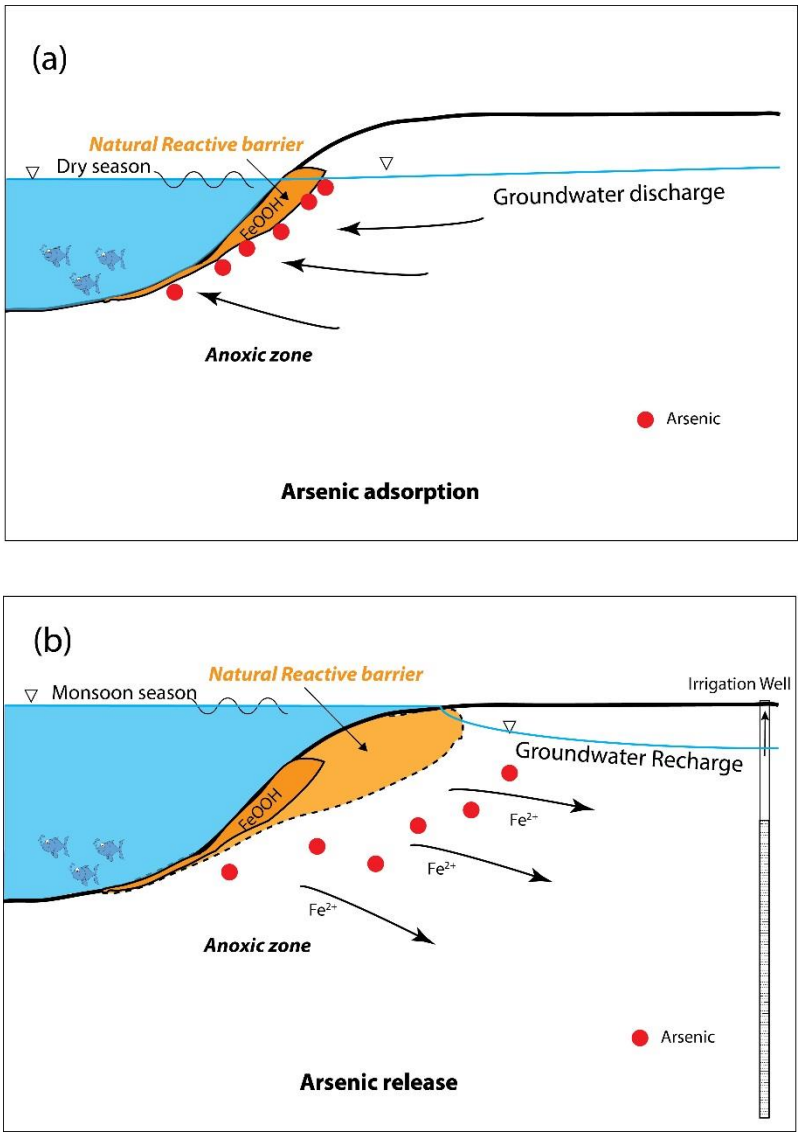

Figure 34. Conceptual model shows (a) The formation of PNRB and Arsenic adsorption during groundwater discharge, and (b) The expansion of PNRB and subsequent Arsenic release during groundwater recharge. Red circle represents arsenic. Black arrows indicate groundwater flow direction.

CHAPTER V

CONCLUSIONS AND FUTURE WORK

5.1 Conclusions

This dissertation uses field investigations and numerical modeling to study biogeochemical cycles, N, Fe and As, under one central theme—groundwater and surface water interactions induced by periodic river fluctuations. The research couples hydrologic dynamics with biogeochemical reactions and reveals the spatial and temporal behavior of reactive solutes as they are transported and transformed in the hyporheic zone. The second chapter explored the role of the HZ in removing nitrate from the river, when there is dam operations upstream. While many of the previous studies have investigated nitrogen cycling driven by river morphology such as point bars and riverbed dunes, the work presented here has shown that transient river stage fluctuations are another important driver that enhances the biogeochemical reactions and nitrate removal within the aquifer. The work described in Chapter 3 evaluated how aquifer physical parameters would affect tidal pulse propagation and how that, in turn, would affect the accuracy of using the tidal method to estimate aquifer diffusivities. As a follow-up study, Chapter 4 investigated the impacts of tidal and seasonal river fluctuations on the transport, release and mobilization of As in the shallow aquifer in Bangladesh. Numerous studies have focused on the mechanism of As release through field and lab experiments under simple flow regime, however, my work here showed that tidal and seasonal fluctuations have significant impact on the spatial-temporal distribution of Fe-

oxides. Human impacts such as irrigation pumping would further complicate our understanding of As release pathways. The key findings from each chapter are summarized below:

Chapter 2: *Denitrification in the banks of fluctuating rivers: the effects of river stage amplitude, sediment hydraulic conductivity and dispersivity, and ambient groundwater flow.* This is the first study to illustrate the role of bank storage induced by periodic river stage fluctuations on nitrification and denitrification within a riparian zone. Hotspots of biogeochemical reactions were found with nitrification occurring in the shallower zone adjacent to the bank where oxic river water and anoxic groundwater mixed, whereas denitrification occurred deeper into the aquifer and below riverbed where oxygen was depleted. River fluctuations greatly enhanced biogeochemical reactions and thus the overall removal rate of nitrate from stream. However, nitrate removal efficiency (the ratio of the mass of reduced nitrate and the total mass of nitrate goes into the HZ) decreased as river stage amplitude or sediment hydraulic conductivity increased. In comparison, nitrate removal efficiency was positively correlated with the sediment dispersivity because dispersivity promoted mixing between oxidants and reductants. Of all the factors evaluated, however, the presence and direction of ambient groundwater flow had the most significant impact on nitrate removal efficiency when compared to neutral conditions. A losing river showed smaller removal efficiency (3.5%) while a gaining river showed larger removal efficiency (17.1%) compared to neutral conditions (5.4%). Our results demonstrated that daily river fluctuations created

denitrification hot spots within the HZ that would not otherwise exist under naturally neutral or gaining conditions.

Chapter 3: *The impact of the degree of aquifer confinement and anisotropy on tidal pulse propagation*. This study set out to tightly constrain the physical properties of an aquifer using different hydraulic testing methods and then evaluate the error in applying a simple 1-D analytical model to estimate physical aquifer properties. An order magnitude of difference in estimated D was observed between the pumping test analysis and the Jacob-Ferris 1D model (tidal method). We used a suite of numerical models to explain the source of discrepancy at our field site, and determine optimal physical aquifer settings where the 1-D analytical model should be used. Numerical simulations showed that the presence of a phreatic surface caused the greatest errors in the estimation of D using 1-D Jacob-Ferris model as this model assumes the aquifer is confined. Modest levels of aquifer anisotropy and confinement, however, tend to compensate for this error, resulting in more accurate estimates of D using the 1-D Jacob-Ferris model. The effect of bank slope is negligible. The Jacob-Ferris model should perform well within a riverbank unconfined aquifer with an anisotropy ratio larger than 10 or a top confining layer K that is smaller than 0.2 m/d (assuming the aquifer K is greater than 20 m/d). Aquifer diffusivity estimated with the time lag method (D_{TLM}) was more accurate than that estimated with the amplitude reduction method (D_{AAM}). When pumping tests are not feasible in some coastal areas due to time, the cost associated with treating contaminated water, or the risk of seawater intrusion, the 1D Jacob-Ferris model

combined with slug tests, borehole lithology and ERT survey is a viable alternative approach for obtaining T and S.

Chapter 4: Modeling Natural Reactive Barrier formation and arsenic mobilization in a riverbank aquifer under the influence of tidal and seasonal fluctuations. This chapter is built on Chapter 3 using the aquifer properties (mainly K) characterized and the numerical flow model that was developed. For Chapter 4, however, I have developed a 2-D reactive transport model to evaluate the impact of tidal forcing and seasonal fluctuation on PNRB formation within the HZ lining a Fe-reducing aquifer that is discharging to a river, and the subsequent mobilization of As into a riverbank aquifer under the influence of groundwater pumping. Simulations predicted the exchange between river water and groundwater, flow and solute transport were strongly impacted by the frequency of tidal fluctuations. More frequent river stage fluctuations enhanced biogeochemical reactions and induced faster buildup of PNRB and larger mass of FeOOH. The spatial extent of the PNRB coincided with the anoxic-oxic boundary with intense FeOOH precipitation occurring at the intercept between mean river stage and riverbank. Sensitivity analyses were conducted by varying K and tidal fluctuation amplitude. Higher K induced more in depth penetration of solutes and the formation of PNRB whereas higher amplitude caused greater expansion of PNRB horizontally. However, increasing either amplitude or K led to faster accumulation of FeOOH mass. In contrast, seasonal fluctuations had the greatest impact on spatial formation of PNRB with the lateral extent of the PNRB (orthogonal to the river shore) spanning 60 m across the top of the aquifer. Our simulations showed that even small

tidal fluctuations (i.e. amplitude of 0.14 m) has significant effect on PNRB formation and thus the trapping and release of As. Therefore, tidal fluctuations effects should be taken into account when predicting the accumulation of reactive Fe-oxides and toxic metals such as As along rivers influenced by tidal fluctuations or river stage regulations.

5.2 Future Work

This dissertation provides new insights into the transport and fate of nutrients and contaminants in dynamically fluctuating rivers. However, there are some limitations in these studies and new questions that need to be addressed in the future work.

For our nitrogen cycling study in Chapter 2, we used a 2-D model assuming homogeneous and isotropic aquifer with constant river-source solute concentration. First of all, our model ignored the third dimension which may include bedforms, point bars and channel-spanning logs along the river reach. These factors may contribute to the removal of nitrate and increase the removal efficiency. Second, the solute concentration in the river may vary over time during high flows and low flows. These variation in concentration may not be significant during one day simulation period. However, if multi-day simulations are considered, the solute concentration in the river may affect the biogeochemical cycle within the HZ. In addition, the lags between the flood pulses and solute pulses cause asynchronous peak concentrations arriving over increasingly disparate time frames with distance downstream. As a result, the biogeochemical reactions diminish as the lag between the flood and solute wave increases. Finally, the heterogeneity of aquifer may play an important role in creating spatial denitrification hotspots. Therefore, a more robust 3-D model considering changing river solute

concentration and aquifer heterogeneity with long term simulations would provide a more realistic understanding of the N cycle. In fact, some of the work is currently under way with Bayani Cardenas (University of Texas, Austin) and Bethany Neilson (Utah State University). They will apply a reach-scale surface water model incorporating our simulation outputs from 2-D river transect to investigate the nitrogen cycling across the whole river reach.

For As mobilization study in Chapter 4, we have investigated the process of the formation of PNRB and As release. However, the initial adsorption of As onto Fe-oxide was not explicitly simulated. Instead, a constant As/Fe ratio was used to incorporate As into Fe-oxide, constrained by field observations. In addition, only a limited set of reactions with few electron donor and acceptors were considered in the model, which may oversimplify the field observations. For example we did not consider Fe(II) oxidation by nitrate. More importantly, many of our kinetic rate constants were not directly measured and were adopted from other studies working in similar environments in Vietnam or Bangladesh. In future work, *in situ* field experiments should be done to identify and constrain the most important biogeochemical parameters such as iron oxidation rate and reduction rate in the presence of varying concentrations of oxygen and nitrate. Further data collection from field sites, especially the mapping of spatial distribution of Fe and As within an PNRB, will provide an excellent testing ground for the modeling approach pioneered in this dissertation.

REFERENCES

Abarca, E., H. Karam, H. F. Hemond, and C. F. Harvey (2013), Transient groundwater dynamics in a coastal aquifer: The effects of tides, the lunar cycle, and the beach profile, *Water Resour. Res.*, *49*(5), 2473–2488, doi:10.1002/wrcr.20075.

Arntzen, E. V., D. R. Geist, and P. E. Dresel (2006), Effects of fluctuating river flow on groundwater/surface water mixing in the hyporheic zone of a regulated, large cobble bed river, *River Res. Appl.*, *22*(8), 937–946, doi:10.1002/rra.947.

Ayotte, J. D., M. Belaval, S. A. Olson, K. R. Burow, S. M. Flanagan, S. R. Hinkle, and B. D. Lindsey (2015), Factors affecting temporal variability of arsenic in groundwater used for drinking water supply in the United States, *Sci. Total Environ.*, *505*, 1370–1379, doi:10.1016/j.scitotenv.2014.02.057.

Baken, S., P. Salaets, N. Desmet, P. Seuntjens, E. Vanlierde, and E. Smolders (2015), Oxidation of iron causes removal of phosphorus and arsenic from streamwater in groundwater-fed lowland catchments, *Environ. Sci. Technol.*, *49*(5), 2886–2894, doi:10.1021/es505834y.

Bardini, L., F. Boano, M. B. Cardenas, R. Revelli, and L. Ridolfi (2012), Nutrient cycling in bedform induced hyporheic zones, *Geochim. Cosmochim. Acta*, *84*, 47–61, doi:10.1016/j.gca.2012.01.025.

Bardini, L., F. Boano, M. B. Cardenas, A. H. Sawyer, R. Revelli, and L. Ridolfi (2013), Small-scale permeability heterogeneity has negligible effects on nutrient cycling in streambeds, *Geophys. Res. Lett.*, *40*(6), 1118–1122, doi:10.1002/grl.50224.

Bates, P. D., M. D. Stewart, A. Desitter, M. G. Anderson, J.-P. Renaud, and J. A. Smith

(2000), Numerical simulation of floodplain hydrology, *Water Resour. Res.*, *36*(9), 2517–2529, doi:10.1029/2000WR900102.

Bearup, L. a., A. K. Navarre-Sitchler, R. M. Maxwell, and J. E. McCray (2012), Kinetic metal release from competing processes in aquifers, *Environ. Sci. Technol.*, *46*(12), 6539–6547, doi:10.1021/es203586y.

Benner, S. G., M. L. Polizzotto, B. D. Kocar, S. Ganguly, K. Phan, K. Ouch, M. Sampson, and S. Fendorf (2008), Groundwater flow in an arsenic-contaminated aquifer, Mekong Delta, Cambodia, *Appl. Geochemistry*, *23*(11), 3072–3087, doi:10.1016/j.apgeochem.2008.06.013.

Berube, M., K. Jewell, K. Myers, P. Knappett, and P. Shuai (2017), The Fate of Arsenic in Groundwater Discharged to the Meghna River, Bangladesh, *Environ. Chem.*, In prep.

Boano, F., A. Demaria, R. Revelli, and L. Ridolfi (2010), Biogeochemical zonation due to intrameander hyporheic flow, *Water Resour. Res.*, *46*(2), 1–13, doi:10.1029/2008WR007583.

Bouwer, H., and R. C. Rice (1976), A slug test for determining hydraulic conductivity of unconfined aquifers with completely or partially penetrating wells, *Water Resour. Res.*, *12*(3), 423–428, doi:10.1029/WR012i003p00423.

Briggs, M. A., F. D. Day-Lewis, J. P. Zarnetske, and J. W. Harvey (2015), A physical explanation for the development of redox microzones in hyporheic flow, *Geophys. Res. Lett.*, *42*(11), 4402–4410, doi:10.1002/2015GL064200.

Briody, A. C., M. B. Cardenas, P. Shuai, P. S. K. Knappett, and P. C. Bennett (2016),

Groundwater flow, nutrient, and stable isotope dynamics in the parafluvial-hyporheic zone of the regulated Lower Colorado River (Texas, USA) over the course of a small flood, *Hydrogeol. J.*, doi:10.1007/s10040-016-1365-3.

Burgin, A. J., and S. K. Hamilton (2007), Have we overemphasized the role of denitrification in aquatic ecosystems? A review of nitrate removal pathways, *Front. Ecol. Environ.*, *5*(2), 89–96, doi:10.1890/1540-9295(2007)5[89:HWOTRO]2.0.CO;2.

Butler, J. J. J. (1997), *The design, performance, and analysis of slug tests*, CRC Press.

Cardenas, M. B. (2009), Stream-aquifer interactions and hyporheic exchange in gaining and losing sinuous streams, *Water Resour. Res.*, *45*(6), n/a-n/a, doi:10.1029/2008WR007651.

Cardenas, M. B., and J. L. Wilson (2007), Dunes, turbulent eddies, and interfacial exchange with permeable sediments, *Water Resour. Res.*, *43*(8), n/a-n/a, doi:10.1029/2006WR005787.

Cardenas, M. B., P. C. Bennett, P. B. Zamora, K. M. Befus, R. S. Rodolfo, H. B. Cabria, and M. R. Lapus (2015), Devastation of aquifers from tsunami-like storm surge by Supertyphoon Haiyan, *Geophys. Res. Lett.*, *42*(8), 2844–2851, doi:10.1002/2015GL063418.

Chang, Y. C., D. S. Jeng, and H. D. Yeh (2010), Tidal propagation in an oceanic island with sloping beaches, *Hydrol. Earth Syst. Sci.*, *14*(7), 1341–1351, doi:10.5194/hess-14-1341-2010.

Chattopadhyay, P. B., N. Vedanti, and V. S. Singh (2015), A conceptual numerical

model to simulate aquifer parameters, *Water Resour. Manag.*, *29*(3), 771–784, doi:10.1007/s11269-014-0841-6.

Chen, X. (2000), Measurement of streambed hydraulic conductivity and its anisotropy, *Environ. Geol.*, *39*(12), 1317–1324, doi:10.1007/s002540000172.

Chuang, M. H., and H. D. Yeh (2007), An analytical solution for the head distribution in a tidal leaky confined aquifer extending an infinite distance under the sea, *Adv. Water Resour.*, *30*(3), 439–445, doi:10.1016/j.advwatres.2006.05.011.

Chuang, M. H., and H. D. Yeh (2008), Analytical solution for tidal propagation in a leaky aquifer extending finite distance under the sea, *J. Hydraul. Eng.*, *134*(4), 447–454, doi:10.1061/(asce)0733-9429(2008)134:4(447).

Chuang, M. H., and H. D. Yeh (2011), A generalized solution for groundwater head fluctuation in a tidal leaky aquifer system, *J. Earth Syst. Sci.*, *120*(6), 1055–1066, doi:10.1007/s12040-011-0128-8.

Chuang, M. H., C. S. Huang, G. H. Li, and H. D. Yeh (2010), Groundwater fluctuations in heterogeneous coastal leaky aquifer systems, *Hydrol. Earth Syst. Sci.*, *14*(10), 1819–1826, doi:10.5194/hess-14-1819-2010.

Chui, T. F. M., and D. L. Freyberg (2009), Implementing hydrologic boundary conditions in a multiphysics model, *J. Hydrol. Eng.*, *14*(12), 1374–1377, doi:10.1061/(ASCE)HE.1943-5584.0000113.

Cooper, H. H. J., and M. I. Rorabaugh (1963), Ground-water movements and bank storage due to flood stages in surface streams, *U. S. Geol. Surv., Water Supply Pap.*, *1536*, 343–366.

Curry, R. A., J. Gehrels, D. L. G. Noakes, and R. Swainson (1994), Effects of river flow fluctuations on groundwater discharge through brook trout, *Salvelinus fontinalis*, spawning and incubation habitats, *Hydrobiologia*, *277*(2), 121–134, doi:10.1007/BF00016759.

Datta, S., B. Mailloux, H. B. Jung, M. A. Hoque, M. Stute, K. M. Ahmed, and Y. Zheng (2009), Redox trapping of arsenic during groundwater discharge in sediments from the Meghna riverbank in Bangladesh, *Proc. Natl. Acad. Sci.*, *106*(40), 16930–16935, doi:10.1073/pnas.0908168106.

Dawson, D. E., M. M. Vanlandeghem, W. H. Asquith, and R. Patino (2015), Long-term trends in reservoir water quality and quantity in two major river basins of the southern Great Plains Long-term trends in reservoir water quality and quantity in two major river basins of the southern Great Plains, *Lake Reserv. Manag.*, *31*(3), 254–279, doi:10.1080/10402381.2015.1074324.

De-Marsily, G. (1986), *Quantitative hydrogeology: groundwater hydrology for engineers*, Acdemic Press, New York.

Desbarats, A. J., C. E. M. Koenig, T. Pal, P. K. Mukherjee, and R. D. Beckie (2014), Groundwater flow dynamics and arsenic source characterization in an aquifer system of West Bengal, India, *Water Resour. Res.*, *50*(6), 4974–5002, doi:10.1002/2013WR014034.

Dhar, R. K., Y. Zheng, C. W. Saltikov, K. A. Radloff, B. J. Mailloux, K. M. Ahmed, and A. Van Geen (2011), Microbes enhance mobility of arsenic in pleistocene aquifer sand from Bangladesh, *Environ. Sci. Technol.*, *45*(7), 2648–2654,

doi:10.1021/es1022015.

Duan, Y., Y. Gan, Y. Wang, Y. Deng, X. Guo, and C. Dong (2014), Temporal variation of groundwater level and arsenic concentration at Jianghan Plain, central China, *J. Geochemical Explor.*, *149*, 106–119, doi:10.1016/j.gexplo.2014.12.001.

Ensign, S. H., M. F. Piehler, and M. W. Doyle (2008), Riparian zone denitrification affects nitrogen flux through a tidal freshwater river, *Biogeochemistry*, *91*(2–3), 133–150, doi:10.1007/s10533-008-9265-9.

Erskine, A. D. (1991), The effect of tidal fluctuation on a coastal aquifer in the UK, *Ground Water*, *29*(4), 556–562, doi:10.1111/j.1745-6584.1991.tb00547.x.

Fendorf, S., H. A. Michael, and A. van Geen (2010), Spatial and Temporal Variations of Groundwater Arsenic in South and Southeast Asia, *Science (80-.).*, *328*(5982), 1123–1127, doi:10.1126/science.1172974.

Ferris, J. G. (1951), Cyclic fluctuations of a water level as a basis for determining aquifer transmissivity., *Int. Assoc. Sci. Hydrol. Publ.*, *33*, 148–155, doi:10.3133/70133368.

Fetter, C. W. (2000), *Applied hydrogeology*, Prentice hall.

Fox, A., F. Boano, and S. Arnon (2014), Impact of losing and gaining streamflow conditions on hyporheic exchange fluxes induced by dune-shaped bed forms, *Water Resour. Res.*, *50*(3), 1895–1907, doi:10.1002/2013WR014668.

Francis, B. A., L. K. Francis, and M. B. Cardenas (2010), Water table dynamics and groundwater-surface water interaction during filling and draining of a large fluvial island due to dam-induced river stage fluctuations, *Water Resour. Res.*, *46*(7),

W07513, doi:10.1029/2009WR008694.

Friesz, P. (1996), Geohydrology of stratified drift and streamflow in the Deerfield River Basin, northwestern Massachusetts, *U.S. Geol. Surv. Water-Resources Investig. Rep.*, *96*, 1–17.

Fritz, B. G., and E. V. Arntzen (2007), Effect of rapidly changing river stage on uranium flux through the hyporheic zone, *Ground Water*, *45*(6), 753–760, doi:10.1111/j.1745-6584.2007.00365.x.

van Geen, A. et al. (2003), Spatial variability of arsenic in 6000 tube wells in a 25 km 2 area of Bangladesh, *Water Resour. Res.*, *39*(5), n/a-n/a, doi:10.1029/2002WR001617.

van Geen, A. et al. (2013), Retardation of arsenic transport through a Pleistocene aquifer., *Nature*, *501*(7466), 204–7, doi:10.1038/nature12444.

Gelhar, L., C. Welty, and K. Rehfeldt (1992), A critical review of data on field-scale dispersion in aquifers, *Water Resour. Res.*

Gerecht, K. E., M. B. Cardenas, A. J. Guswa, A. H. Sawyer, J. D. Nowinski, and T. E. Swanson (2011), Dynamics of hyporheic flow and heat transport across a bed-to-bank continuum in a large regulated river, *Water Resour. Res.*, *47*(3), W03524, doi:10.1029/2010WR009794.

Goodbred, S. L., P. M. Paolo, M. S. Ullah, R. D. Pate, S. R. Khan, S. A. Kuehl, S. K. Singh, and W. Rahaman (2014), Piecing together the Ganges-Brahmaputra-Meghna river delta: Use of sediment provenance to reconstruct the history and interaction of multiple fluvial systems during Holocene delta evolution, *Bull. Geol. Soc. Am.*,

126(11–12), 1495–1510, doi:10.1130/B30965.1.

Gu, C., G. M. Hornberger, A. L. Mills, J. S. Herman, and S. A. Flewelling (2007), Nitrate reduction in streambed sediments: Effects of flow and biogeochemical kinetics, *Water Resour. Res.*, *43*(12), W12413, doi:10.1029/2007WR006027.

Gu, C., W. Anderson, and F. Maggi (2012), Riparian biogeochemical hot moments induced by stream fluctuations, *Water Resour. Res.*, *48*(9), W09546, doi:10.1029/2011WR011720.

Guo, H., J. J. Jiao, and H. Li (2010), Groundwater response to tidal fluctuation in a two-zone aquifer, *J. Hydrol.*, *381*(3–4), 364–371, doi:10.1016/j.jhydrol.2009.12.009.

Hanrahan, T. P. (2008), Effects of river discharge on hyporheic exchange flows in salmon spawning areas of a large gravel-bed river, *Hydrol. Process.*, *22*(1), 127–141, doi:10.1002/hyp.6605.

Hantush, M. S., and C. E. Jacob (1955), Non-steady radial flow in an infinite leaky aquifer, *Eos, Trans. Am. Geophys. Union*, *36*(1), 95–100, doi:10.1029/TR036i001p00095.

Harvey, C. F. et al. (2002), Arsenic Mobility and Groundwater Extraction in Bangladesh, *Science (80-.).*, *298*(5598), 1602–1606, doi:10.1126/science.1076978.

Harvey, C. F. et al. (2006), Groundwater dynamics and arsenic contamination in Bangladesh, *Chem. Geol.*, *228*(1–3), 112–136, doi:10.1016/j.chemgeo.2005.11.025.

Hassan, M. A., D. Tonina, R. D. Beckie, and M. Kinnear (2015), The effects of discharge and slope on hyporheic flow in step-pool morphologies, *Hydrol. Process.*, *29*(3), 419–433, doi:10.1002/hyp.10155.

Hazen, A. (1911), Discussions: Dams on sand foundations, *Trans. Am. Soc. Civ. Eng.*, 73:199.

Hicks, S. D., R. L. Sillcox, C. R. Nichols, B. Via, and E. C. Mccray (2000), Tide and current glossary. Silver Spring, MD: NOAA National Ocean Service, *Cent. Oper. Oceanogr. Prod. Serv.*, 1–29.

Hohmann, C., E. Winkler, G. Morin, and A. Kappler (2010), Anaerobic Fe(II)-Oxidizing Bacteria Show As Resistance and Immobilize As during Fe(III) Mineral Precipitation, *Environ. Sci. Technol.*, *44*(1), 94–101, doi:10.1021/es900708s.

Horneman, A. et al. (2004), Decoupling of As and Fe release to Bangladesh groundwater under reducing conditions. Part I: Evidence from sediment profiles, *Geochim. Cosmochim. Acta*, *68*(17), 3459–3473, doi:10.1016/j.gca.2004.01.026.

Hvorslev, M. J. (1951), Time lag and soil permeability in ground-water observations, *Bull. No. 36 U.S. Army Corps Eng.*, (36), 53.

Jacob, C. E. (1950), Flow of ground-water, *Eng. Hydraul. H. (Ed). Wiley New York*, (5), 321–386.

Jardine, P. M., F. M. Dunnivant, J. F. McCarthy, and H. M. Selim (1992), Comparison of Models for Describing the Transport of Dissolved Organic Carbon in Aquifer Columns, *Soil Sci. Soc. Am. J.*, *56*(2), 393, doi:10.2136/sssaj1992.03615995005600020009x.

Jeng, D. S., L. Li, and D. A. Barry (2002), Analytical solution for tidal propagation in a coupled semi-confined/phreatic coastal aquifer, *Adv. Water Resour.*, *25*(5), 577–584, doi:10.1016/S0309-1708(02)00016-7.

Jennings, A. A. (1987), Critical chemical reaction rates for multicomponent groundwater contamination models, *Water Resour. Res.*, *23*(9), 1775–1784, doi:10.1029/WR023i009p01775.

Jha, M. K., and A. Singh (2014), Application of genetic algorithm technique to inverse modeling of tide-aquifer interaction, *Environ. Earth Sci.*, *71*(8), 3655–3672, doi:10.1007/s12665-013-2758-4.

Jha, M. K., Y. Kamii, and K. Chikamori (2003), On the estimation of phreatic aquifer parameters by the tidal response technique, *Water Resour. Manag.*, *17*(1), 69–88, doi:10.1023/A:1023018107685.

Jha, M. K., D. Namgial, Y. Kamii, and S. Peiffer (2008), Hydraulic Parameters of Coastal Aquifer Systems by Direct Methods and an Extended Tide–Aquifer Interaction Technique, *Water Resour. Manag.*, *22*(12), 1899–1923, doi:10.1007/s11269-008-9259-3.

Jiao, J. J., and Z. Tang (1999), An analytical solution of groundwater response to tidal fluctuation in a leaky confined aquifer, *Water Resour. Res.*, *35*(3), 747–751, doi:10.1029/1998WR900075.

Johnson, A. I., and D. A. Morris (1962), *Physical and hydrologic properties of water-bearing deposits from core holes in the Los Banos-Kettleman City area, California*.

Jung, H. B., M. A. Charette, and Y. Zheng (2009), Field, Laboratory, and Modeling Study of Reactive Transport of Groundwater Arsenic in a Coastal Aquifer, *Environ. Sci. Technol.*, *43*(14), 5333–5338, doi:10.1021/es900080q.

Jung, H. B., B. C. Bostick, and Y. Zheng (2012), Field, experimental, and modeling

study of arsenic partitioning across a redox transition in a bangladesh aquifer, *Environ. Sci. Technol.*, *46*(3), 1388–95, doi:10.1021/es2032967.

Jung, H. B., Y. Zheng, M. W. Rahman, M. M. Rahman, and K. M. Ahmed (2015), Redox zonation and oscillation in the hyporheic zone of the Ganges-Brahmaputra-Meghna Delta: Implications for the fate of groundwater arsenic during discharge, *Appl. Geochemistry*, *63*, 647–660, doi:10.1016/j.apgeochem.2015.09.001.

Khan, M. R. et al. (2016), Megacity pumping and preferential flow threaten groundwater quality, *Nat. Commun.*, *7*, 12833, doi:10.1038/ncomms12833.

Knappett, P. S. K. et al. (2012), Implications of fecal bacteria input from latrine-polluted ponds for wells in sandy aquifers., *Environ. Sci. Technol.*, *46*(3), 1361–70, doi:10.1021/es202773w.

Knappett, P. S. K. et al. (2016), Vulnerability of low-arsenic aquifers to municipal pumping in Bangladesh, *J. Hydrol.*, *539*, 674–686, doi:10.1016/j.jhydrol.2016.05.035.

Knights, D., A. H. Sawyer, R. T. Barnes, C. T. Musial, and S. Bray (2017), Tidal controls on riverbed denitrification along a tidal freshwater zone, *Water Resour. Res.*, 2207, doi:10.1002/2016WR019405.

Kocar, B. D., S. G. Benner, and S. Fendorf (2014), Deciphering and predicting spatial and temporal concentrations of arsenic within the Mekong Delta aquifer, *Environ. Chem.*, *11*(5), 579, doi:10.1071/EN13244.

Kolker, A., J. Cable, and K. Johannesson (2013), Pathways and processes associated with the transport of groundwater in deltaic systems, *J. Hydrol.*, *498*, 319–334,

doi:10.1016/j.jhydrol.2013.06.014.

Larkin, R. G., and J. M. Sharp, Jr. (1992), On the relationship between river-basin geomorphology, aquifer hydraulics, and ground-water flow direction in alluvial aquifers, *Geol. Soc. Am. Bull.*, *104*(12), 1608–1620, doi:10.1130/0016-7606(1992)104<1608:OTRBRB>2.3.CO;2.

LCRA (2014), Basin highlights report: a summary of water quality in the Colorado River basin during 2013. Lower Colorado River Authority, Austin, TX,

Lee, J., C. Robinson, and R. M. Couture (2014), Effect of groundwater-lake interactions on arsenic enrichment in freshwater beach aquifers, *Environ. Sci. Technol.*, *48*(17), 10174–10181, doi:10.1021/es5020136.

Li, H., P. Sun, S. Chen, Y. Xia, and S. Liu (2010), A falling-head method for measuring intertidal sediment hydraulic conductivity, *Ground Water*, *48*(2), 206–211, doi:10.1111/j.1745-6584.2009.00638.x.

Li, L., D. A. Barry, C. Cunningham, F. Stagnitti, and J. Y. Parlange (2000), A two-dimensional analytical solution of groundwater responses to tidal loading in an estuary and ocean, *Adv. Water Resour.*, *23*(8), 825–833, doi:10.1016/S0309-1708(00)00016-6.

Liu, Y., F. Xu, and C. Liu (2017), Coupled Hydro-Biogeochemical Processes Controlling Cr Reductive Immobilization in Columbia River Hyporheic Zone, *Environ. Sci. Technol.*, *51*(3), 1508–1517, doi:10.1021/acs.est.6b05099.

Loheide, S. P., and J. D. Lundquist (2009), Snowmelt-induced diel fluxes through the hyporheic zone, *Water Resour. Res.*, *45*(7), W07404, doi:10.1029/2008WR007329.

MacKay, A. A., P. Gan, R. Yu, and B. F. Smets (2014), Seasonal Arsenic Accumulation in Stream Sediments at a Groundwater Discharge Zone, *Environ. Sci. Technol.*, *48*(2), 920–929, doi:10.1021/es402552u.

Maji, R., and L. Smith (2009), Quantitative analysis of seabed mixing and intertidal zone discharge in coastal aquifers, *Water Resour. Res.*, *45*(11), W11401, doi:10.1029/2008WR007532.

Marzadri, A., D. Tonina, and A. Bellin (2011), A semianalytical three-dimensional process-based model for hyporheic nitrogen dynamics in gravel bed rivers, *Water Resour. Res.*, *47*(11), W11518, doi:10.1029/2011WR010583.

McArthur, J. M., P. Ravenscroft, D. M. Banerjee, J. Milsom, K. a. Hudson-Edwards, S. Sengupta, C. Bristow, A. Sarkar, S. Tonkin, and R. Purohit (2008), How paleosols influence groundwater flow and arsenic pollution: A model from the Bengal Basin and its worldwide implication, *Water Resour. Res.*, *44*(11), n/a-n/a, doi:10.1029/2007WR006552.

McCallum, J. L., and M. Shanafield (2016), Residence times of stream-groundwater exchanges due to transient stream stage fluctuations, *Water Resour. Res.*, *52*(3), 2059–2073, doi:10.1002/2015WR017441.

Merill, L., and D. J. Tonjes (2014), A Review of the Hyporheic Zone, Stream Restoration, and Means to Enhance Denitrification, *Crit. Rev. Environ. Sci. Technol.*, (March 2014), 140225123451005, doi:10.1080/10643389.2013.829769.

Millham, N. P., and B. L. Howes (1995), A comparison of methods to determine K in a shallow coastal aquifer, *Ground Water*, *33*(1), 49–57, doi:10.1111/j.1745-

6584.1995.tb00262.x.

Mohanty, B. P., R. S. Kanwar, and C. J. Everts (1994), Comparison of Saturated Hydraulic Conductivity Measurement Methods for a Glacial-Till Soil, *Soil Sci. Soc. Am. J.*, *58*(3), 672–677, doi:10.2136/sssaj1994.03615995005800030006x.

Molz, F. J., M. A. Widdowson, and L. D. Benefield (1986), Simulation of Microbial Growth Dynamics Coupled to Nutrient and Oxygen Transport in Porous Media, *Water Resour. Res.*, *22*(8), 1207–1216, doi:10.1029/WR022i008p01207.

Musial, C. T., A. H. Sawyer, R. T. Barnes, S. Bray, and D. Knights (2016), Surface water-groundwater exchange dynamics in a tidal freshwater zone, *Hydrol. Process.*, *30*(5), 739–750, doi:10.1002/hyp.10623.

Nakaya, S., H. Natsume, H. Masuda, M. Mitamura, D. K. Biswas, and A. A. Seddique (2011), Effect of groundwater flow on forming arsenic contaminated groundwater in Sonargaon, Bangladesh, *J. Hydrol.*, *409*(3–4), 724–736, doi:10.1016/j.jhydrol.2011.09.006.

Naranjo, R. C. (2015), Mixing effects on nitrogen and oxygen concentrations and the relationship to mean residence time in a hyporheic zone of a riffle-pool sequence, *Water Resour. Res.*, *51*, 9127–9140, doi:10.1002/2014WR016259.

Neumann, R. B., K. N. Ashfaque, a. B. M. Badruzzaman, M. Ashraf Ali, J. K. Shoemaker, and C. F. Harvey (2010), Anthropogenic influences on groundwater arsenic concentrations in Bangladesh, *Nat. Geosci.*, *3*(1), 46–52, doi:10.1038/ngeo685.

Nickson, R., J. McArthur, W. Burgess, K. M. Ahmed, P. Ravenscroft, and M. Rahman

(1998), Arsenic poisoning of Bangladesh groundwater., *Nature*, *395*(6700), 338, doi:10.1038/26387.

Nilsson, C., C. A. Reidy, M. Dynesius, and C. Revenga (2005), Fragmentation and Flow Regulation of the World's Large River Systems, *Science (80-.).*, *308*(5720), 405–408, doi:10.1126/science.1107887.

Nyquist, J. E., P. A. Freyer, and L. Toran (2008), Stream bottom resistivity tomography to map ground water discharge, *Ground Water*, *46*(4), 561–569, doi:10.1111/j.1745-6584.2008.00432.x.

Pinder, G. F., and S. P. Sauer (1971), Numerical Simulation of Flood Wave Modification Due to Bank Storage Effects, *Water Resour. Res.*, *7*(1), 63–70, doi:10.1029/WR007i001p00063.

Polizzotto, M. L., B. D. Kocar, S. G. Benner, M. Sampson, and S. Fendorf (2008), Near-surface wetland sediments as a source of arsenic release to ground water in Asia., *Nature*, *454*(7203), 505–508, doi:10.1038/nature07093.

Postma, D., F. Larsen, N. T. Minh Hue, M. T. Duc, P. H. Viet, P. Q. Nhan, and S. Jessen (2007), Arsenic in groundwater of the Red River floodplain, Vietnam: Controlling geochemical processes and reactive transport modeling, *Geochim. Cosmochim. Acta*, *71*(21), 5054–5071, doi:10.1016/j.gca.2007.08.020.

Postma, D., S. Jessen, N. T. M. Hue, M. T. Duc, C. B. Koch, P. H. Viet, P. Q. Nhan, and F. Larsen (2010), Mobilization of arsenic and iron from Red River floodplain sediments, Vietnam, *Geochim. Cosmochim. Acta*, *74*(12), 3367–3381, doi:10.1016/j.gca.2010.03.024.

Postma, D., T. K. T. Pham, H. U. Sø, V. H. Hoang, M. L. Vi, T. T. Nguyen, F. Larsen, H. V. Pham, and R. Jakobsen (2016a), A model for the evolution in water chemistry of an arsenic contaminated aquifer over the last 6000years, Red River floodplain, Vietnam, *Geochim. Cosmochim. Acta*, *195*, 277–292, doi:10.1016/j.gca.2016.09.014.

Postma, D., N. T. H. Mai, V. M. Lan, P. T. K. Trang, H. U. Sø, P. Q. Nhan, F. Larsen, P. H. Viet, and R. Jakobsen (2016b), Fate of arsenic during Red River water infiltration into aquifers beneath Hanoi, Vietnam., *Environ. Sci. Technol.*, acs.est.6b05065, doi:10.1021/acs.est.6b05065.

Radloff, K. A. et al. (2011), Arsenic migration to deep groundwater in Bangladesh influenced by adsorption and water demand., *Nat. Geosci.*, *4*(11), 793–798, doi:10.1038/ngeo1283.

Reeves, H. W., P. M. Thibodeau, R. G. Underwood, and L. R. Gardner (2000), Incorporation of Total Stress Changes into the Ground Water Model SUTRA, *Ground Water*, *38*(1), 89–98, doi:10.1111/j.1745-6584.2000.tb00205.x.

Rotzoll, K., and A. I. El-Kadi (2008), Estimating hydraulic properties of coastal aquifers using wave setup, *J. Hydrol.*, *353*(1–2), 201–213, doi:10.1016/j.jhydrol.2008.02.005.

Rotzoll, K., A. I. El-Kadi, and S. B. Gingerich (2008), Analysis of an unconfined aquifer subject to asynchronous dual-tide propagation, *Ground Water*, *46*(2), 239–250, doi:10.1111/j.1745-6584.2007.00412.x.

Rotzoll, K., S. B. Gingerich, J. W. Jenson, and A. I. El-Kadi (2013), Estimating

hydraulic properties from tidal attenuation in the Northern Guam Lens Aquifer, territory of Guam, USA, *Hydrogeol. J.*, *21*(3), 643–654, doi:10.1007/s10040-012-0949-9.

Sawyer, A. H. (2015), Enhanced removal of groundwater-borne nitrate in heterogeneous aquatic sediments, *Geophys. Res. Lett.*, *42*(2), 403–410, doi:10.1002/2014GL062234.

Sawyer, A. H., and M. B. Cardenas (2009), Hyporheic flow and residence time distributions in heterogeneous cross-bedded sediment, *Water Resour. Res.*, *45*(8), 1–12, doi:10.1029/2008WR007632.

Sawyer, A. H., M. B. Cardenas, A. Bomar, and M. Mackey (2009), Impact of dam operations on hyporheic exchange in the riparian zone of a regulated river, *Hydrol. Process.*, *23*(15), 2129–2137, doi:10.1002/hyp.7324.

Schaefer, M. V., S. C. Ying, S. G. Benner, Y. Duan, Y. Wang, and S. Fendorf (2016), Aquifer Arsenic Cycling Induced by Seasonal Hydrologic Changes within the Yangtze River Basin, *Environ. Sci. Technol.*, *50*(7), 3521–3529, doi:10.1021/acs.est.5b04986.

Schaefer, M. V., X. Guo, Y. Gan, S. G. Benner, A. M. Griffin, C. A. Gorski, Y. Wang, and S. Fendorf (2017), Redox controls on arsenic enrichment and release from aquifer sediments in central Yangtze River Basin, *Geochim. Cosmochim. Acta*, *204*, 104–119, doi:10.1016/j.gca.2017.01.035.

Schultz, G., and C. Ruppel (2002), Constraints on hydraulic parameters and implications for groundwater flux across the upland–estuary interface, *J. Hydrol.*, *260*(1–4),

255–269, doi:10.1016/S0022-1694(01)00616-3.

Shuai, P., M. B. Cardenas, P. S. K. Knappett, P. C. Bennett, and B. T. Neilson (2017a), Denitrification in the banks of fluctuating rivers: the effects of river stage amplitude, sediment hydraulic conductivity and dispersivity, and ambient groundwater flow, *Water Resour. Res.*, Under review.

Shuai, P., P. S. K. Knappett, S. Hossain, A. Hosain, K. Rhodes, K. M. Ahmed, and M. B. Cardenas (2017b), The Impact of the Degree of Aquifer Confinement and Anisotropy on Tidal Pulse Propagation, *Groundwater*, doi:10.1111/gwat.12509.

Slater, L. (2002), Electrical-hydraulic relationships observed for unconsolidated sediments, *Water Resour. Res.*, *38*(10), 33–46, doi:10.1029/2001WR001075.

Slater, L. D., D. Ntarlagiannis, F. D. Day-Lewis, K. Mwakanyamale, R. J. Versteeg, A. Ward, C. Strickland, C. D. Johnson, and J. W. Lane (2010), Use of electrical imaging and distributed temperature sensing methods to characterize surface water-groundwater exchange regulating uranium transport at the Hanford 300 Area, Washington, *Water Resour. Res.*, *46*(10), 1–13, doi:10.1029/2010WR009110.

Slingerland, R., and N. D. Smith (2004), River avulsions and their deposits, *Annu. Rev. Earth Planet. Sci.*, *32*(1), 257–285, doi:10.1146/annurev.earth.32.101802.120201.

Song, Z., L. Li, J. Kong, and H. Zhang (2007), A new analytical solution of tidal water table fluctuations in a coastal unconfined aquifer, *J. Hydrol.*, *340*(3–4), 256–260, doi:10.1016/j.jhydrol.2007.04.015.

Squillace, P. J. (1996), Observed and Simulated Movement of Bank-Storage Water, *Ground Water*, *34*(1), 121–134, doi:10.1111/j.1745-6584.1996.tb01872.x.

Stahl, M. O., C. F. Harvey, A. van Geen, J. Sun, P. Thi Kim Trang, V. Mai Lan, T. Mai Phuong, P. Hung Viet, and B. C. Bostick (2016), River bank geomorphology controls groundwater arsenic concentrations in aquifers adjacent to the Red River, Hanoi Vietnam, *Water Resour. Res.*, *52*(8), 6321–6334, doi:10.1002/2016WR018891.

Steckler, M. S., S. L. Nooner, S. H. Akhter, S. K. Chowdhury, S. Bettadpur, L. Seeber, and M. G. Kogan (2010), Modeling Earth deformation from monsoonal flooding in Bangladesh using hydrographic, GPS, and Gravity Recovery and Climate Experiment (GRACE) data, *J. Geophys. Res.*, *115*(B8), B08407, doi:10.1029/2009JB007018.

Stegen, J. C. et al. (2016), Groundwater–surface water mixing shifts ecological assembly processes and stimulates organic carbon turnover, *Nat. Commun.*, *7*, 11237, doi:10.1038/ncomms11237.

Stollenwerk, K. G., G. N. Breit, A. H. Welch, J. C. Yount, J. W. Whitney, A. L. Foster, M. N. Uddin, R. K. Majumder, and N. Ahmed (2007), Arsenic attenuation by oxidized aquifer sediments in Bangladesh, *Sci. Total Environ.*, *379*(2–3), 133–150, doi:10.1016/j.scitotenv.2006.11.029.

Sun, P., H. Li, M. C. Boufadel, X. Geng, and S. Chen (2008), An analytical solution and case study of groundwater head response to dual tide in an island leaky confined aquifer, *Water Resour. Res.*, *44*(12), 1–7, doi:10.1029/2008WR006893.

Teo, H. T., D. S. Jeng, B. R. Seymour, D. A. Barry, and L. Li (2003), A new analytical solution for water table fluctuations in coastal aquifers with sloping beaches, *Adv.*

Water Resour., *26*(12), 1239–1247, doi:10.1016/j.advwatres.2003.08.004.

Theis, C. V. (1935), The relation between the lowering of the Piezometric surface and the rate and duration of discharge of a well using ground-water storage, *Trans. Am. Geophys. Union*, *16*, 519, doi:10.1029/TR016i002p00519.

Tonina, D., and J. M. Buffington (2007), Hyporheic exchange in gravel bed rivers with pool-riffle morphology: Laboratory experiments and three-dimensional modeling, *Water Resour. Res.*, *43*(1), 1–16, doi:10.1029/2005WR004328.

Trefry, M. G., and E. Bekele (2004), Structural characterization of an island aquifer via tidal methods, *Water Resour. Res.*, *40*(1), W01505, doi:10.1029/2003WR002003.

Trefry, M. G., and C. D. Johnston (1998), Pumping test analysis for a tidally forced aquifer, *Ground Water*, *36*(3), 427–433, doi:10.1111/j.1745-6584.1998.tb02813.x.

Valett, H. M., C. C. Hakenkamp, and A. J. Boulton (1993), Perspectives on the Hyporheic Zone: Integrating Hydrology and Biology. Introduction, *J. North Am. Benthol. Soc.*, *12*(1), 40–43, doi:10.2307/1467683.

Van, der Kamp, G. (1972), Tidal fluctuations in a confined aquifer extending under the sea, *Int. Geol. Congr.*, *24*(11), 101–106.

Weinman, B., S. L. Goodbred, Y. Zheng, Z. Aziz, M. Steckler, A. van Geen, A. K. Singhvi, and Y. C. Nagar (2008), Contributions of floodplain stratigraphy and evolution to the spatial patterns of groundwater arsenic in Araihazar, Bangladesh, *Bull. Geol. Soc. Am.*, *120*(11–12), 1567–1580, doi:10.1130/B26209.1.

Widdowson, M. A., F. J. Molz, and L. D. Benefield (1988), A numerical transport model for oxygen- and nitrate-based respiration linked to substrate and nutrient

availability in porous media, *Water Resour. Res.*, *24*(9), 1553–1565, doi:10.1029/WR024i009p01553.

Wilson, A. M., and L. R. Gardner (2006), Tidally driven groundwater flow and solute exchange in a marsh: Numerical simulations, *Water Resour. Res.*, *42*(1), 1–9, doi:10.1029/2005WR004302.

Xia, Y., H. Li, M. C. Boufadel, Q. Guo, and G. Li (2007), Tidal wave propagation in a coastal aquifer: Effects of leakages through its submarine outlet-capping and offshore roof, *J. Hydrol.*, *337*(3–4), 249–257, doi:10.1016/j.jhydrol.2007.01.036.

Xie, X., Y. Wang, J. Li, Q. Yu, Y. Wu, C. Su, and M. Duan (2015), Effect of irrigation on Fe(III)–SO42− redox cycling and arsenic mobilization in shallow groundwater from the Datong basin, China: Evidence from hydrochemical monitoring and modeling, *J. Hydrol.*, *523*, 128–138, doi:10.1016/j.jhydrol.2015.01.035.

Xin, P., L. R. Yuan, L. Li, and D. A. Barry (2011), Tidally driven multiscale pore water flow in a creek-marsh system, *Water Resour. Res.*, *47*(7), 1–19, doi:10.1029/2010WR010110.

Yeh, H. D., C. S. Huang, Y. C. Chang, and D. S. Jeng (2010), An analytical solution for tidal fluctuations in unconfined aquifers with a vertical beach, *Water Resour. Res.*, *46*(10), 1–12, doi:10.1029/2009WR008746.

Zarnetske, J. P., R. Haggerty, S. M. Wondzell, and M. A. Baker (2011a), Dynamics of nitrate production and removal as a function of residence time in the hyporheic zone, *J. Geophys. Res.*, *116*(G1), G01025, doi:10.1029/2010JG001356.

Zarnetske, J. P., R. Haggerty, S. M. Wondzell, and M. A. Baker (2011b), Labile

dissolved organic carbon supply limits hyporheic denitrification, *J. Geophys. Res. Biogeosciences*, *116*(4), doi:10.1029/2011JG001730.

Zarnetske, J. P., R. Haggerty, S. M. Wondzell, V. a. Bokil, and R. González-Pinzón (2012), Coupled transport and reaction kinetics control the nitrate source-sink function of hyporheic zones, *Water Resour. Res.*, *48*(11), 1–15, doi:10.1029/2012WR011894.

Zheng, L., M. B. Cardenas, and L. Wang (2016), Temperature effects on nitrogen cycling and nitrate removal-production efficiency in bed form-induced hyporheic zones, *J. Geophys. Res. Biogeosciences*, *121*(4), 1086–1103, doi:10.1002/2015JG003162.

Zheng, Y. et al. (2005), Geochemical and hydrogeological contrasts between shallow and deeper aquifers in two villages of Araihazar, Bangladesh: Implications for deeper aquifers as drinking water sources, *Geochim. Cosmochim. Acta*, *69*(22), 5203–5218, doi:10.1016/j.gca.2005.06.001.

Zhou, X. (2008), Determination of aquifer parameters based on measurements of tidal effects on a coastal aquifer near Beihai, China, *Hydrol. Process.*, *22*(16), 3176–3180, doi:10.1002/hyp.6906.